

Deterministic Diffusion
in
One-Dimensional Chaotic Dynamical Systems

von
Dipl.-Phys. Rainer Klages
aus Berlin

Zusammenfassung

Die vorliegende Arbeit beschäftigt sich mit der theoretischen Analyse einfacher eindimensionaler Modelle für deterministische Diffusion. Diese Modelle bestehen aus einer periodischen Anordnung identischer Streuzentren, in denen sich wechselwirkungsfreie Punktteilchen bewegen. Der mikroskopische chaotische Streuprozess dieser Teilchen kann durch Variation eines einzelnen Systemparameters kontinuierlich verändert werden, wodurch eine Parameterabhängigkeit für den makroskopischen Diffusionskoeffizienten des Systems erzeugt wird.

Zur Berechnung dieses Diffusionskoeffizienten werden eine Reihe analytischer und numerischer Methoden entwickelt, die auf Grundlagen der Theorie chaotischer dynamischer Systeme und der Transporttheorie der statistischen Mechanik beruhen. Der erhaltene parameterabhängige Diffusionskoeffizient besitzt eine überraschend komplexe fraktale Struktur, die im Rahmen dieser Arbeit zum erstenmal in einem dynamischen System nachgewiesen wurde.

Eine eingehende Analyse der deterministischen Diffusion, die zur Entstehung dieses fraktalen Diffusionskoeffizienten führt, zeigt, daß das System makroskopische dynamische Eigenschaften besitzt, die denjenigen eines einfachen statistischen Diffusionsprozesses entsprechen. Auf einer feinen Skala dagegen tauchen Strukturen auf, die durch die deterministischen mikroskopischen Eigenschaften der Streuzentren bestimmt werden.

Um die Struktur des fraktalen Diffusionskoeffizienten zu verstehen, werden qualitative und quantitative Methoden entwickelt. Diese setzen die Abfolge von Oszillationen der Stärke des Diffusionskoeffizienten in Beziehung zur mikroskopischen Kopplung der einzelnen Streuer untereinander, die sich bei Variation des Systemparameters ändert. Auf der Grundlage einer neudefinierten Klasse von fraktalen Funktionen werden systematische analytische und numerische Näherungsmethoden vorgeschlagen, die ein besseres Verständnis bestimmter Details des fraktalen Diffusionskoeffizienten ermöglichen. Es werden einfache Modelle der Zufallsbewegung und deren Anwendbarkeit auf den Prozess deterministischer Diffusion diskutiert. Dies führt zur Voraussage von universalen Gesetzen für den parameterabhängigen Diffusionskoeffizienten auf einer groben Skala. Darüberhinaus gibt es Hinweise auf einen dynamischen Phasenübergang, der in Analogie zu ähnlichen Phänomenen in dynamischen Systemen als eine Krise in deterministischer Diffusion gedeutet werden kann.

Es ist zu vermuten, daß fraktale Diffusionskoeffizienten, zusammen mit den für sie charakteristischen dynamischen Eigenschaften, in einer Vielzahl dynamischer Systeme zu finden sind. Da derartige Systeme bis zu einem gewissen Grad bereits experimentell realisiert werden konnten, sollten diese Ergebnisse nicht nur zur Klärung physikalischer Grundlagenfragen beitragen, die den mikroskopischen Ursprung makroskopischer Transportphänomene betreffen, sondern sie könnten unter Umständen auch langfristig Bedeutung für spezielle Anwendungen, wie zum Beispiel in der Halbleitertechnologie, gewinnen.

Abstract

A theoretical analysis of simple one-dimensional models for deterministic diffusion has been performed. The models which are in the center of this investigation consist of arrays of identical scatterers, in which point particles get scattered without interacting with each other. The microscopic chaotic scattering process of these particles can be changed continuously by switching a single control parameter. This induces a parameter dependence for the macroscopic diffusion coefficient of the system.

For the calculation of this diffusion coefficient, new analytical and numerical methods are developed. They are based on the theory of chaotic dynamical systems and on the theory of transport of statistical mechanics. The computed parameter-dependent diffusion coefficient shows a surprisingly complex fractal structure, which is obtained here for the first time in a dynamical system.

A detailed analysis of the process of deterministic diffusion which leads to this fractal diffusion coefficient shows that the system has macroscopic dynamical properties analogous to the ones of a simple statistical diffusion process. On a fine scale, however, structures appear which are inherent to the deterministic microscopic properties of the scatterers.

To explain the structure of the fractal diffusion coefficient, qualitative and quantitative methods are developed. These methods relate the sequence of oscillations in the strength of the parameter-dependent diffusion coefficient to the microscopic coupling of the single scatterers, which changes by varying the control parameter. By employing a newly-defined class of fractal functions, a systematic analytical and numerical approximation procedure is introduced, which provides a better understanding of certain details of the parameter-dependent diffusion coefficient. Simple random walk models are applied to the process of deterministic diffusion. This leads to the prediction of universal laws for the parameter-dependent diffusion coefficient on a large scale. Moreover, there is evidence for the existence of a dynamical phase transition. In analogy to related phenomena recently discovered in dynamical systems, this transition can be understood as a crisis in deterministic diffusion.

It is supposed that fractal diffusion coefficients, and characteristic properties of their underlying diffusion processes, are obtained for a variety of deterministic dynamical systems. To a certain extent, such systems could already be realized experimentally. Thus, the results presented in this work should not only give more insight into fundamental questions concerning the microscopic origin of macroscopic transport, but they could also become important for special technological applications as, e.g., in the field of semi-conductor devices.

Acknowledgements

In the first place, I wish to thank Prof. Dr. S. Hess and Prof. Dr. J. R. Dorfman, without either of whom this work would not have been possible: Prof. Dr. S. Hess for introducing me to the interesting field of transport theory, and for his continuing support over many years in many different ways; and Prof. Dr. J. R. Dorfman for giving me the opportunity to jointly discover with him the equally fascinating field of chaos theory, which finally led to the subject of this thesis.

I am indebted to Prof. Dr. E. Schöll, Ph.D., for his role as an additional referee, for his continuing interest in this work, and for several helpful hints. Thanks go also to Prof. Dr. A. Hese for his efforts of being the head on the examination board.

Valuable discussions with some experts in this field are gratefully acknowledged. Their various hints helped me enormously in pursuing this work: Prof. Dr. Chr. Beck, Prof. Dr. H. van Beijeren, Prof. Dr. L. Bunimovich, Prof. Dr. E. G. D. Cohen, Prof. Dr. P. Gaspard, Prof. Dr. C. Grebogi, Dr. H.-P. Herzel, Dr. B. Hunt, Prof. Dr. R. Kapral, Prof. Dr. J. Kurths, Prof. Dr. H. E. Nusse, Dr. A. Pikowsky, Prof. Dr. T. Tél, and Prof. Dr. J. Yorke. Recent discussions with Prof. Dr. W. G. Hoover and Prof. Dr. H. A. Posch are also very much appreciated.

Special thanks go to Dr. J. Groeneveld for enlightening e-mail discussions and for his critical comments to parts of this work. I am obliged to my colleagues and friends Dr. R. E. Kunz, Dr. A. Latz, Dr. B. Leeb, F. Lledó, and Dr. Chr. Papenfuß for some helpful remarks.

S. Bose and D. Merbach helped me considerably by advice in certain computer problems. Dr. M. Kröger kindly supported me in taking the last steps for publishing my thesis from abroad.

Financial support by the German Academic Exchange Service (DAAD) and by the NaFöG commission Berlin over the last three years is gratefully acknowledged.

I thank the Institute for Physical Science and Technology (IPST), College Park, and Prof. Dr. T.R. Kirkpatrick for their hospitality during a 1 1/2-year stay, sponsored by the DAAD, when this work got started; Prof. Dr. J. R. Dorfman and the IPST again for support in several subsequent visits; J. Latz and Dr. A. Latz for their kind hospitality during all these stays; Prof. Dr. M. H. Ernst for financial support in a short visit to Utrecht; Prof. Dr. S. Hess and the Society of Friends of the Technical University of Berlin for financial support, especially during the last stages of this work; and the secretaries of the IPST, Mrs. M. Spell, Mrs. J. Provost, and Mrs. C. Brannan, and of the Institute for Theoretical Physics in Berlin, Mrs. U. Wolfram and Mrs. K. Ludwig, for their help in organizational affairs.

Finally, I want to thank my parents, Ursula and Günter Klages, and my brother, Michael Klages, for their support in various ways during the time this work has been performed.

Contents

1	Introduction	1
2	Simple maps with fractal diffusion coefficients	5
2.1	A simple model for deterministic diffusion	6
2.1.1	What is deterministic diffusion?	6
2.1.2	Physical motivation of the deterministic model	9
2.1.3	Formal definition of the deterministic model	11
2.2	First passage method	13
2.3	Solution of the Frobenius-Perron equation	15
2.3.1	Transition matrix method	16
2.3.2	Markov partitions	25
2.4	Fractal diffusion coefficients: results	35
2.5	Conclusions	46
3	Dynamics of deterministic diffusion	49
3.1	Principles of numerics: Iteration method and simulations	50
3.2	Time-dependent statistical dynamical quantities: results	52
3.2.1	Probability densities	53
3.2.2	Probability density averages and ensemble averages	55
3.3	Fractal diffusion coefficients, time-dependent dynamical quantities, and stability of dynamical systems	62
3.4	Conclusions	66
4	Crisis in deterministic diffusion	67
4.1	Simple models for crises in chaotic scattering	68
4.2	Parameter-dependent diffusion coefficients and random walks	72
4.3	Understanding the structure of fractal diffusion coefficients	79
4.3.1	Counting wiggles and plus-minus dynamics	79
4.3.2	Turnstile dynamics	84
4.4	Conclusions	89

5	Fractal Functions for fractal diffusion coefficients	91
5.1	Construction of jump-velocity functions	92
5.2	Approximation procedures for fractal diffusion coefficients	95
5.3	Fractal generalized Takagi functions	99
5.4	Computation of invariant probability densities on the unit interval	102
5.5	Conclusions	107
6	Concluding remarks	109
6.1	Summary of main results	109
6.2	Outlook	111
	References	115

1

Introduction

“Was ist Physik? Ist sie der Gehorsam des Denkens gegenüber der Wirklichkeit?” [vW95]

C.F. von Weizsäcker

The project of connecting *transport theory* to the *theory of dynamical systems* is a quite recent field of research. It was basically started about fifteen years ago,¹ initiated by the developments of what is popularly known as *chaos* theory. The theory of chaos itself is not much older [Cvi89], although its roots may be dated back to H. Poincaré and his work about the turn of the century, or even earlier, to J.C. Maxwell’s and L. Boltzmann’s discussions of microscopic scattering processes in the framework of developing kinetic theory.

The modern theory of chaos may be said to be initiated, at least for non-mathematicians, by the famous article of E.N. Lorenz Ref. [Lor63] about thirty years ago [Gle88]. Since then, the mathematical theory of dynamical systems has been employed with increasing success as a suitable tool to analyze the dynamics not only of physical systems, but also of dynamical systems important in many other branches of science. The reason for this success is that the complete dynamics of even simple models is usually highly nonlinear and difficult to describe by conventional methods. Thus, an arsenal of refined methods, as provided by the theory of dynamical systems, is needed if one wants to achieve an understanding of the dynamics beyond the range of linear approximations.

Transport theory, on the other hand, is a traditional branch of non-equilibrium statistical mechanics and deals basically with the calculation of quantities which are called *transport coefficients*, as, e.g., viscosity, thermal conductivity, or diffusion coefficients. These quantities are employed to describe the macroscopic behaviour of physical systems like gases or liquids with respect to the variation of certain parameters as, e.g., temperature, density of a fluid, or applied external fields. This way, certain parts of transport theory are of great practical importance for chemists, materials scientists, and engineers.

In the picture of classical physics, any macroscopic transport is caused mechanically by microscopic dynamics. If one follows this line of reductionism, one may raise the question about the intrinsic connection between the microscopic “chaotic” dynamics of a physical system and its macroscopic statistical be-

¹ see, e.g., Refs. [Lic92, Mei92, Wig92, Dor95a, Cvi95] and further references therein

haviour. The essential new feature of the theory of dynamical systems is now that it allows a description of the *deterministic* dynamics of a chaotic system, i.e., the movements of all single particles of, e.g., a gas are taken into account completely, without any approximation, and are characterized by evaluating respectively defined dynamical systems quantities. This is in contrast to the mainstream of previous traditional approaches to transport theory, where always a suitable “coarse graining” has been employed in one way or the other. A famous coarse graining is, e.g., Boltzmann’s hypothesis of molecular chaos, which provides the key for the derivation of the powerful Boltzmann equation of transport theory and, furthermore, has led to heated discussions about the origin of the second law of thermodynamics in the framework of the atomic theory of matter [Bru76].

The modern theory of chaotic dynamical systems thus provides an opportunity to “take microscopic dynamics seriously” in the calculation of macroscopic statistical quantities in the sense that the *complete*, usually highly nonlinear deterministic dynamics of a system can be taken into account. Applied to the problem of computing transport coefficients, this alliance between transport theory and the theory of deterministic dynamical systems leads, as a *deterministic theory of transport*, to the evaluation of quantities like *deterministic diffusion coefficients* (see Section 2.1 for a detailed definition), which have been moved into the focus of many investigations in recent literature. It may be stated as the main goal of a deterministic theory of transport to investigate the precise relation between microscopic deterministic dynamics and macroscopic statistical transport by analyzing models of physical dynamical systems with respect to their chaotic properties.

However, confronted with the analysis of the complete dynamics of a chaotic system, one has to pay a price: The chaotic model has to be sufficiently “simple” so that the methods of dynamical systems theory can be applied to their full extent. Thus, there is much reason for the common tendency in nonlinear dynamics to “reduce” complex, i.e., usually high-dimensional systems to less complex, i.e., usually low-dimensional models, which are supposed to be simple enough to enable a detailed analysis. This leads to an “abstraction from reality”, anticipating that the simple model one arrives at still contains “some” essential features of the original system, and at least for physicists the challenge must be to “invert” this direction after a successful analysis of the supposedly simple model to get back to physical reality. This working principle may explain the existence of a large variety of one- and two-dimensional dynamical systems in the literature, as, e.g., coupled map lattices and cellular automata. There is of course a great danger that physicists stick too much to the fascinating properties of chaotic dynamical systems, without keeping any connection to actual physical problems in mind anymore.

Nevertheless, paraphrasing von Weizsäcker, in this work it shall be taken the

risk to be a bit “disobedient” to physical reality. It deals with a supposedly simple, quite abstract model for deterministic diffusion which may be physically motivated in a long line, starting from quite realistic physical systems described by Newton’s equations of motion [Hes92a, Hes92b, Kla92, Coh93, Dor77] over certain two-dimensional models [Woo71, Mac83b, Kon89, Gas90] to finally the type of one-dimensional model to be considered here [Fuj82, Gas92a, Gas92d]. The hope of the author, as a physicist, is still that some results of the following investigations may turn out to be helpful to gain a better understanding of “real” physical systems, and that in the long run some of the features described here may be discovered in certain physical experiments [Gei85, Wei95, Fle95]. Connections to experimental aspects, as far as they occur, will be pointed out in the course of the investigations, and some possible first steps on a “road to reality” will be briefly sketched in the final chapter.

It shall be concluded with some brief remarks about the contents of this work, and about the style in which these pages are written. This book consists of four main chapters in which different facets of deterministic diffusion will be discussed. Chapter 2 starts with a definition of the model to be investigated and leads to the most important result of this work: the existence of *fractal diffusion coefficients*. Chapter 3 is concerned with the *dynamics of deterministic diffusion*, i.e., an analysis of the time-dependent behaviour of diffusing particles in the model system will be performed. In Chapter 4, a relative of the first map under consideration will be introduced, motivated by a phenomenon recently discovered in dynamical systems theory, which is called a *crisis in chaotic scattering*. The methods developed before will be applied to answer the question whether this phenomenon is of any importance for the process of deterministic diffusion. Finally, in Chapter 5 a refined approach to compute fractal diffusion coefficients will be presented by employing some newly-defined *fractal functions*, which can be used to generate a systematical series of numerical and analytical approximations for fractal diffusion coefficients.

This work has been written in a rather “soft” and introductory manner. It is directed basically to physicists as potential readers, although it has been tried to give some clues to mathematically oriented researchers by formulating certain conjectures. For the main conjectures, which are labeled as such in the following chapters, either numerical evidence has been obtained or a sketch of a proof could be worked out. If there was a choice, always a more “physically intuitive” approach has been preferred to introduce important theoretical objects and techniques instead of favorizing a strictly formal way (see especially Section 2.3). The specialist might be a bit disappointed about that treatment, but it is

intended to give details² in a series of subsequent papers.³ In the comprehensive work presented here, any of these details have been either skipped or just briefly mentioned in footnotes with further references. This way, only a limited background of dynamical systems theory and transport theory is required, as provided by some introductory texts.⁴ More special notations will again be briefly explained in footnotes with suitable references.

Section 2.1.2 provides an introduction of the model to be considered, which should even be understandable to non-physicists. The hurried reader may be referred to the respective introductions and conclusions of the single chapters, which contain brief motivations of the problems and the main results, and to the final chapter. Although it has been tried to write the single chapters in a way that they can be read separately, certain cross-references could not be avoided.

²These details are: some formal definitions (Markov partitions and transition matrices, see Chapter 2); the derivation of various specific analytical results obtained by the so-called transition matrix method (see Chapters 2 and 4); some details to the derivation of the Green-Kubo formula employed in Chapter 5; and the proof of the corollary, or the respective theorem, of Chapter 5.

³It is planned to publish slightly extended versions of the four chapters mentioned above as separate articles in different journals.

⁴A choice are, e.g., the following references: [Ott93, Pei92, Sch89, Lev89, Eck85, Dor95a, Dor77, Rei87, Hes92b, Hes92a].

2

Simple maps with fractal diffusion coefficients

Low-dimensional dynamical systems provide a good starting point to investigate fundamental problems of dynamical systems theory. Thus, there exists a large literature about such models, which includes various investigations about transport in simple low-dimensional maps. Certain groups have early been interested in the behaviour of deterministic diffusion coefficients by switching a single parameter value, especially Geisel et al. [Gei82, Gei84, Gei85], Grossmann et al. [Gro82, Fuj82, Gro83a], and Kapral et al. [Sch82]. However, in their articles usually a more statistical approach to compute parameter-dependent diffusion coefficients has been preferred. On the other hand, refined new methods of dynamical systems theory like cycle expansion [Cvi91a, Cvi91b, Art91, Art93, Art94] or other techniques [Cla93, Bre94, Vol94, Tel95] have been reported in recent literature, and they have been applied to the problem of transport in one and two dimensions. Moreover, for simple systems fundamental relations between dynamical systems quantities and transport coefficients have been discovered by Gaspard et al. [Gas90, Gas92a, Gas92d]. However, in case of all these new dynamical systems methods the problem about the parameter dependence of diffusion coefficients has not been appreciated in more detail.

The idea of this chapter is to bring these different lines of research together by applying new methods of dynamical systems theory to the problem of parameter-dependent diffusion coefficients in simple models. In Section 2.1, the term deterministic diffusion will be explained, and the dynamical system to be analyzed will be introduced in detail. In Section 2.2, some background about the approach to be employed here will be briefly discussed, and in Section 2.3, a method will be presented which enables for the first time the computation of diffusion coefficients for a broad range of parameter values. The results for these diffusion coefficients turn out to be surprisingly complex so that additional investigations, as performed in Section 2.4, are required as an attempt to understand the origin of this unexpected non-trivial diffusive behaviour.¹

¹A summary of this chapter has already been published as a letter, see Ref. [Kla95b].

2.1 A simple model for deterministic diffusion

2.1.1 What is deterministic diffusion?

In a first approach, one may think about diffusion as a simple *random walk* [Wax54, Wan66, vK92, Rei87, Tod92]. In Fig. 2.1, a one-dimensional model of such a random walk is sketched. One starts by choosing an initial position x_0 of a point particle on the real line, e.g., $x_0 = 0$, as is shown in the figure. The dynamics of the particle is then determined by fixing a probability density $\tilde{p}(s)$ such that

$$p(s) = \tilde{p}(s) ds \quad (2.1)$$

gives the transition probability $p(s)$ for the particle to travel from its old position x_0 over a distance $s = x_1 - x_0$ to its new position x_1 . The same procedure can be applied to any further changes in the position of the particle. For sake of simplicity, it is assumed that the probability density $\tilde{p}(s)$ is symmetric with respect to $s = 0$. The quantity of interest is here the *orbit* of the particle, which is represented by a collection of points $\{x_0, x_1, x_2, \dots, x_n\}$ on the real line. n refers to the discrete time, which is given by the number of iterations, or “jumps”, of the particle.

For performing a simple random walk, it is assumed that the probability density $\tilde{p}(s)$ is independent of the position x_n of the particle and of the discrete time n , i.e., it is fixed in time and space. In other words, there is *no history* in the dynamics of the particle, i.e., the single iteration steps are *statistically independent* from each other. This is called a *Markov process* in statistical physics [Wax54, vK92].

A random walk can be employed as a simple model for diffusion: One starts with an ensemble of particles at, e.g., $x_0 = 0$, and applies the iteration procedure introduced above to each of the particles. If one separates the real line into a number of subintervals of size Δx , the number n_p of particles in any such small interval after n iterations can be counted. Divided by the total number N_P of particles, these results determine the probability density $\rho_n(x)$, which is given schematically in Fig. 2.2 for a sufficiently large number of particles. This quantity can be interpreted as the probability to encounter one particle at a displacement x after n iterations.

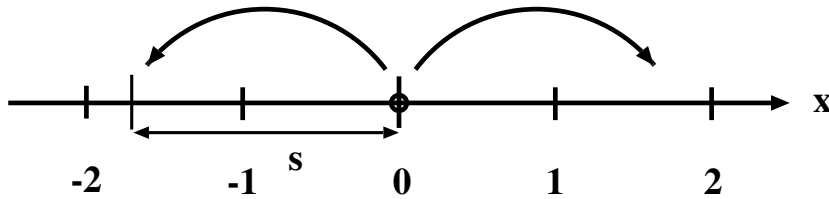


FIGURE 2.1. A simple one-dimensional random walk model, in contrast to deterministic dynamics.

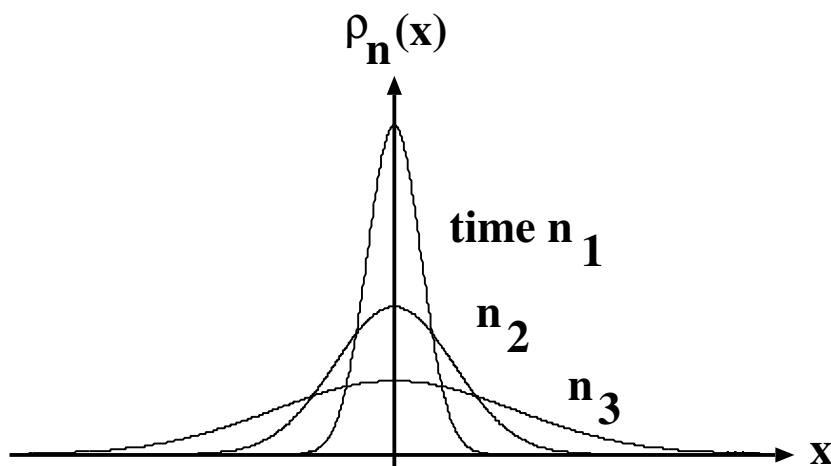


FIGURE 2.2. Probability densities for an ensemble of particles in the simple random walk model of Fig. 2.1 after certain numbers of iteration $n_1 < n_2 < n_3$ (see text).

The reader should note the fundamental difference between the two probability densities involved here: While $\tilde{\rho}(s)$ *defines* the model inherently, $\rho_n(x)$ is a dynamical quantity *produced* by the model. To put it in more physical terms, $\tilde{\rho}(s)$ determines the *microscopic* scattering rules the particles suffers at position x , whereas $\rho_n(x)$ provides information about the *macroscopic* distribution of an ensemble of particles, or of the position of one particle as a mean value, respectively.

The diffusion coefficient D can now be obtained by the second moment of the probability density $\rho_n(x)$ via

$$D = \lim_{n \rightarrow \infty} \frac{\langle x^2 \rangle}{2n} , \quad (2.2)$$

where

$$\langle \dots \rangle := \int dx \rho_n(x) \dots \quad (2.3)$$

represents the probability density average. If one has Gaussian probability densities as the ones shown in Fig. 2.2, the diffusion coefficient of Eq. (2.2) is well-defined. This is the case for a *stochastic* diffusion process as the one modeled above by a simple random walk.

In contrast to this traditional picture of diffusion as an uncorrelated random walk, the modern theory of dynamical systems enables to consider diffusion as a *deterministic dynamical process*: In a plot of time n versus position x , Fig. 2.3 shows

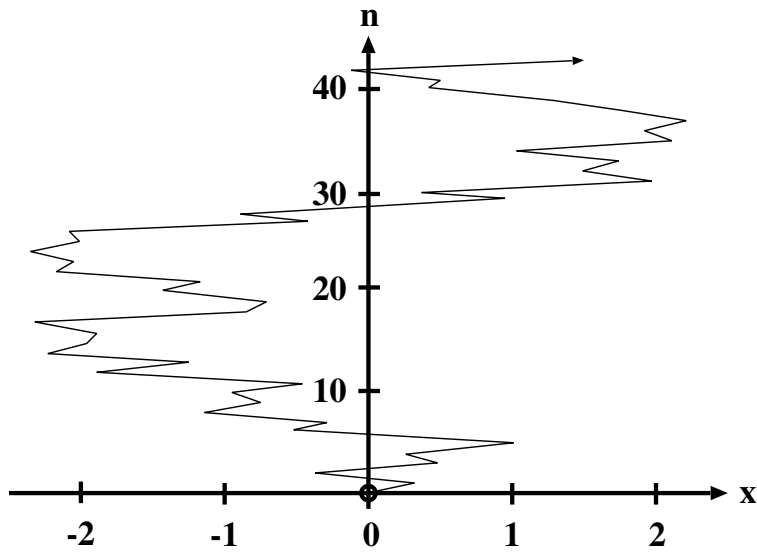


FIGURE 2.3. Sketch of the movement of a point particle in one dimension, generated by a deterministic dynamical system.

the orbit of a point particle with initial condition $x_0 = 0$, as it may be generated by a *chaotic dynamical system*

$$x_{n+1} = M(x_n) \quad . \quad (2.4)$$

$M(x)$ is here a one-dimensional map which prescribes how a particle gets mapped from position x_n to position x_{n+1} .² The map $M(x)$ plays now the role of the model-inherent probability density $\tilde{p}(s)$ of the previous random walk. By defining $M(x)$ and using Eq. (2.4), one obtains the full microscopic equations of motion of the system. Thus, the decisive new fact which distinguishes this dynamical process from the one of a simple random walk is that here the *complete history* of the particle is taken into account. This is emphasized in Fig. 2.3 by connecting the single points of the orbit of the moving particle by lines. If the resulting macroscopic process of an ensemble of particles, governed by a deterministic dynamical system like map $M(x)$, turns out to obey a law like Eq. (2.2), i.e., if a diffusion coefficient exists for the system,³ one denotes this process as *deterministic diffusion*.

²More details about such a map will be given in Section 2.1.3.

³This is not in advance clear, even in supposedly "simple" dynamical systems, see, e.g., Section 2.3.2.

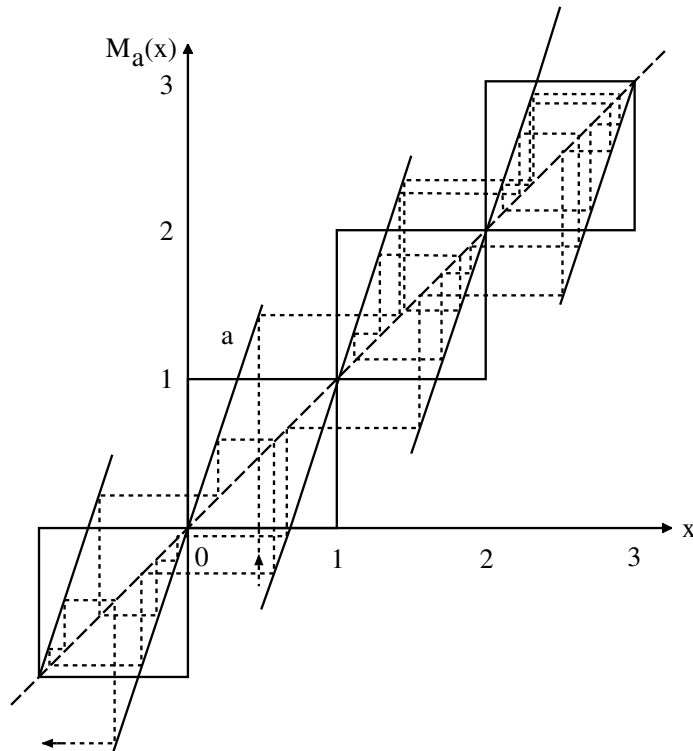


FIGURE 2.4. Illustration of a simple model for deterministic diffusion, see the dynamical system map \mathcal{L} , Eqs.(2.5) to (2.8), for the particular slope $a = 3$.

It may be remarked that, according to the picture of classical determinism, it seems more natural to start with the actual equations of motion of the particles for describing a diffusion process than to employ an approximation like a random walk, where any correlations in time and space have been neglected. However, as will be shown in this work, and as is shown in recent literature, this task is not that simple and has never been successfully performed in the general case of Newton's equations of motion so far.

2.1.2 Physical motivation of the deterministic model

Fig. 2.4 shows the model which shall be considered in this chapter. One can see part of a "chain of boxes", which continues periodically in both directions to in-

finity, and the trajectory⁴ of a moving point particle. The movement of the particle obeys the following rules: Choose any point on the x -axis as an initial condition. Draw a vertical line at this point. If this (dotted) line hits one of the inclined (full) lines which exceed the box boundaries, the particle gets scattered horizontally until it hits the (dashed) diagonal which goes straight through all the boxes, where the particle gets reflected again vertically. The number of times the particle is scattered by an inclined line will be called the number of iterations of the particle.⁵ One can play this game for any other initial condition, and one will obtain all kinds of different trajectories. Especially, one will observe that, after a certain number of iterations, the distance between the respective coordinate of the particle on the x -axis and its initial condition will vary drastically, even if one changes the initial condition only a little bit. Thus, one encounters a *sensitive dependence on initial conditions*. The diffusion coefficient in this model is determined by the square of the displacement of the particle in the x -direction, averaged over a large set of initial conditions and divided by two times the number of iterations in the limit of very large iteration numbers.⁶

Now, one can vary the “scattering rules” smoothly by stretching or squeezing the inclined lines such that they remain parallel, and that still any vertical line hits an inclined line at precisely one point. The question one might ask is how the diffusion coefficient in this model, which shall be assumed to exist as a working hypothesis, changes by varying the scattering rules this way.

It has been proposed to compare the dynamics in this chain of boxes to the process of *Brownian motion*:⁷ If a particle stays in a box for a few iterations, its *internal* box motion is supposed to be getting randomized and may resemble the microscopic fluctuations of a Brownian particle, whereas its *external* jumps between the boxes could be interpreted as sudden “kicks” the particle suffers by some strong collision. This suggests that “jumps between boxes” contribute most to the actual value of the diffusion coefficient.

⁴A trajectory is considered here as a continuous version of the orbit of the moving particle, although this distinction is quite arbitrary.

⁵Note that actually there is *no* independent movement of the particle in the y -direction, since the rules are that it just gets reflected at the diagonal, which “transfers” the y - to the x -coordinate. Thus, the movement of the particle is essentially one-dimensional.

⁶Under certain quite general conditions, this expression for the diffusion coefficient is identical to the one given previously by Eq. (2.2); it is called the *Einstein formula of diffusion*, since it was first derived by A. Einstein in Ref. [Ein05] at the beginning of this century (see also Refs. [Sta89, vK92, Wax54]).

⁷The irregular movement of a microscopic particle suspended in a liquid is called *Brownian motion* after the botanist R. Brown, who has first studied this process in detail experimentally around 1828. For a survey about the history of Brownian motion see, e.g., Ref. [Bru76, Sta89]; for a brief introduction into basic concepts see, e.g., Ref. [Wan66]; for fundamental physical and mathematical aspects of Brownian motion, see, e.g., Refs. [Wax54, vK92]; see also Ref. [Man82].

Such a picture may be helpful to get a physical intuition about diffusion in this model. One should note that the strength of diffusion, and therefore the magnitude of the diffusion coefficient, are related to the probability of the particle to *escape* out of a box, i.e., to perform a jump into another box. This escape probability, however, as well as the mean distance a particle travels by performing such a jump, varies with varying the scattering rules. The reader is invited to make an intuitive guess at this point about how the diffusion coefficient changes with varying the scattering rules of the system.

As has been mentioned in the introductory Chapter 1, and as has been briefly discussed in terms of a random walk in the previous section, Brownian motion is usually described in statistical physics by introducing some stochasticity into the equations which model a diffusion process. The main advantage of the simple model discussed here is that diffusion can be treated by taking the full dynamics of the system into account, i.e., the *complete trajectory* of the moving particle is considered, without any additional approximations. To distinguish this kind of diffusion from stochastic approaches, it is called *deterministic diffusion*. In this case, the trajectory of the particle is fixed by determining its initial condition.⁸ To the knowledge of the author, models of chains of one-dimensional maps have, with respect to diffusion, first been discussed extensively in 1982 by Fujisaka and Grossmann [Gro82, Fuj82], who also employed the analogy of Brownian motion, by Geisel and Nierwetberg [Gei82], and by Schell, Fraser, and Kapral [Sch82].

2.1.3 Formal definition of the deterministic model

Let

$$M_a : R \rightarrow R, \quad x_n \mapsto M_a(x_n) = x_{n+1}, \quad a > 0, \quad x_n \in R, \quad n \in N_0 \quad (2.5)$$

be a map modelling the chain of boxes introduced above, i.e., a *periodic continuation* of *discrete one-dimensional piecewise linear*⁹ *expanding*¹⁰ *maps* with *uniform slope*. The index a holds for the control parameter, which is the absolute value of the slope of the map, x_n stands for the position of a point particle, and n labels the discrete time. Since the map is expanding, its Lyapunov exponent can straightforward be calculated to $\ln a$, and thus $M_a(x)$ is chaotic. Note that the expanding condition, together with the map being piecewise linear, ensures

⁸For more details see the previous section.

⁹The term *piecewise linear* should be understood in the sense that the interval of the map which is periodically continued consists of a finite number of subintervals, on the interiors of which the map is linear.

¹⁰A one-dimensional map $M_a(x)$ is *expanding* if $|dM_a(x)/dx| > 1$ for all x in the intervals of differentiability, see Ref. [Bec93]. For a more rigorous mathematical notion see Ref. [dM93].

the existence of certain points of discontinuity and/or non-differentiability. These points reflect the chaoticity of $M_a(x)$ despite its property of being piecewise linear. The expanding condition also ensures that $M_a(x)$ is hyperbolic.¹¹

The term “chain” in the characterization of $M_a(x)$ can be made mathematically more precise as a *lift of degree one* [Mis89, Als89b, Kat95],

$$M_a(x+1) = M_a(x) + 1 \quad , \quad (2.6)$$

for which the acronym *old* has been introduced.¹² In physical terms, this means that $M_a(x)$ is to a certain extent translational invariant.

Being *old*, the full map $M_a(x)$ is generated by the map of one box, e.g., on the unit interval $0 < x \leq 1$, which will be referred to as the *box map*. It shall be assumed that the graph of this box map is central symmetric with respect to the center of the box at $(x,y) = (1/2, 1/2)$. This induces that the graph of the full map $M_a(x)$ is anti-symmetric with respect to $x = 0$,

$$M_a(x) = -M_a(-x) \quad , \quad (2.7)$$

so that there is no “drift” in the chain of boxes.

For convenience, the class of maps defined by Eqs. (2.5), (2.6), and (2.7) shall be denoted as *class \mathcal{P}* , and maps which fulfill the requirements of class \mathcal{P} shall be referred to as *class \mathcal{P} -maps*.

In Fig. 2.4, which contains a section of a simple class \mathcal{P} -map, the box map has been chosen to

$$M_a(x) = \left\{ \begin{array}{ll} ax & , \quad 0 < x \leq \frac{1}{2} \\ ax + 1 - a & , \quad \frac{1}{2} < x \leq 1 \end{array} \right\} \quad , \quad a \geq 2 \quad , \quad (2.8)$$

cf. Refs, [Gro82, Gas92d, Ott93]. This example can be best classified as a *Lorenz map with escape*.¹³ The chaotic dynamics of these maps is generated by a “stretch-split-merge”-mechanism for a density of points on the real line [Pei92]. As a class

¹¹For one-dimensional maps, the hyperbolicity immediately follows from the expanding condition, see Ref. [Bec93]. Definitions of hyperbolicity are also given in Ref. [Bec93], for a more rigorous mathematical notion in case of one-dimensional dynamical systems see Ref. [dM93]. The basic idea of hyperbolicity stems from higher-dimensional dynamical systems, see Refs. [Eck85, Guc90, Bow75, Lev89, Ott93].

¹²This abbreviation was apparently created by Misiurewicz, changing the order of the first characters in the main words (see Ref. [Mis89] and references therein); Refs. [Als89b, Als93] provide some remarks about the analysis of *old* maps in the mathematical literature, as well as some examples.

¹³One-dimensional Lorenz maps have in fact been introduced as suitable Poincaré surfaces of section of the Lorenz attractor [Guc90, Pei92]. The idea of this reduction is due to Lorenz, although originally he obtained a different one-dimensional map [Guc90, Pei92, Ott93].

A rigorous definition of Lorenz maps can be found in Refs, [Gle93, Hub90], or, more specialized, in Ref. [Als89a], respectively. The main difference between these Lorenz maps and the map defined in

\mathcal{P} -map, Eq.(2.8), together with Eqs.(2.5), (2.6), and (2.7), will be referred to as map \mathcal{L} . Other class \mathcal{P} -maps have been considered in Refs. [Gro82, Fuj82, Gro83b, Tho83, Art91, Gas92d], another example will be discussed in Chapter 4.

More precisely than stated in Section 2.1.2, the problem of this chapter can be formulated as to develop a method for computing parameter-dependent diffusion coefficients $D(a)$ for class \mathcal{P} -maps, as far as they exist. In this and most of the following chapters, map \mathcal{L} will serve as an example. However, it is believed that the methods to be presented here will work as well for any other class \mathcal{P} -map, supposedly with similar results.

2.2 First passage method

The methodology of first passage has been developed in the framework of statistical physics (see, e.g., Refs. [Wax54, vK92] and further references therein). It deals with the calculation of decay- or escape rates for ensembles of statistical systems with certain boundary conditions. In recent work, these methods have very successfully been applied to the theory of dynamical systems [Gas90, Gas92a, Gas92d, Gas93, Dor95b, Gas95].¹⁴

Following the presentations in Refs. [Gas90, Gas92a, Gas92d], the principles of first passage will be outlined for the “class \mathcal{P} ” of dynamical systems defined above. The method will turn out to provide a convenient starting point for computing parameter-dependent diffusion coefficients.

One may distinguish three different steps in applying the method:

Step 1: Solve the one-dimensional *diffusion equation*

$$\frac{\partial n}{\partial t} = D \frac{\partial^2 n}{\partial x^2} \quad (2.9)$$

with suitable boundary conditions, where $n := n(x, t)$ stands for the macroscopic density of particles at a point x at time t . This equation serves here as a *definition* for the diffusion coefficient D .

Eq.(2.8) is that they originally do not include *escape*, i.e., they map strictly from an interval onto itself, whereas the map here provides an escape from the (unit) interval to other intervals of the chain.

It should be noted that the motivation of choosing such a map here has nothing to do with the Lorenz attractor (in fact, it is due to Prof. Dorfman’s reading of Refs. [Ott93, Gas92d]). However, for the specialist this remark might serve as a hint how to classify the box map under consideration with respect to its detailed mathematical properties.

¹⁴See Ref. [Gas92d] for a brief overview.

Step 2: Solve the *Frobenius-Perron equation*¹⁵

$$\rho_{n+1}(x) = \int dy \rho_n(y) \delta(x - M_a(y)) \quad , \quad (2.10)$$

which represents the continuity equation for the probability density $\rho_n(x)$ of the dynamical system $M_a(y)$ [Ott93, Las94].

Step 3: Now, for a chain of boxes of chainlength L , consider the limit chainlength L and time n to infinity: *If* for given slope a the first few largest eigenmodes of n and ρ turn out to be identical in an appropriate scaling limit, *then* $D(a)$ can be computed by matching the eigenmodes of the probability density ρ to the particle density n : For *periodic boundary conditions*, i.e.,

$$n(0,t) = n(L,t) \quad \text{and} \quad \rho_n(0) = \rho_n(L) \quad , \quad (2.11)$$

one obtains

$$D(a) = \lim_{L \rightarrow \infty} \left(\frac{L}{2\pi} \right)^2 \gamma_{dec}(a) \quad , \quad (2.12)$$

where $\gamma_{dec}(a)$ is the decay rate in the closed system to be calculated directly from the Frobenius-Perron equation and therefore determined by quantities of the deterministic dynamical system.

For *absorbing boundary conditions*, i.e.,

$$n(0,t) = n(L,t) = 0 \quad \text{and} \quad \rho_n(0) = \rho_n(L) = 0 \quad , \quad (2.13)$$

the same procedure leads to

$$D(a) = \lim_{L \rightarrow \infty} \left(\frac{L}{\pi} \right)^2 \gamma_{esc}(a) \quad , \quad (2.14)$$

where $\gamma_{esc}(a)$ is the escape rate for the open system. This quantity can be further determined by the escape rate formalism (see Ref. [Eck85, Dor95a] and references therein) to

$$\gamma_{esc}(a) = \lambda(\mathcal{R}; a) - h_{KS}(\mathcal{R}; a) \quad , \quad (2.15)$$

where the Lyapunov exponent $\lambda(\mathcal{R}; a)$ and the Kolmogorov-Sinai (KS) entropy $h_{KS}(\mathcal{R}; a)$ have to be defined on the repeller \mathcal{R} of the dynamical system.¹⁶ This

¹⁵For sake of simplicity, here and in the following the parameter index a for the slope as a has been avoided for the probability density. It will be introduced if it is needed explicitly, see Chapter 5.

¹⁶The notations *metric* [Lev89, Ott93] and *measure-theoretic* entropy [Eck85] are synonymous to KS entropy.

equation can be considered as an extension of Pesin's formula to open systems.¹⁷ Eqs.(2.12) and (2.14) have been applied to a variety of models, like the periodic Lorentz gas, two-dimensional chains of baker transformations and certain one-dimensional chains of maps, by Gaspard and coworkers [Gas92a, Gas92d]. They provide suitable starting points for detailed analytical and numerical calculations, as will be explained further in the following section.

Eq.(2.14), together with Eq.(2.15), has first been presented for the two-dimensional periodic Lorentz gas by Gaspard and Nicolis [Gas90]. Further generalizations of this formula to other transport coefficients and dynamical systems have been worked out recently [Dor95b, Gas95]. However, although of fundamental physical importance, it seems in general to be difficult to use this equation for practical evaluations of $D(a)$, because usually the KS entropy is hard to calculate [Ott93]. Instead, Eq.(2.14) with Eq.(2.15) can be inverted to get the KS entropy via the decay rate of the dynamical system of Eq.(2.12) to

$$h_{KS}(\mathcal{R}; a) = \lambda(\mathcal{R}; a) - \frac{1}{4}\gamma_{dec}(a) \quad (L \rightarrow \infty) \quad . \quad (2.16)$$

Apart from the results mentioned above, another fundamental relation, which expresses transport coefficients in terms of Lyapunov exponents, has been obtained for a different type of model in the framework of molecular dynamics computer simulations [Pos88, Pos89, Eva90a, Bar93a, Coh95]. In the spirit of this approach [Mor87], it has recently been possible to obtain Ohm's law for a periodic Lorentz gas with external field, starting from the microscopic dynamics of the system [Che93a, Che93b]. The precise relation between these two approaches, and their resulting different formulas, respectively, is an open question and a matter of active recent research.¹⁸

2.3 Solution of the Frobenius-Perron equation

Following the first passage method, the problem of computing parameter-dependent diffusion coefficients essentially reduces to solving the Frobenius-Perron equation for the dynamical system in a certain limit.

In this section, a method will be presented by which this goal can be achieved. Its principles will be illustrated by some simple examples. It should be mentioned that the basic idea of this method is again due to the work of Gaspard [Gas92a]. However, technical refinements, a critical discussion of the limits of the method,

¹⁷One obtains Pesin's formula from Eq.(2.15) for $\gamma_{esc} = 0$, i.e., it establishes the relation between Lyapunov exponents and KS entropy for closed systems [Gas90].

¹⁸For introductions see Refs. [Dor95a, Hoo91, Eva90b].

previous section.

Step 1: The one-dimensional diffusion equation Eq.(2.9) can be solved with periodic boundary conditions straightforward to

$$n(x,t) = a_0 + \sum_{m=1}^{\infty} \exp\left(-\left(\frac{2\pi m}{L}\right)^2 Dt\right) \left(a_m \cos\left(\frac{2\pi m}{L}x\right) + b_m \sin\left(\frac{2\pi m}{L}x\right) \right) , \quad (2.17)$$

where a_0 , a_m and b_m are Fourier coefficients to be determined by an initial particle density $n(x,0)$.

Step 2: To solve the Frobenius-Perron equation, the key idea is to write this equation as a matrix equation [Gas92a, Bec93]. For this purpose, one needs to find a suitable *partition* of the map, i.e., a decomposition of the real line into a set of subintervals, called *elements*, or *parts* of the partition. The single parts of the partition have to be such that they do not overlap except at boundary points, which are referred to as *points of the partition*, and that they cover the real line completely [Bec93]. In case of slope $a = 4$, such a partition is naturally provided by the box boundaries. The grid of dashed lines in Fig. 2.5 represents a two-dimensional image of the one-dimensional partition introduced above, which is generated by the application of the map.

Now, an initial density of points shall be considered which covers, e.g., the interval in the second box of Fig. 2.5 uniformly. By applying the map, one observes that points of this interval get mapped two-fold on the interval in the second box again, but that there is also escape from this box which covers the third and the first box intervals, respectively. Since map \mathcal{L} is *old*, this mechanism applies to any box of the chain of chainlength L , modified only by the boundary conditions. Taking into account the stretching of the density by the slope a at each iteration, this leads to a matrix equation of

$$\rho_{n+1} = \frac{1}{a} T(a) \rho_n , \quad (2.18)$$

where for $a = 4$ the $L \times L$ -transition matrix $T(4)$ can be constructed to

$$T(4) = \begin{pmatrix} 2 & 1 & 0 & 0 & \dots & 0 & 0 & 1 \\ 1 & 2 & 1 & 0 & 0 & \dots & 0 & 0 \\ 0 & 1 & 2 & 1 & 0 & 0 & \dots & 0 \\ \vdots & & & \vdots & \vdots & & & \vdots \\ 0 & \dots & 0 & 0 & 1 & 2 & 1 & 0 \\ 0 & 0 & \dots & 0 & 0 & 1 & 2 & 1 \\ 1 & 0 & 0 & \dots & 0 & 0 & 2 & 1 \end{pmatrix} . \quad (2.19)$$

The matrix elements in the upper right and lower left edges are due to periodic boundary conditions and reflect the motion of points from the L th box of the chain

to the first one and *vice versa*.

In Eq.(2.18), the transition matrix $T(a)$ is applied to a column vector ρ_n of the probability density $\rho_n(x)$ which, in case of $a = 4$, can be written as

$$\rho_n \equiv |\rho_n(x)\rangle := (\rho_n^1, \rho_n^2, \dots, \rho_n^k, \dots, \rho_n^L)^* \quad , \quad (2.20)$$

where “*” denotes the transpose, and ρ_n^k represents the component of the probability density in the k th box, $\rho_n(x) = \rho_n^k$, $k - 1 < x \leq k$, $k = 1, \dots, L$, ρ_n^k being constant on each part of the partition.

In case of $a = 4$, the transition matrix is symmetric and can be diagonalized by spectral decomposition. Solving the eigenvalue problem

$$T(4) |\phi_m(x)\rangle = \chi_m(4) |\phi_m(x)\rangle \quad , \quad (2.21)$$

where $\chi_m(4)$ and $|\phi_m(x)\rangle$ are the eigenvalues and eigenvectors of $T(4)$, respectively, one obtains

$$\begin{aligned} |\rho_n(x)\rangle &= \frac{1}{4} \sum_{m=0}^{L-1} \chi_m(4) |\phi_m(x)\rangle \langle \phi_m(x) | \rho_n(x)\rangle \\ &= \sum_{m=0}^{L-1} \exp\left(-n \ln \frac{4}{\chi_m(4)}\right) |\phi_m(x)\rangle \langle \phi_m(x) | \rho_0(x)\rangle \quad , (2.22) \end{aligned}$$

where $|\rho_0(x)\rangle$ is an initial probability density vector and $\ln 4$ gives the Lyapunov exponent of the map. Note that the choice of initial probability densities is restricted by this method to functions which can be written in the vector form of Eq.(2.20).

For matrices of the type of $T(4)$, it is well-known how to solve their eigenvalue problems [Ber52, Kow54, Dav79]. For slope $a = 4$, one gets

$$\begin{aligned} \chi_m(4) &= 2 + 2 \cos \theta_m \quad , \quad \theta_m := \frac{2\pi}{L} m \quad , \quad m = 0, \dots, L-1 \quad ; \\ |\phi_m(x)\rangle &= (\phi_m^1, \phi_m^2, \dots, \phi_m^k, \dots, \phi_m^L)^* \quad , \quad \phi_m^k = \tilde{a}_m \phi_{m,1}^k + \tilde{b}_m \phi_{m,2}^k \quad , \\ \phi_{m,1}^k &:= \cos \theta_m (k-1) \quad , \quad \phi_{m,2}^k := \sin \theta_m (k-1) \quad , \\ &k = 1, \dots, L \quad , \quad k-1 < x \leq k \quad (2.23) \end{aligned}$$

with \tilde{a}_m and \tilde{b}_m to be fixed by suitable normalization conditions.²⁰

Step 3: To compute the diffusion coefficient $D(4)$, it remains to match the first few

²⁰In case of $a = 4$, Eq.(2.22), supplemented by Eq.(2.23), represents the complete solution of the Frobenius-Perron equation; see Chapter 3 for the time-dependent behaviour of probability densities and the dynamics of diffusion.

largest eigenmodes of the diffusion equation to the ones of the Frobenius-Perron equation: In the limit time t and system size L to infinity, the particle density $n(x, t)$, Eq.(2.17), of the diffusion equation reduces to

$$n(x, t) \simeq \text{const.} + \exp\left(-\left(\frac{2\pi}{L}\right)^2 Dt\right) \left(A \cos\left(\frac{2\pi}{L}x\right) + B \sin\left(\frac{2\pi}{L}x\right)\right) \quad , \quad (2.24)$$

where the constant represents the uniform equilibrium density of the equation.

Analogously, for discrete time n and chainlength L to infinity, one obtains for the probability density $\rho_n(x)$ of the Frobenius-Perron equation, Eq.(2.22) with Eq.(2.23),

$$\rho_n(x) \simeq \text{const.} + \exp(-\gamma_{dec}(4)n) \left(\tilde{A} \cos\left(\frac{2\pi}{L}(k-1)\right) + \tilde{B} \sin\left(\frac{2\pi}{L}(k-1)\right)\right) \quad , \\ k = 1, \dots, L \quad , \quad k-1 < x \leq k \quad (2.25)$$

with a decay rate of

$$\gamma_{dec}(4) = \ln \frac{4}{2 + 2 \cos \frac{2\pi}{L}} \quad (2.26)$$

of the dynamical system, determined by the second largest eigenvalue of the matrix $T(4)$, see Eq.(2.23). Note that the largest eigenvalue is equal to the slope of the map so that for the first term in Eq.(2.25) the exponential vanishes, and one obtains a uniform equilibrium density.

Apart from generic discretization effects in the time and position variables, which may be neglected in the limit of time to infinity and after a suitable spatial coarse graining, the eigenmodes of Eqs.(2.24) and (2.25) match precisely so that, according to Eq.(2.12), the diffusion coefficient $D(4)$ can be computed to

$$D(4) = \left(\frac{L}{2\pi}\right)^2 \gamma_{dec}(4) = \frac{1}{4} + O(L^{-4}) \quad . \quad (2.27)$$

This result is identical to what is obtained from a simple random walk model (see Section 4.2 or Ref. [Sch82]), which does not take the full deterministic dynamics of the system into account.

The procedure can be generalized straightforward to all even integers values of the slope and leads to a parameter-dependent diffusion coefficient of

$$D(a) = \frac{1}{24}(a-1)(a-2) \quad , \quad a = 2k \quad , \quad k \in N \quad , \quad (2.28)$$

in agreement with results of Fujisaka and Grossmann [Fuj82].

Although this method seems to work perfectly, first subtleties appear for odd integer values of the slope. They shall be illustrated by the example of slope $a = 3$,

see, e.g., Fig. 2.4.

Analogously to the previous example, for $a = 3$ a simple partition can be constructed, the parts of which are all of length $1/2$. According to this partition, a transition matrix $T(3)$ can be determined, given schematically by

$$T(3) = \begin{pmatrix} 1 & 1 & 0 & 0 & \cdots & 0 & 0 & 1 & 0 \\ 1 & 1 & 0 & 1 & 0 & 0 & \cdots & 0 & 0 \\ 1 & 0 & 1 & 1 & 0 & 0 & \cdots & 0 & 0 \\ 0 & 0 & 1 & 1 & 0 & 1 & 0 & 0 & \cdots \\ 0 & 0 & 1 & 0 & 1 & 1 & 0 & 0 & \cdots \\ \vdots & & & & \vdots & & & & \vdots \\ 0 & 1 & 0 & 0 & \cdots & 0 & 0 & 1 & 1 \end{pmatrix}. \quad (2.29)$$

Note that, in contrast to the case $a = 4$, here the matrix is formed by single *blocks* which move periodically to the right. Since the partition of $a = 3$ is slightly more complicated than for $a = 4$, the blocks refer to the partition in each box, whereas the shift again is related to the lift property of the *old* map.

Now, one observes that the matrix $T(3)$ is not symmetric. However, the eigenvalue problem of this matrix can still be solved analogously to the case $a = 4$. The spectrum of the matrix turns out to be highly degenerate, and therefore $T(3)$ cannot be diagonalized anymore [Zur84].²¹ Since the probability density of the Frobenius-Perron equation is determined by iteration of transition matrices, cf. Eq. (2.18), for slope $a = 3$ it is not in advance clear how the single eigenmodes “mix” in the limit time and chainlength to infinity and whether they can be matched to the solutions of the diffusion equation as before so that the diffusion coefficient $D(3)$ is again simply determined by the second largest eigenvalue of the matrix.

One might first approach this problem pragmatically. Analogously to the analytical solutions of Eqs. (2.24) and (2.25) for slope $a = 4$, Fig. 2.6 shows a plot of the two second largest eigenmodes of $T(3)$ in comparison to the solution of the diffusion equation. Again, one observes total agreement, except differences in the fine structure. The same is true for the other first few largest eigenmodes of $T(3)$. Thus, although straightforward diagonalization and, therefore, a simple solution of the Frobenius-Perron equation like Eq. (2.22) are not possible anymore, it looks as if the largest eigenmodes of $T(3)$ behave “nicely” so that it is suggestive to compute the diffusion coefficient $D(3)$ via the second largest eigenvalue of

²¹The matrix $T(3)$ is called *non-normal*, i.e., $T(3)T^*(3) \neq T^*(3)T(3)$, which means that it does *not* provide a system of orthogonal eigenvectors. Non-normal matrices have recently achieved much attention in other branches of dynamical systems theory as well [Gro95b].

Of course still a transformation onto Jordan normal form to “block-diagonalize” this matrix could be applied. However, this is of no use for straightforward analytical calculations, but rather for rigorous mathematical proofs of certain theorems; see Conjecture 2.2, Footnote 40, and Theorem 5.1.

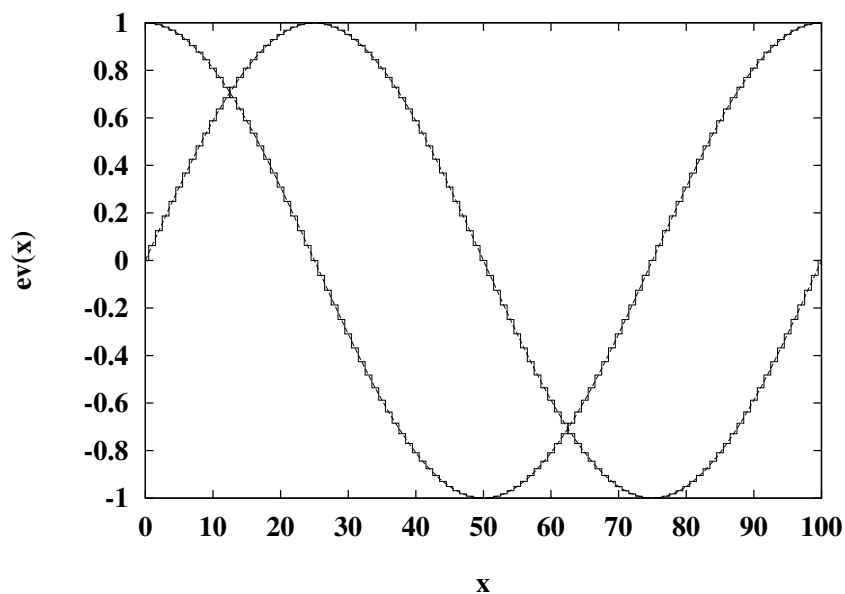


FIGURE 2.6. Second largest eigenmodes for map \mathcal{L} , chainlength $L = 100$, for slope $a = 3$ with periodic boundary conditions and comparison to the solutions of the diffusion equation Eq.(2.9).

$T(3)$ again. With

$$\gamma(3) = \ln \frac{3}{1 + 2 \cos(2\pi/L)} \quad , \quad (2.30)$$

and Eq.(2.12), one gets

$$D(3) = \frac{1}{3} + O(L^{-4}) \quad . \quad (2.31)$$

As for $a = 4$, this result is obtained as well from a simple random walk model. However, to produce this value, the respective random walk has to be defined in a slightly different way than for $a = 4$ (see the corresponding remark in Section 4.2).

Analogously to the case of even integer slopes, the exact calculations can be generalized to all odd integer values of the slope and lead to

$$D(a) = \frac{1}{24}(a^2 - 1) \quad , \quad a = 2k - 1 \quad , \quad k \in \mathbb{N} \quad , \quad (2.32)$$

which again is identical to the result of Fujisaka and Grossmann [Fuj82].

One might conclude that the method still works, even if its mathematical details

are not clear at this stage. As an explanation, it is tempting to assume that in simple dynamical systems as class \mathcal{P} -maps “nothing can go wrong” and that they are always diffusive in a simple manner. However, it should be noted that so far no proof has been given in the literature for the existence of diffusion coefficients in class \mathcal{P} -maps for general values of the slope. In fact, dealing with a proper foundation of the transition matrix method turns out to be intimately connected to proving the existence of diffusion coefficients in this class of dynamical systems. A preliminary answer to this question will be given in the next section after setting up a more general framework.

It remains to deal with three other questions raised by the calculations above: A special feature of the diffusion coefficient results for integer slopes shall be pointed out; further limits of this method with respect to generalized diffusion coefficients shall be critically discussed; and at last the application of the method to absorbing boundary conditions shall be briefly outlined.

1. diffusion coefficients for integer slopes: Eqs. (2.27) and (2.31) show already that $D(4) < D(3)$, which might at first sight be counterintuitive. By evaluating the general formulas of $D(a)$ given by Eqs. (2.28) and (2.32) at other even and odd integer slopes, one realizes that this inequality reflects a general oscillatory behaviour of $D(a)$ at integer slopes,²² as it has similarly been observed for deterministic diffusion in certain classes of two-dimensional maps [Rec80, Rec81, Dan89b, Dan89a]. This behaviour cannot be understood completely by one consistent random walk model, as will be explained in more detail in Section 4.2.

2. matching lower eigenmodes: One encounters serious problems if one wants to extend the matching eigenmodes procedure to arbitrary low eigenmodes, even in case of $a = 4$, where the matrix is diagonalizable. With Eq.(2.23), one can check that

$$\phi_{m,1}^k = \phi_{L-m,1}^k, \quad \phi_{m,2}^k = -\phi_{L-m,2}^k; \quad k = 1, \dots, L, \quad m = 1, \dots, L-1, \quad (2.33)$$

i.e., in contrast to the m eigenmodes of the diffusion equation Eq.(2.9), the frequency of the eigenmodes of $T(4)$ does not increase monotonically with m , but gets “turned over” at the $(L/2)$ th (for L even) eigenmode such that the first and the last half of the number of eigenmodes are identical, except a minus sign. This is due to the discretization of the position variable x in the diffusion equation to k in the Frobenius-Perron *matrix* equation Eq.(2.18), which was one of the basic ingredients for the possibility to construct transition matrices.

Moreover, one should note that, according to Eq.(2.23), the smallest eigenvalue of $T(4)$ is equal to zero. For $T(3)$, a large number of eigenvalues is even less

²²As mentioned before, this result has already been obtained by Fujisaka and Grossmann [Fuj82], although it has not been discussed in further detail by these authors.

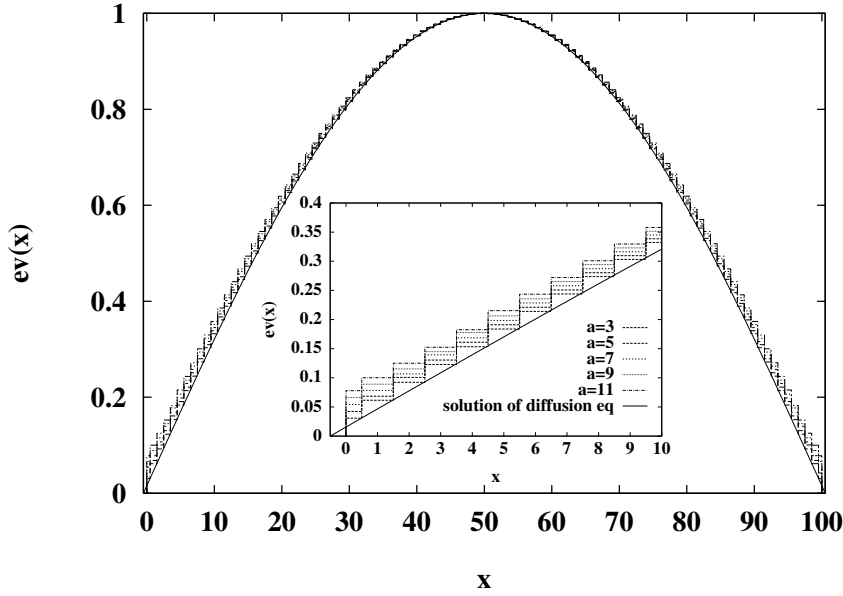


FIGURE 2.7. Largest eigenmodes of map \mathcal{L} for odd integer values of the slope a with absorbing boundary conditions, and comparison to the solution of the diffusion equation Eq.(2.9).

than zero. Thus, except for the first few largest eigenmodes, which still match reasonably well to the eigenmodes of the diffusion equation in the limit time n and chainlength L to infinity, one cannot expect the method to work simply that the components of a “time-dependent” diffusion coefficient $D_n(a)$ are determined by smaller eigenvalues of the transition matrices in straight analogy to Eq.(2.12). This could be taken as a hint that, to obtain more details of the dynamics, refined methods are needed. For example, in Ref. [Gas92b] the first orders of a position-dependent diffusion coefficient have been determined for a class \mathcal{P} -map according to a procedure which avoids the discretization of the real line.

3. absorbing and periodic boundary conditions: The same procedure as outlined for periodic boundary conditions can also be employed for absorbing boundaries. It shall be sketched briefly, according to the three steps distinguished before:

Step 1: The one-dimensional diffusion equation with absorbing boundary conditions can be solved to

$$n(x,t) = \sum_{m=1}^{\infty} a_m \exp\left(-\left(\frac{\pi m}{L}\right)^2 Dt\right) \sin\left(\frac{\pi m}{L}x\right) \quad (2.34)$$

with a_m denoting again the Fourier coefficients.

Step 2: The transition matrices for $a = 4$ and $a = 3$ at these boundary conditions are identical to the ones of Eqs.(2.19),(2.29), except that the matrices now contain plain zeros as matrix elements in the upper right and lower left corners. However, due to this slight change in their basic structure there is no general method to solve the eigenvalue problems for this type of matrices anymore, in contrast to the case of periodic boundary conditions.

At least for $a = 3$ and $a = 4$, it is still possible to obtain analytical solutions by straightforward calculations analogously to the ones performed in Ref. [Gas92a], but for any higher integer value of the slope even these basic methods fail. This appears to be caused by strong boundary layers. Fig. 2.7 shows numerical solutions²³ for the largest eigenmodes of the first odd integer slope transition matrices in comparison to the solutions of the diffusion equation Eq.(2.9). It can be seen that next to the boundaries, there are pronounced deviations between the Frobenius-Perron and the diffusion equation solutions. These deviations are getting smaller in the interior region of the chain, but are gradually getting stronger with increasing the value of the slope, as is shown in the magnification. The same behaviour can be found for even integer slopes, although the quantitative deviation of these eigenmodes to the ones of the diffusion equation solutions is slightly less than for odd values of the slope. Thus, obviously absorbing boundary conditions disturb the deterministic dynamics significantly, whereas similar effects do not occur for periodic boundary conditions, which therefore could be characterized as a kind of “natural boundary conditions” for this periodic dynamical system.

Step 3: The different boundary conditions do not only show up in the eigenmodes of the transition matrices, but also in the calculation of the diffusion coefficients. In analogy to periodic boundary conditions, the escape rate of the dynamical system at $a = 3$ and $a = 4$ is determined to

$$\gamma_{esc}(a) = \ln \frac{a}{\chi_{max}(a)} \quad (2.35)$$

with $\chi_{max}(a)$ being the largest eigenvalue of the transition matrix,

$$\chi_{max}(3) = 1 + 2 \cos \frac{\pi}{L+2} \quad \text{and} \quad \chi_{max}(4) = 2 + 2 \cos \frac{\pi}{L+1} \quad . \quad (2.36)$$

Feeding this into Eq.(2.14) via matching eigenmodes, one obtains

$$\begin{aligned} D(3) &\simeq \frac{1}{3} \frac{L^2}{(L+2)^2} + O(L^{-4}) \rightarrow \frac{1}{3} \quad (L \rightarrow \infty) \quad , \\ D(4) &\simeq \frac{1}{4} \frac{L^2}{(L+1)^2} + O(L^{-4}) \rightarrow \frac{1}{4} \quad (L \rightarrow \infty) \quad , \end{aligned} \quad (2.37)$$

²³Details of the numerics applied here will be given in Section 2.3.2.

which gives a convergence of the diffusion coefficient with the chainlength L significantly below that to be obtained by periodic boundary conditions. For example, for a chainlength of $L = 100$ the convergence is about two orders of magnitude worse.

It can be concluded that the transition matrix method works in principle for absorbing boundary conditions as well, but that here its range of application to compute diffusion coefficients is qualitatively and quantitatively more restricted because of long-range boundary layers.

2.3.2 Markov partitions

In the previous section, the choice of simple partitions enabled the construction of transition matrices. These matrices provided a way to solve the Frobenius-Perron equation in a certain limit. However, so far this method has only been applied to very special cases of map \mathcal{L} , defined by integer slopes. This raises the question whether an extension of this method to other values of the slope is possible.

For this purpose, the idea of choosing a suitable partition of the map has to be generalized. Taking a look at Fig. 2.5 again, one observes that the graph of the map “crosses” or “touches” a vertical line of the grid, which represents, as explained before, a two-dimensional image of the partition, only at some grid points. Furthermore, the local extrema of the map, which are here identical to the points of discontinuity, are situated on, or just “touch” horizontal lines of the grid, whereas other crossovers of horizontal lines occur at no specific point. The same characteristics can be verified, e.g., for the respective partition of slope $a = 3$. These conditions ensure that it is possible to obtain a correct transition matrix from a partition, since to be modeled by a matrix, a density of points, which covers parts of the partition completely, has to get mapped in a way that its image again covers parts of the partition completely, and not partially.

This basic property of a “suitable partition to construct transition matrices” is already the essence of what is known as a *Markov partition*:

Definition 2.1 (Markov partition, verbal definition) *For one-dimensional maps, a partition is a Markov partition if and only if parts of the partition get mapped again onto parts of the partition, or unions of parts of the partition [Bec93].*

A more formal definition of one-dimensional Markov partitions, as well as further details, can be found in Refs. [Rue89, dM93, Bow79].²⁴

²⁴Again, the notion of one-dimensional Markov partitions is a reduced form of a more general definition for higher-dimensional dynamical systems, see, e.g., Refs. [Guc90, Kat95, Bow75, Sin68, Sin68, Cor82, Sin89, Rue78]. One-dimensional maps which possess Markov partitions are often re-

Now, the next goal must be to find a general rule how to construct Markov partitions for map \mathcal{L} at other, non-trivial parameter values of the slope. Because of the periodicity of the chain of maps it suffices to find a Markov partition for a single *box map*, i.e., for the respective map on the unit interval, cf. Section 2.1.2. Here, the fact can be used that the extrema, which are the *critical points* of the box map, have to touch horizontal lines, as explained before, which means that to obtain a Markov partition the extrema have to get mapped onto partition points.

Taking the central symmetry of the box map with respect to the center of the box at $x = 1/2$ into account, the problem reduces to considering only one of the extrema in the following, e.g., the maximum. Changing the height of the maximum corresponds to changing the slope of the map. Therefore, if one wants to find Markov partitions for parameter values of the slope, one can do it the other way around by the following *Markov condition*:²⁵

Definition 2.2 (Markov condition, verbal definition) *For map \mathcal{L} , Markov partition values of the slope are determined by choosing the slope such that the maximum of the box map gets mapped onto a point of the partition again.*

In Fig. 2.8, some examples of non-trivial Markov partitions for map \mathcal{L} are illustrated for a broad range of values of the slope by their box maps. Note that a modulus of one has been applied to the coordinate x_n in case of iterations.

One may verify that the two “handwaving” conditions to obtain “good” partitions, derived at the beginning of this section on the basis of the integer slope examples, are also fulfilled in these cases and that these partitions obey the Markov partition definition 2.1 as well. With respect to the structure of the partitions, it is obvious that the single parts of the partition do not necessarily have to be equal, but that in fact the partitions can be arbitrarily complex. The bold lines with the arrows represent what will be called the *generating orbit* of a Markov partition: The initial condition of each such orbit refers to the injection of the maximum (Fig. 2.8 (a) to (c)) or the minimum (Fig. 2.8 (d)) of a preceding or a following box map, respectively. It can be observed that the iterations of this orbit generate the structure of the partition, and that this way the number of partition parts is related to

ferred to as *Markov maps*, however, the definition of Markov maps does not seem to be unique in the literature, since usually additional properties are required for the map, which are different in different publications [dM93, Bow79, Moo75, Boy79, Bal94].

It should be mentioned that the Markov partitions considered here are not necessarily *generating* partitions, i.e., where an isomorphism between any orbit in phase space and a symbol sequence of a symbolic dynamics, induced by the partition, exists [Bec93, Cor82].

²⁵The possibility to construct Markov partitions this way was pointed out by Profs. L. Bunimovich and J. Yorke, in discussions together with Prof. J.R. Dorfman, to whom the author is very much indebted for this hint.

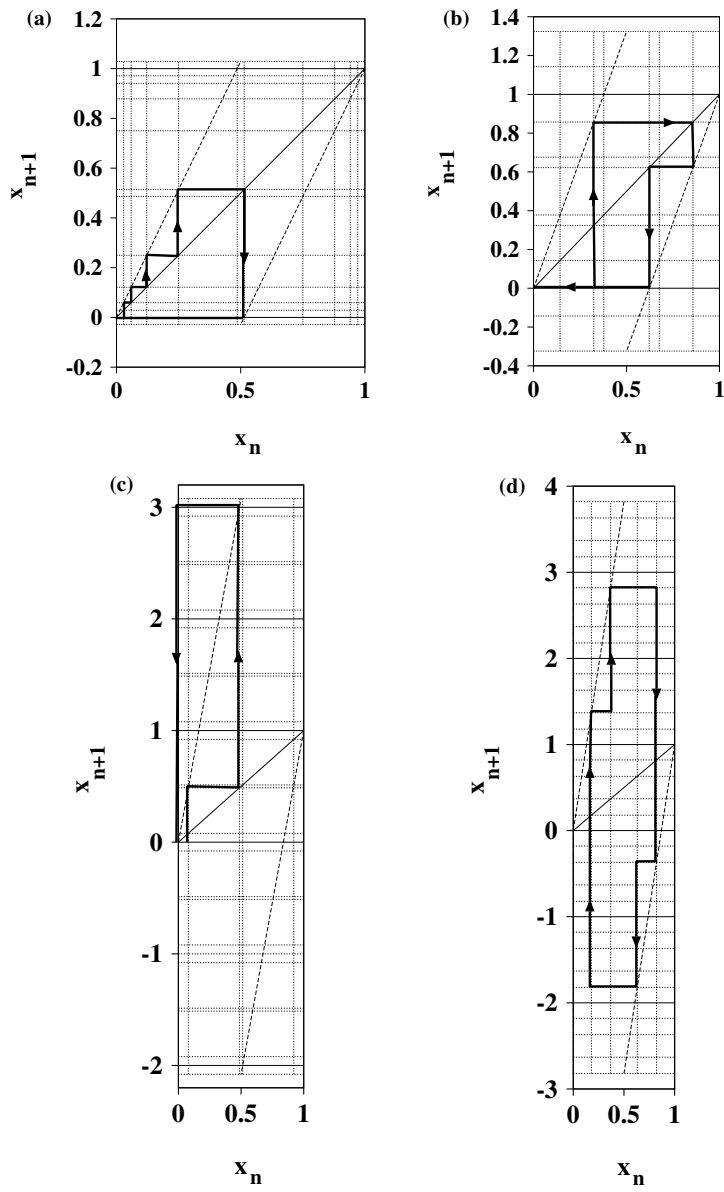


FIGURE 2.8. Examples of non-trivial Markov partitions of map \mathcal{L} at various values of the slope. The bold black lines with the arrows give their generating orbits, see text. Diagram (a) is for the slope $a \simeq 2.057$, (b) for $a \simeq 2.648$, (c) for $a \simeq 6.158$ and (d) for $a = 7.641$.

the iteration number of the generating orbit. It is important to note that in case of (Fig. 2.8 (a) to (c)) the orbit is eventually periodic, i.e., it finally gets mapped onto the fixed point $x = 0$, whereas in case of (Fig. 2.8 (d)), the Markov partition is generated by a periodic orbit of period four. Thus, while the generating orbit itself provides the skeleton for the actual construction of the Markov partition in the chain of boxes, the special type of generating orbit refers to the key how to find Markov partition values of the slope in a systematical way.

In fact, a general algebraic procedure to compute such values of the slope can be developed. One starts with a further *topological reduction* of the whole chain of boxes.²⁶ Since map \mathcal{L} is *old*, it is possible to construct the Markov partition for the whole chain from a *reduced map*

$$\tilde{M}_a(\tilde{x}) := M_a(\tilde{x}) \pmod{1} \quad (2.38)$$

via periodic continuation, where $\tilde{x} := x - [x]$ is the fractional part of x , $\tilde{x} \in (0, 1]$, and $[x]$ denotes the largest integer less than x .

Therefore, it remains to find Markov partitions for map $\tilde{M}_a(\tilde{x})$ of the equation above. This can be done in the following way:

Let

$$\varepsilon := \min \left\{ \tilde{M}_a\left(\frac{1}{2}\right), 1 - \tilde{M}_a\left(\frac{1}{2}\right) \right\} \quad , \quad \varepsilon \leq \frac{1}{2} \quad , \quad (2.39)$$

be the minimal distance of a maximum of the box map $M_a(\tilde{x})$ to an integer value. With respect to the Markov condition given by Definition 2.2, it is clear that ε has to be a partition point. Since $\tilde{M}_a(\tilde{x})$ is central symmetric, $1 - \varepsilon$ also has to be a partition point, and because of map \mathcal{L} being *old*, the fixed point $x = 0$ is necessarily another partition point.

Now, the reduced map governs its internal box dynamics according to

$$\tilde{x}_{n+1} = \tilde{M}_a(\tilde{x}_n) \quad , \quad \tilde{x}_n = \tilde{M}_a^n(\tilde{x}) \quad , \quad \tilde{x} \equiv \tilde{x}_0 \quad . \quad (2.40)$$

Since $0, \varepsilon$ and $1 - \varepsilon$ have to be partition points, the Markov condition Definition 2.2 can be formalized to

$$\tilde{M}_a^n(\varepsilon) \equiv \delta \quad , \quad \delta = 0, \varepsilon, 1 - \varepsilon \quad , \quad (2.41)$$

i.e., the generating orbit of a Markov partition is defined by the initial condition ε , its end point δ and the iteration number n . According to Eq.(2.39), ε is determined

²⁶An analogous *dynamical reduction* of the chain of boxes, as sketched in Sect. 2.1.2, which is based on a distinction between internal box motion and external jumps between boxes, is also possible [Fuj82, Tho83, Gas92a] and leads to another method to compute diffusion coefficients, see Section 5.1.

by the slope a . Therefore, for map \mathcal{L} Markov partition values of the slope can be computed as solutions of Eq.(2.41).

The evaluation of this equation can be performed numerically as well as, to a certain degree, analytically. To obtain analytical results for Markov partition values of the slope, one has to determine the structure of the generating orbit in advance, i.e., one has to know whether it hits the left or the right branch of the box map at the next iteration. Then, one can write down an algebraic equation, which remains to be solved. For example, for the Markov partition Fig. 2.8 (c), the generating orbit is determined to

$$\begin{aligned} x_1 &= \tilde{M}_a(\varepsilon) \quad , \quad \varepsilon \leq \frac{1}{2} \\ \delta &\equiv \tilde{M}_a(x_1) - 3 \quad , \quad x_1 \leq \frac{1}{2} \end{aligned} \quad (2.42)$$

with $a = 2(3 + \varepsilon)$ and $\delta = 0$ at iteration number $n = 2$. This leads to

$$a^3 - 6a^2 - 6 = 0 \quad , \quad a \geq 2 \quad , \quad (2.43)$$

for which one may verify $a \simeq 6.158$ as the correct solution. This way, all Markov partition values of the slope are the roots of algebraic equations of $(n + 1)$ th order. Since one usually faces the problem to solve algebraic equations of order greater than three, numerical solutions of Eq.(2.41) are desirable, although one should take into account that iterations of the reduced map $\tilde{M}_a(\tilde{x})$ contain many discontinuities, due to the original discontinuity of $\tilde{M}_a(\tilde{x})$ at $\tilde{x} = 1/2$ as well as due to applying the modulus to $M_a(\tilde{x})$ in Eq.(2.38).²⁷

With respect to the three different end points δ of the generating orbit in the formal Markov condition Eq.(2.41), three series of Markov partitions can be distinguished. For each series one can increase the iteration number n , and one can vary the range of the slope a systematically. These three series have been used as the basis for numerical calculations of the diffusion coefficient $D(a)$, as will be explained below. However, there exist additional suitable end points δ for the generating orbit. As an example, one can choose δ to be a point on a two-periodic orbit,

$$\tilde{M}_a(\delta) = \delta \quad , \quad a = 2(1 + \varepsilon) \quad , \quad 0 \leq \varepsilon \leq \frac{1}{2} \quad \Rightarrow \quad \delta = \frac{1 + 2\varepsilon}{4(1 + \varepsilon)^2 - 1} \quad (2.44)$$

²⁷Standard root-finding procedures of software packages like NAG and IMSL require the respective functions to be continuous. Thus, for the problem here a grid method has been developed, where $\tilde{M}_a^n(\varepsilon) - \delta$, cf. Eq. (2.41), has been discretized and where it has been checked whether a value of this difference is close to zero by varying ε . Within a range of some CPU seconds of computing time on workstations like, e.g., SUN SPARCs, a precision of up to eight digits behind the dot could easily be obtained.

so that the generating orbit is again eventually periodic, but now being mapped on a periodic orbit which is part of the Markov partition instead of being mapped on a simple fixed point. This way, certain periodic orbits can serve for defining an arbitrary number of new Markov partition series with respect to the choice of respective new end points δ . On the other hand, the set of Markov partition generating orbits is *not* equal to the set of *all* periodic orbits. For example, for the range $2 \leq a \leq 3$, Eq.(2.44) shows that there exists a two-periodic orbit for any slope a , but *not any* maximum of the map in this range necessarily maps onto this periodic orbit, as is already illustrated by Fig. 2.8 (a) and (b), or by other simple solutions of Eq.(2.41), respectively. This proves that Markov partition generating orbits are in fact a subset of the periodic orbits of the map.²⁸

With respect to varying the iteration number n and the end point δ , one can expect to get an infinite number of Markov partition values of the slope. In fact, for certain classes of maps the existence of Markov partitions can be considered as a natural property of the map.²⁹ According to the explanations above, this does not seem to be true for map \mathcal{L} . Instead, there is numerical evidence³⁰ for the following conjecture:³¹

Conjecture 2.1 (Denseness property of Markov partitions) *For map \mathcal{L} , the Markov partition values of the slope a are dense on the real line with $a \geq 2$.*

This denseness conjecture should ensure that it is possible to obtain a representative curve for the parameter-dependent diffusion coefficient $D(a)$ solely by com-

²⁸This proof makes also clear that it is not a sufficient, but only a necessary condition for a Markov partition to require that “partition points get mapped onto partition points” [Boy79], since this is also true for choosing, e.g., any two-periodic orbit defined by Eq.(2.44) as a generating orbit for a partition.

²⁹At least two theorems about the existence of Markov partitions are well-known in the literature. They can be roughly stated as the following:

1. For any Axiom A diffeomorphism of an n -dimensional manifold onto itself, there exists a Markov partition (Sinai [Sin68] and Bowen [Bow75]; see also Ref. [Sin89, Guc90] for an overview).
2. For any C^r -continuous expanding map of a compact interval onto itself, there exists a Markov partition (Ruelle [Rue78, Rue89]).

(for a rigorous mathematical formulation of these theorems see the references cited)

It should first be mentioned that Anosov diffeomorphisms are also Axiom A [Eck85, Bow75] and that to be Anosov, the whole manifold of the diffeomorphism has to be hyperbolic (for definitions of Anosov and Axiom A see Refs. [Eck85, Bow75, dM93]). However, although being Anosov, the reduced map of map \mathcal{L} is neither a diffeomorphism nor is it C^r -continuous so that these theorems do not apply to this case.

³⁰Numerical evidence has been obtained from plots which show Markov partition values of the slope with respect to their iteration numbers n : It could be observed that for the three series of Markov partition values defined above, the number of Markov partitions in a certain range of the slope increases like a power law with respect to the iteration number n and that the Markov partition values of the slope seem to cover the real line dense, although not uniformly, in certain regions of the slope, with respect to increasing the iteration number n .

³¹Meanwhile, it has been claimed that this conjecture can be proved [Gro95a].

puting diffusion coefficients at Markov partition values of the slope.³² It may be conjectured that Conjecture 2.1 also holds for all other class \mathcal{P} -maps as well.³³

To do such computations, one needs to construct the corresponding transition matrices to the Markov partitions obtained, as it has been shown for the slopes $a = 3$ and $a = 4$ of map \mathcal{L} . This can be done according to the following rule: Take as an example one of the box map Markov partitions illustrated in Fig. 2.8. If one refers to a dashed rectangle as a *cell of the partition*, and if one takes these cells as the “body” of the matrix to be obtained, the transition matrix corresponding to a Markov partition can be constructed by checking where the graph of the map goes across a cell of the partition, counting the number of these occurrences in each cell and writing down these values as the matrix elements. For map \mathcal{L} , usually these matrix elements will consist of zeroes and ones, but the way they are defined here they can also take other integer values, depending on the choice of the partition, as, e.g., illustrated in case of $a = 4$, Eq. (2.15).

The construction of the box map transition matrix can be simplified by taking the central symmetry of the box map into account. The transition matrix of the full chain of chainlength L again follows by periodic continuation. These matrices can be denoted as *topological transition matrices*, since they reflect purely the topology of the map with respect to the Markov partitions, without involving any transition probabilities at this point [Rue89, Guc90, Rue78, Bow75, Sin68].

The property of map \mathcal{L} being *old* induces a certain structure in the topological transition matrices. They are said to be *banded square block Toeplitz matrices*, i.e., they consist of certain submatrices, called *blocks*, corresponding to the box map Markov partitions, and these blocks are the same along diagonals of the topological transition matrix parallel to the main diagonal, forming *bands* [Dav79, Bea91, Tre85]. Applying periodic boundary conditions to the chain of boxes defines a subclass of these Toeplitz matrices, called *block circulants*, where each row is constructed by cycling the previous row forward one block [Ber52, Kow54, Dav79, Bea91], see, e.g., the matrices $T(4)$, Eq.(2.19), as an example for a simple circulant and $T(3)$, Eq.(2.29), for a block circulant.

According to the transition matrix method outlined in the previous section, it remains to solve the eigenvalue problems of these matrices and to match the respective eigenmodes to the ones of the diffusion equation for computing the corresponding diffusion coefficients $D(a)$. Here, periodic boundary condi-

³²Certain techniques have been developed to approximate maps which do not possess Markov partitions via series of Markov partitions and their corresponding transition matrices, see Refs. [Boy88, Gor89, Gor91, Bal94]. However, such a procedure is expected to be very time-consuming for computing diffusion coefficients in this case.

The problem of non-Markovian values of the slope will also be briefly discussed in the context of computer simulations, see Chapter 3.

³³Again, it has been claimed that this conjecture can be proved [Gro95a].

tions are of great advantage. Analytically, as mentioned before, there exists a general procedure how to solve the eigenvalue problems of simple circulants [Ber52, Kow54, Dav79], and in some cases it is possible to reduce the eigenvalue problem of a block circulant to that of a simple circulant. If this method works, it automatically provides “nice eigenmodes”, i.e., eigenvectors of the form of sines and cosines with some fine structure. These eigenmodes are similar to the eigenmodes of the diffusion equation at this stage, i.e., before iterating the matrices according to the Frobenius-Perron matrix equation Eq.(2.18).³⁴ The situation is quite different for absorbing boundary conditions, where no such general procedure exists.

If analytical solutions of the eigenvalue problems are not possible anymore, one can try to obtain numerical solutions. Well-known software packages like NAG and IMSL³⁵ provide subroutines to solve the eigenvalue problems of these matrices. Unfortunately, the numerically obtained results for the full spectra turned out not to be very reliable to a certain extent: In comparison to analytical results for periodic boundaries, the NAG package does not compute all eigenvectors correctly, i.e., in the numerical results usually some linear independent eigenvectors are missing. Moreover, both packages provide spectra of eigenvalues which, although partly identical to the analytical solutions, in their full range differ quantitatively from the ones analytically calculated for some examples, not taking any degeneracy into account.³⁶ Such numerical problems seem to be inherent to the class of non-normal Toeplitz matrices, as has already been pointed out by Beam and Warming in a not very widely known report [Bea91]. In fact, solving eigenvalue problems for Toeplitz matrices can be considered as a field of active recent research in numerical mathematics [Rei92, Bas94].

However, solely for the purpose of computing diffusion coefficients not the full spectra of the transition matrices are required, but only the few largest eigenvalues and eigenvectors are of interest. With respect to eigenvectors, the IMSL package has been checked to be reliable in this range, and with respect to eigenvalues, both packages provide exact and identical numerical results, especially for the second largest eigenvalue, which determines the diffusion coefficients. From a practical point of view, the NAG package is considerably more efficient in the use of computing time than IMSL and more flexible in its subroutines. Therefore, for

³⁴The reason for this universal behaviour is that the eigenmodes of simple circulants are always sines and cosines, see Ref. [Ber52].

³⁵For the computations discussed here, the versions IMSL 1.1 and 2.0 and NAG MK14B and 15A have been used.

³⁶For example, for slope $a \simeq 6.8729834$, chainlength $L = 100$ and periodic boundary conditions, one finds numerically a considerable number of eigenvalues less than zero, and the smallest numerical eigenvalue is less than -1 , whereas analytical solutions give only a few eigenvalues less than zero, and the smallest one is only slightly below zero and clearly greater than -1 .

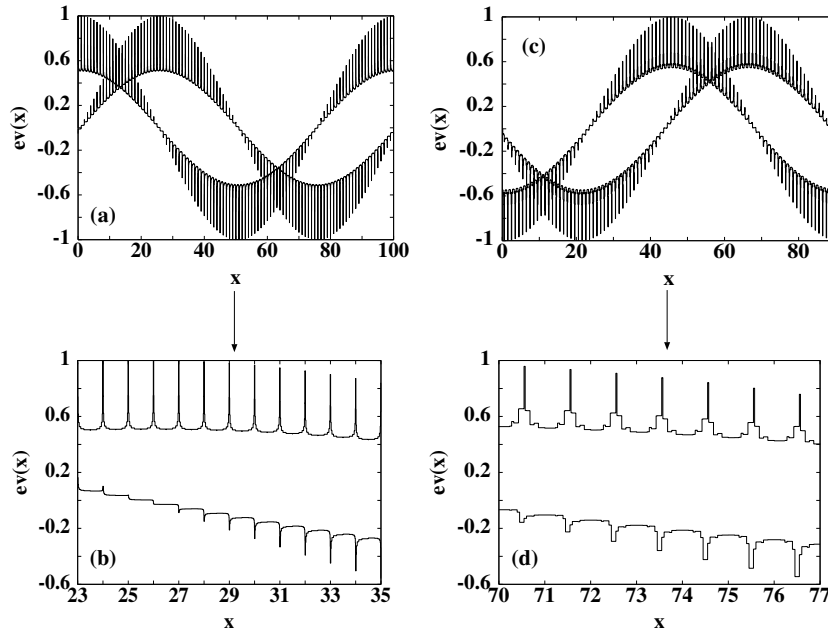


FIGURE 2.9. Second largest eigenmodes for map \mathcal{L} at two non-trivial Markov partition values of the slope with periodic boundary conditions. Diagrams (a) and (b) are for slope $a = 3.0027$, chainlength $L = 100$, (c) and (d) for $a = 2.0148$, chainlength $L = 90$.

quantitative computations of eigenvalues and diffusion coefficients NAG routines have been used, whereas for eigenvector computations IMSL procedures have been employed. For computations of diffusion coefficients, it is also favourable to consider only the case of periodic boundary conditions, i.e., solving eigenvalue problems for block circulants, respectively, since it has already been discussed in Sect 2.3.1 that absorbing boundaries lead to a poor convergence rate of the diffusion coefficient with the chainlength L .

Fig.(2.9) presents two examples of second largest eigenmodes for chains of boxes with periodic boundaries and non-trivial Markov partitions. Again, one gets “nice” second largest eigenmodes, i.e., functions which behave like sines and cosines on a large scale. However, the structure of these eigenmodes is much more complex on a fine scale, as one can see in the magnifications of certain regions. The periodic continuation of the fine structure suggests that it is related to the dynamics of the box map, and therefore varies with changing the slope, whereas the general large-scale behaviour of the eigenmodes seems to be a property of the chain of boxes which shows up independently from such microscopic details. These characteristics have been checked numerically for a variety of other

Markov partition values of the slope and seem to be a universal feature of map \mathcal{L} , and probably of all class \mathcal{P} -maps. One may assume that the fine structure is somehow related to the strength of the diffusion coefficient and that, on the other hand, the universal large-scale structure of the eigenmodes is related to the existence of diffusion coefficients for non-trivial Markov partition values of the slope. It should be reminded that the fundamental problem of the existence of diffusion coefficients for class \mathcal{P} -maps as has been posed as an open question in the previous section.

In fact, the specific character of the eigenmodes discussed above, which shows up in any analytical solution of (block) circulants and which is supported by numerical results, forms the basis for the following conjecture:

Conjecture 2.2 (Existence of diffusion coefficients) *Let $M_a(x)$ be a class \mathcal{P} -map. If for given value of the slope the map is uniquely ergodic and if there exists a Markov partition, then the map is diffusive.*

Without going into too much detail here, some remarks are in order to provide at least a motivation for this conjecture: The existence of Markov partitions guarantees that transition matrices can be used at all. The restriction to class \mathcal{P} -maps ensures that topological transition matrices can be constructed in the simple way outlined before,³⁷ and the *old* property included in the definition of class \mathcal{P} determines the global structure of the topological transition matrices such that the eigenmodes are “nice”, at least for periodic boundary conditions. The requirement to be uniquely ergodic establishes the possibility of diffusion in the chain of boxes and confirms also the uniqueness of the diffusion coefficient to be obtained.³⁸ Finally, the term diffusive shall be understood in the sense that a diffusion coefficient exists, defined by the statistical diffusion equation Eq.(2.9), which has been introduced to the dynamical system by successfully performing the matching eigenmodes procedure outlined in the previous section.

Therefore, the main proposition of this conjecture is that the matching eigenmodes procedure required by the first passage method works for any value of the slope, if the respective conditions are fulfilled. As a corollary to this conjecture, it can be formulated that in the limit of time n and chainlength L to infinity, the Frobenius-Perron equation of the respective class \mathcal{P} -dynamical systems always provides “nice”, i.e., the correct diffusive eigenmodes.³⁹ As another corollary, it

³⁷This condition might be extendable to piecewise linear maps with piecewise uniform slopes without too much effort.

³⁸A simple counterexample shows that not any chain of boxes with escape out of one box is automatically diffusive.

³⁹In Ref. [Gas92a], such a statement for specific cases of class \mathcal{P} -maps has been considered as the main result of the paper. The conjecture above may be regarded as an attempt to generalize this statement.

follows that there occurs no anomalous diffusion in class \mathcal{P} -maps, i.e., that normal diffusion is “typical” for such piecewise linear maps. A rigorous mathematical proof of Conjecture 2.2 seems to be possible along the lines of first passage and transition matrix method.⁴⁰

The conjecture stated above may be understood as an attempt to establish a more proper mathematical foundation for computing diffusion coefficients by first passage and transition matrix method. Results based on this method shall be presented in the next section.

It should be mentioned in advance that the results provided by this approach have been verified by another numerical method (see Chapter 3), another analytical method which has been implemented numerically (see Chapter 5), as well as, to a certain degree, by straightforward computer simulations (see Chapter 3).⁴¹

2.4 Fractal diffusion coefficients: results

Based on the methods presented in the previous section, the parameter-dependent diffusion coefficient $D(a)$ has been computed for map \mathcal{L} numerically for a broad range of values of the slope. The main results are presented in Fig. 2.10. The numerical precision obtained depends on the convergence of the diffusion coefficients with the chainlength, cf. Eq.(2.37), and has been estimated to be better than 10^{-4} for each $D(a)$ so that error bars do not appear in the diagrams. It should be stressed that the numerical method employed here was the first one by which these curves of $D(a)$ have been obtained. It is by far not the best one of the procedures developed until now to compute such diffusion coefficients with respect to numerical efficiency, see Chapters 3 to 5.

Fig. 2.10 (a) shows the diffusion coefficient of map \mathcal{L} for values of the slope in the range $2 \leq a \leq 8$. One can see that the strength of diffusion increases globally by increasing the slope from $a = 2$ to $a = 8$. This might be expected intuitively,

⁴⁰The main problem of diagonalization mentioned in Section 2.3.1 might be circumvented by transformation onto Jordan normal forms, employing certain theorems about the characteristics of eigenvalue spectra of block Toeplitz matrices and applying the Perron-Frobenius theorem of matrix theory. Together with the knowledge that block circulants always provide the correct eigenmodes, this might show a way how to prove this conjecture rigorously. A first sketch of such a proof has been worked out [Kla95a], however, the lack of a theorem about a certain continuity property of block Toeplitz eigenvalue spectra and of an analytical proof for the “correct form” of the block Toeplitz eigenvectors seem to be the main obstacles for completing such a proof.

Other methods might even offer simpler ways to prove the existence of diffusion coefficients, see, e.g., Chapter 5.

⁴¹Recently, the same results have been obtained independently by another author with a different method [Gro95a].

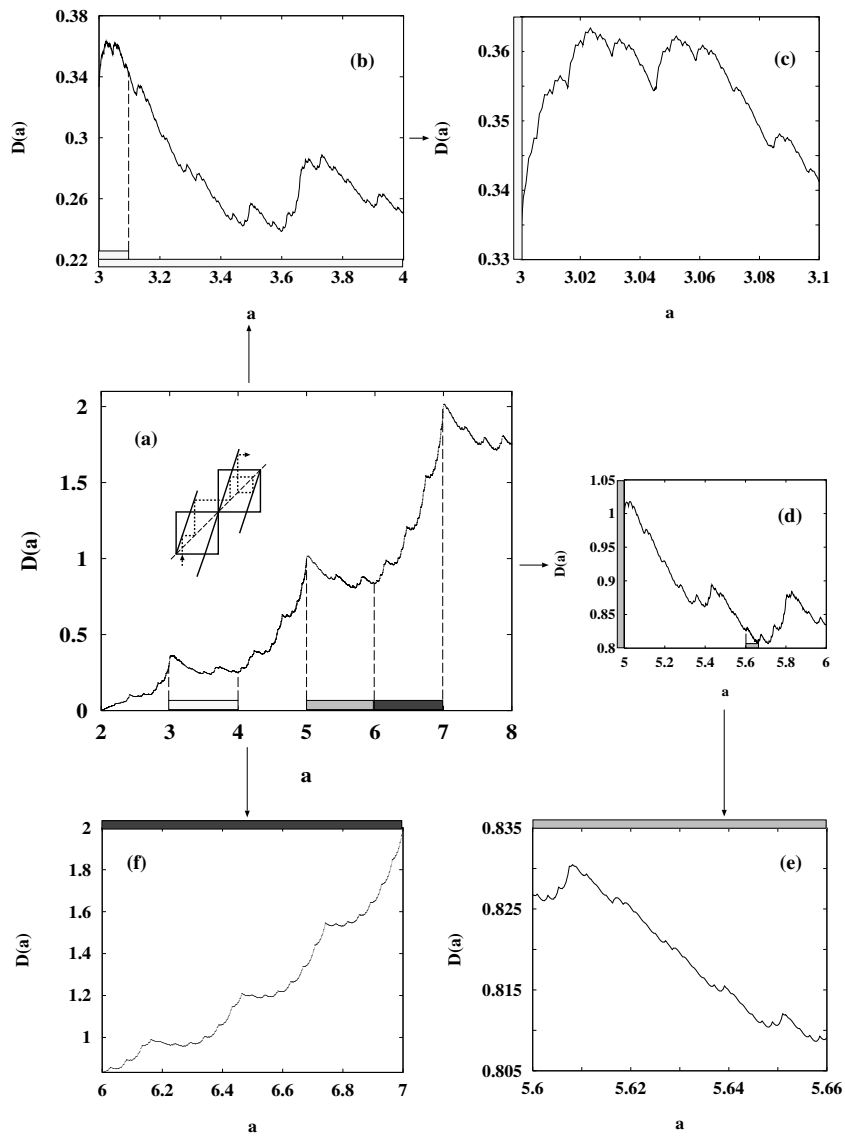


FIGURE 2.10. Parameter-dependent diffusion coefficient $D(a)$ computed for map \mathcal{L} and some enlargements. In graph (b)-(e), the dots are connected with lines. The number of data points is 7,908 for (a), 1,078 for (b), 476 for (c), 1,674 for (d), 530 for (e) and 1,375 for (f).

as motivated in Section 2.1.2, since the probability of a particle to escape out of a box, as well as the mean distance a particle travels by performing a jump, are getting larger with larger value of the slope.⁴² However, the increase of the diffusion coefficient is not monotone and consists of oscillations not only at integer values of the slope, as has already been mentioned in Section 2.2, but also on much finer scales between integer values. In fact, Fig. 2.10 (a) shows a certain regularity in the appearance of “wiggles”, i.e., local maxima and minima. If one denotes the local maxima at odd integer slopes a as wiggles of 0th order and any smaller local maxima systematically as wiggles of higher order, one can find one maximum of first order below $a = 3$, three maxima of first order in the range $3 \leq a \leq 5$, five maxima of first order in the range $5 \leq a \leq 7$, This regularity even persists to a certain extent on finer scales, although according to a slightly different rule, as can be seen, e.g., in the magnification Fig. 2.10 (f), $6 \leq a \leq 7$, where exactly six wiggles of second order appear between the respective wiggles of first order. The same way, six wiggles of third order can be observed in this region in further magnifications, and similar structures show up in the region of $4 \leq a \leq 5$ with four wiggles of second and four wiggles of third order. The region of $2 \leq a \leq 3$ is somehow special and will be discussed separately. Thus, while the number of wiggles of first order increases by a step of two with increasing the slope, the number of wiggles of higher order remains constant in the region between two respective wiggles of first order, even by increasing the order of the wiggles to be considered.

On the other hand, magnifications of other regions of the slope show that the structure of the curve is not everywhere that simple. For example, blow-ups of the regions $3 \leq a \leq 4$, Fig. 2.10 (b), and $5 \leq a \leq 6$, Fig. 2.10 (d), do not enable a clear distinction between “wiggles of different orders” anymore. Instead, they provide complex structures, which further magnifications, as, e.g., Figs. 2.10 (c) and (e), reveal to be self-similar.

It can be summarized at this stage that different regions of the curve exhibit different kinds of self-similarity, partly being fairly simple, but partly also being highly non-trivial. Thus, the results of Fig. 2.10 suggest that the parameter-dependent diffusion coefficient $D(a)$ for map \mathcal{L} is fractal [Man82]. More evidence for the fractality of the curve can be obtained in three different ways: Firstly, qualitative and quantitative explanations for the wiggles in certain regions of the slope will be provided, which ensure that these regions exhibit non-trivial self-similar behaviour. This will be demonstrated in the following. Secondly, it is striking to observe that especially diagrams (c), (e), and (f) resemble graphs of some fractal functions, which have been obtained in Refs. [Tas93a, Tas94, Tas95] by working

⁴²This will be made more quantitative in Section 4.2 by computing diffusion coefficients for simple random walk models.

on dynamical systems being very close to the ones considered here. These functions have been shown to possess fractal dimensions close to one [Tas93a]. On the one hand, this gives further evidence for the fractality of the curves of Fig. 2.10. On the other hand, this raises the new question whether there is an analytical fractal representation for certain regions of the curve, or maybe even for the full parameter-dependent diffusion coefficient of map \mathcal{L} . Such problems will be discussed in detail in Chapter 5. Thirdly, it should be mentioned that numerical computations of the box counting dimension⁴³ of the curve have been performed. The results indicate that the curves shown in Fig. 2.10 (a) - (f) have fractal dimensions d very close, but not equal to one in a range of $d = 1 + \Delta d$, $0 < \Delta d \leq 10^{-2}$. Because of the limited data set and due to well-known fundamental problems to determine fractal dimensions via conventional methods [Pei92, Bar93b], as, e.g., box counting, better values are difficult to get, especially since the fractal dimension is expected to be close to one in this case. Nevertheless, more detailed investigations of the fractal dimension for various regions of the curve could be of much interest. With respect to the magnifications in Fig. 2.10, it may even be conjectured that the full $D(a)$ -curve is multifractal.⁴⁴

Fig. 2.11 illustrates the principles of a first rough qualitative approach to understand the occurrence of wiggles of 0th and 1st order. It will be called *plus-minus approach*. The basic idea of this approach is to establish a connection between the appearance of wiggles in the $D(a)$ -graphs and the occurrence of certain dynamical correlations in the chain of boxes. These correlations are a main feature of the transport of particles from one box to another, and they show up and vanish with varying the slope of the map. In the following, particles will be referred to solely by their positions, i.e., by points on the real line. Fig. 2.11 (a) and (b) sketch correlations of 0th order: As a starting point, the escape of particles out of one box in one direction, i.e., to the right, will be considered for varying the slope in the range $2 \leq a \leq 4$. Such an escape of points is related to a certain subinterval of the box which will be called *escape region*, as is shown in the figure. If points get mapped to the right at the next iteration, the respective subinterval will be denoted with a plus sign. The same way, subintervals will be denoted with a minus if points get mapped to the left. Therefore, the escape region marked in Fig. 2.11 is part of a plus region, and for small enough slope after only one iteration points of it get mapped directly into another plus region. This enhances diffusion, since particles can move continuously in one direction, i.e., here to the right. The behaviour persists for increasing the slope up to $a = 3$. For slopes above this value, an increasing number of points of the escape region is now mapped into the

⁴³The box counting dimension is sometimes also referred to as capacity, see, e.g., Ref. [Ott93].

⁴⁴Such multifractal characteristics may become important in the context of certain physical phenomena, see, e.g., the discussion in Section 4.3.2.

and $1/2 < x \leq 1$ with a minus.⁴⁵

In Fig. 2.11 (c) the number of iterations has been increased to two. The method is the same as explained before, however, a further distinction has been made after the first iteration: new subintervals have been defined, which refer to points of the escape region being mapped to another plus or minus region at the second iteration. One can see that increasing the slope corresponds to creating different plus-minus sequences for orbits close to, but less than $x = 1/2$. This leads to the particles being in a good or bad position for going further in one direction with respect to the next iteration, depending on the value of the slope. The $D(a)$ -graph in Fig. 2.11 (d) again gives the qualitative behaviour of $D(a)$ to be expected with respect to the dynamical correlations after two iterations, up to $a = 5$. This result corresponds well to the number of wiggles of first order estimated in the respective regions of the slope. Again, the plus-minus sequences give the symbolic dynamics of points close to, but less than $x = 1/2$ after two iterations.

The plus-minus method works on this level as well for any higher values of the slope and leads to a qualitative explanation for the number of wiggles of first order for any region of the slope. To a certain degree, it can even explain additional features of the structure of the $D(a)$ -curves: For example, in Fig. 2.10 (b) one observes that the local maximum is not precisely at $a = 3$, although one could expect this from the results of the plus-minus method of 0th order. Actually, particles of the escape region close to $x = 1/2$ can still achieve a good position for further movement in one direction, even for slopes slightly above $a = 3$. This is due to the fact that, although such points get first scattered back into the previous box after two iterations, here they are now in an excellent position for further jumps to the right again. This way, these orbits perform a kind of “spiral” and seem to be responsible for the surprising fact that the odd integer slope values of $D(a)$ are *not* precisely identical to the local extrema of the curve, but that there is always a kind of overhang, i.e., a further increase of the diffusion coefficient right above odd integer slopes, as, e.g., shown in detail in Fig. 2.10 (c).

Although the plus-minus method can be applied to achieve a qualitative understanding of the wiggles of 0th and 1st order, further refinements of this method to obtain wiggles of higher order generally turned out not to be very promising. The main reason is that in case of more iterations of points of the escape region, the dynamics is getting quite complicated and is not easy to handle anymore in the qualitative way illustrated in Fig. 2.11.

However, the basic idea of this method can be made more quantitative by a procedure which shall be called *turnstile dynamics*. The principle of turnstile dynamics

⁴⁵For more details about symbolic dynamics, see, e.g., Ref. [Ott93]; techniques like the one sketched above have been used by Hsu and Kim to compute topological entropies via kneading theory for maps like the one under consideration, see Ref. [Hsu85].

is again to investigate the appearance and disappearance of long-range dynamical correlations by iterating points with respect to varying the slope. The new feature is now that not the full intervals of all single boxes are taken into account. Instead, the analysis is restricted solely to the regions of the boxes where transport of particles from one box to another occurs in form of jumps. These regions are called *turnstile*:

Definition 2.3 (turnstile) *Turnstiles are the “coupling regions” of the single boxes of a chain of class \mathcal{P} , where points of one unit interval get mapped outside that particular interval into another unit interval.*

This notation has been borrowed from the theory of transport for two-dimensional twist maps, such as sawtooth maps, where turnstiles turned out to be crucial for understanding large-scale diffusion [Mac84, Che89, Che90, Mei92].⁴⁶ The escape region introduced above in the context of the plus-minus method represents precisely one half of such a turnstile.

The main idea is now to study the *interaction* of turnstiles, i.e., varying the slope it shall be investigated whether one obtains “good” or “bad” conditions for particles to get from one turnstile into another, or maybe even to get mapped successively through a series of turnstiles. As before in case of the plus-minus method, such dynamical correlations are expected to show up in the curve for the parameter-dependent diffusion coefficient $D(a)$. The advantage of turnstile dynamics is that it can be made quantitative by exemplifying all turnstiles with certain points of these regions. For instance, the peak of the turnstile one starts with may be represented by the critical point, $x = 1/2$. Now, one can try to compute the slopes for which this point maps into other turnstiles again, being exemplified by certain points, after certain numbers of iterations.

This has been done in detail for the region $2 \leq a \leq 3$, as shown in Fig. 2.12. The dashed line in the figure represents the prediction of $D(a)$ for a simple random-walk model suggested by Schell, Fraser, and Kapral [Sch82], see Section 4.2. Note that, on a large scale, the model correctly accounts for the behaviour of $D(a)$ near $a = 2$, but that with respect to any fine structure, such a simple model is clearly totally apart. One can recognize three distinct series of values of a in the figure. To understand the nature of these series, one should consider the trajectory of the critical point. The first iterate of $x = 1/2$ is in the second interval, $(1, 2)$. The *series* α values of a are defined by the condition that the second iterate of $x = 1/2$ is at the leftmost point of the upward turnstile in the second interval

⁴⁶The term turnstile has been introduced by McKay, Meiss and Percival in Ref. [Mac84]. It refers to the analogy of a real turnstile: In the map under consideration, transport is caused analogously by a mechanism which acts on particles in certain regions of the dynamical system, shuffling them to the left and to the right.

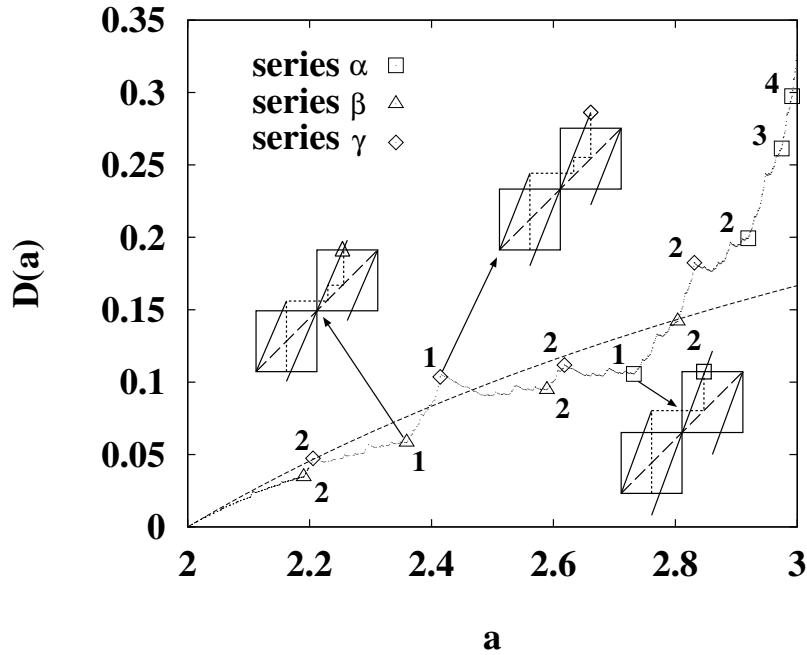


FIGURE 2.12. Enlargement of the region of slope $a \leq 3$ for map \mathcal{L} with the solution for a simple random walk model (dashed line) and labels for the values which are significant for “turnstile dynamics” (see text). For some points, the turnstile coupling is shown by pairs of boxes. The graph consists of 979 single data points.

$(1, 2)$ ($a = 2.732$), or that the third iterate is at the corresponding point in the third interval ($a = 2.920$), etc. The numbers on the $D(a)$ -curve refer to the number of intervals the image of $x = 1/2$ has travelled before it gets to the appropriate point on the turnstiles. *Series* β points are defined in a similar way, but they are allowed to have two or more internal reflections within an interval before reaching the left edge of a turnstile. *Series* γ points are defined by the condition that some image of $x = 1/2$ has reached the rightmost edge of an upward turnstile, i.e., some point $x = k + 1/2$, where k is an integer.

One observes that each series produces a cascade of apparently self-similar regions of decreasing size, as the limits $a \rightarrow 2$ or $a \rightarrow 3$ are approached. These cascades provide a basis for a physical understanding of the features of $D(a)$ in this region: Particles leave a particular unit interval through a turnstile and undergo a number of iterations before they are within another turnstile. Whether they continue to move in the same or the reverse direction at the next and later turnstiles is a sensitive function of the slope of the map. Thus, the fractal structure

of the $D(a)$ curve is due to the effects of long-range correlations among turnstiles, and these correlations lead to changes of $D(a)$ on an infinitely fine scale.

One should note that series γ points completely label the maxima of higher order introduced before, and series β points mark the respective minima. This way, in the region of the slope $a \leq 3$ the picture of quantitative turnstile dynamics is in full agreement with the results obtained by the qualitative plus-minus method outlined above.⁴⁷

However, the application of turnstile dynamics has its limits: First, this method is of no use anymore for any higher value of the slope above $a = 3$. Thus, there is no other understanding of the structure in this range than the one provided qualitatively by the plus-minus approach. And second, even for values below $a = 3$ turnstile dynamics is quantitatively not completely correct: Apart from the lack of explaining the existence of the overhang above $a = 3$, a detailed analysis reveals further “tiny overhangs” at maxima of higher order, as, e.g., right above the maximum of first order in the region $2 \leq a \leq 3$ at $a = 2.414$.⁴⁸ In other words, the “turnstile values” marked in Fig. 2.12 by series γ -points represent rigorously not the exact local maxima of higher order of the curve. The true local maxima are in fact shifted slightly to the right from these points, as in case of $a = 3$. The phenomenon of overhangs will be further elucidated in Chapter 5. However, apart from the qualitative remarks in the context of the plus-minus approach and the additional insight provided by the approach in Chapter 5, a detailed explanation of these overhang effects is still missing.

Two further remarks regarding the turnstile dynamics method presented here are in order: First, with respect to the Markov partition series of the slope introduced in Section 2.3.2, it is clear that the turnstile dynamics series distinguished in Fig. 2.12 refer to Markov partition series with end points of the generating orbit of $\delta = 0$ and $\delta = \varepsilon$, respectively. Thus, on the one hand, certain Markov partition series have been related to certain features of the structure of the $D(a)$ -curve via turnstile dynamics. On the other hand, it has been claimed that computing solely Markov partition diffusion coefficients gives a representative $D(a)$ -curve for any region of the slope. One may raise the objection that, this way, Markov partition values show only special features of the curve. However, apart from the denseness conjecture regarding Markov partitions stated in Conjecture 2.1 it should be taken into account that to compute Markov partitions it suffices to consider only reduced maps and their topology. These reduced maps model only internal box motion, whereas turnstile dynamics, and with it the structure of the $D(a)$ -curve, feature the occurrence of certain dynamical correlations with respect to

⁴⁷The agreement has been checked to persist at least up to a level of extrema of second order.

⁴⁸The more precise values are $a \simeq 2.41421/D(a) \simeq 0.10358$, $a \simeq 2.41645/D(a) \simeq 0.10493$; and for a maximum of second order, e.g., $a \simeq 2.20557/D(a) \simeq 0.04737$, $a \simeq 2.20724/D(a) \simeq 0.04744$.

i	0	1	2	3	4
$s_a(i)$	3.902	3.423	3.186	3.079	3.033
$s_D(i)$	1.128	1.510	1.721	1.892	2.038

TABLE 2.1. Scaling factors for the initial region $2 \leq a \leq 3$ of the parameter-dependent diffusion coefficient $D(a)$, see text.

external jumps between boxes. Thus, computing the diffusion coefficient curve via Markov partitions and applying turnstile dynamics does not necessarily lead to a contradiction.

Second, since turnstile dynamics points seem to separate self-similar regions, it is suggestive to use them as a tool to do some scaling. Series γ -values are especially suitable for this purpose, because they form a series of points which converges monotonically to $a = 3$, defining self-similar regions of decreasing size. These regions have been scaled according to the size of the intervals of the slope and of the respective diffusion coefficient intervals, defined by⁴⁹

$$\begin{aligned} \Delta a_i &:= a(\text{series } \gamma\text{-point } (i+1)) - a(\text{series } \gamma\text{-point } i) \\ \Delta D_i &:= D(\text{series } \gamma\text{-point } (i+1)) - D(\text{series } \gamma\text{-point } i) \quad , \\ & \quad i = 0, \dots, 4 \quad . \end{aligned} \quad (2.45)$$

To obtain scaling factors, the fractions

$$s_a(i) := \frac{\Delta a_i}{\Delta a_{i-1}} \quad \text{and} \quad s_D(i) := \frac{\Delta D_i}{\Delta D_{i-1}} \quad (2.46)$$

have been computed. They led to the two series of values given in Table 2.1. $s_a(i)$ seems to converge quite rapidly to a value around 3, whereas $s_D(i)$ approaches not that fast a value maybe between 2 and 3, but this is of course no more than a guess based on the first five values of two infinite series, since the data set of slopes and $D(a)$ -values is not sufficient for obtaining better results. At least these values suggest that some quantitative scaling is possible in this region.

At this point, it should be stressed that the region below $a = 3$ is special, compared to any other region of the slope: Firstly, the structure of the curve is remarkably simple, as shown in Fig. 2.12. Secondly, the number of wiggles of higher order is not constant with increasing order, but grows according to the structure described by the turnstile dynamics performed above. This is in contrast to the behaviour of $D(a)$ in the ranges $4 \leq a \leq 5$ and $6 \leq a \leq 7$, where one may have expected similar generalities. Thirdly, the region below $a = 3$ is the only one which is simple

⁴⁹ $a = 2$ has been taken here as series γ point 0.

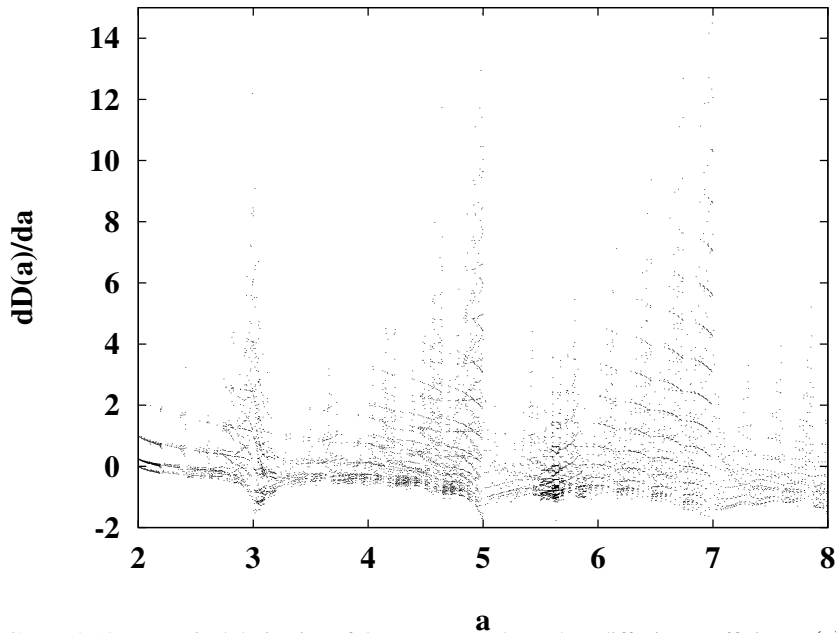


FIGURE 2.13. Numerical derivative of the parameter-dependent diffusion coefficient $D(a)$ of map \mathcal{L} .

enough so that turnstile dynamics can successfully be applied at all, and this region seems to provide some simple scaling laws. All this nice behaviour suddenly breaks down at the value $a = 3$, which is marked by the largest overhang of the whole curve. Therefore, it might be assumed that the point at $a = 3$ separates regions of fundamental different dynamical behaviour of the map, i.e., the dynamics seems to be sufficiently simple below, but suddenly gets quite complicated above this value. In fact, there is further evidence that such a transition exists, as will be discussed in detail in Chapter 4.

At last, another interesting feature of the parameter-dependent diffusion coefficient for map \mathcal{L} shall be pointed out. To obtain Fig. 2.13, the first “derivative” of the $D(a)$ -curve of Fig. 2.10 has been computed with respect to the full data set of $D(a)$ -values available. This has been done in linear approximation, i.e., two adjacent points of the data set have been connected with straight lines, and the “derivative” $D'(a) := \Delta D / \Delta a$ for $\Delta a \ll 1$ has been computed. However, since the curve of $D(a)$ is expected to be nowhere differentiable with respect to the slope (see Section 5.2), the derivative defined above should be better denoted as a “pseudo-derivative”, i.e., as a kind of mean value of ΔD over tiny regions of Δa

which are approaching zero. Thus, the pseudo-derivative presented in Fig. 2.13 is mathematically not well-defined. Nevertheless, the numerical results turn out to be quite reasonable in the sense that they reflect to a certain degree the fractal structure of the actual $D(a)$ -curve. For instance, the three “bands” right above $a = 2$ seem to be due to the “triangle-like” self-similar structure of the region presented in Fig. 2.13, and the “bursts” at odd integer values correspond to the occurrence of local maxima and to the deformations of simple self-similar structures.⁵⁰ More details of this curve will be discussed in Section 5.2.

2.5 Conclusions

(1) A simple model for deterministic diffusion has been defined and discussed, where the microscopic scattering rules can be varied smoothly by switching a single control parameter. The diffusion coefficient of this model has been computed for a broad range of parameter values and shows a fractal structure as a function of the slope of the map. This result appears to be the first example of a dynamical system whose diffusion coefficient has an unambiguously fractal structure.

(2) A general method to compute parameter-dependent diffusion coefficients for a whole class of piecewise linear maps has been developed. It is based on the first passage method, which provides the definition of the diffusion coefficient for the dynamical system, in combination with the use of Markov partitions and transition matrices, which have been employed to solve the Frobenius-Perron equation of the dynamical system. For periodic boundary conditions, the parameter-dependent diffusion coefficient could be related to the second largest eigenvalue of the topological transition matrix. This method provides analytical solutions in simple cases and is also accessible to numerical implementations.

(3) The method described above has also been applied to absorbing boundary conditions. Long-range boundary layers have been found in the eigenmodes of the deterministic dynamical system. They also show up in quantitative calculations of the diffusion coefficient.

(4) Certain limits of the first passage method in combination with the use of transition matrices have been discussed: Drawbacks are especially the restriction to certain initial probability densities suitable for the application of transition

⁵⁰It should be remarked that in Fig. 2.13 the number of slopes for which $D(a)$ -values have been calculated is not homogeneously distributed over the whole range $2 \leq a \leq 8$, but that the number of points per interval is greater in certain regions of the slope, as, e.g., right above $a = 2$, $a = 3$ and around $a = 5.6$. These regions thus show up as slightly pronounced parts in the derivative plot, however, the structure of the curve does not seem to be influenced by it.

matrices, as well as the “external” definition of the diffusion coefficient by the “matching eigenmodes” procedure of first passage. It turned out that this procedure is not well-defined anymore for smaller eigenmodes of the dynamical system.

(5) A systematical way to find Markov partitions for the class of maps under consideration has been developed. This method has been used as the basis for computing the parameter-dependent diffusion coefficient for the dynamical system mentioned above. For this map, as well as for the whole class of maps under consideration, the Markov partitions are conjectured to be dense in the set of parameter values.

(6) A large number of eigenvalue problems of topological transition matrices, based on Markov partitions, has been solved numerically to compute the parameter-dependent diffusion coefficient for the model system. In the course of these calculations, the reliability of well-known standard software routines for computing eigenvalue spectra has been checked critically, and numerical errors have been pointed out.

(7) Certain large- and small-scale structures in the eigenmodes of the topological transition matrices have been found. The large-scale structures support the existence of statistical diffusion in the dynamical system, whereas the small-scale structures refer to the specific microscopic deterministic dynamics of the model system. These results suggest that the strength of the fractal diffusion coefficient is related to the fine-scale structure of the eigenmodes.

(8) A conjecture about the existence of diffusion coefficients for a broad class of one-dimensional maps has been made. This conjecture may shed more light on the origin of diffusion generated by a simple deterministic dynamical system and may show a way how to put the theory outlined in this chapter onto more solid mathematical grounds.

(9) Qualitative explanations for the structure of the parameter-dependent diffusion coefficient over the full range of parameter value have, to a certain extent, been provided by simple heuristic considerations.

(10) A more refined “turnstile dynamics” has been developed as a more quantitative approach to explain the structure of the parameter-dependent diffusion coefficient. It works in certain regions of the parameter values and provides a starting point for a scaling of certain self-similar structures.

(11) By employing these qualitative and quantitative methods, certain interesting features of the diffusion coefficient have been discussed, i.e., the phenomenon of “overhangs” at local extrema, and the special simple character of an “initial region” for small parameter values, where diffusion sets in.

(12) The numerically computed pseudo-derivative of the parameter-dependent diffusion coefficient seems to provide another characteristic property of fractal diffusion coefficients.

(13) It may be conjectured that similar results are obtained not only for other simple one-dimensional periodic dynamical systems of the type of the one considered here, but that fractal diffusion coefficients also show up in more complex dynamical systems, as, e.g., climbing-sine maps. They may be encountered as well in higher-dimensional dynamical systems, as, e.g., in certain two-dimensional maps, where oscillations of the diffusion coefficient with respect to a control parameter have already been observed. Moreover, fractal transport coefficients may even occur in more realistic dynamical systems, as, e.g., in the periodic Lorentz gas (see also Chapter 6).

3

Dynamics of deterministic diffusion

In the previous chapter, a parameter-dependent fractal diffusion coefficient has been obtained for the deterministic dynamical system denoted as map \mathcal{L} , which has been introduced in Section 2.1. The diffusion coefficient has been computed only in the long-time limit so far, i.e., as a time-independent quantity. Nevertheless, its value is very well determined by the complete deterministic dynamics of the system, i.e., it is sensitive even to certain short-time characteristics of the single orbits. This feature has been employed in the methods of “plus-minus dynamics” and “turnstile dynamics” of the previous chapter, which served to explain the oscillations in certain regions, and on certain scales, of the diffusion coefficient curves.

This leads to the problem of this chapter, which is the *dynamics* of deterministic diffusion. The goal is to understand the time-dependent behaviour of ensembles of diffusing particles in map \mathcal{L} by analyzing certain statistical dynamical quantities. For this purpose, suitable numerical methods will be developed (see Section 3.1) to evaluate the time-dependent probability density, the time-dependent diffusion coefficient, and the velocity autocorrelation function of the dynamical system (see Section 3.2). A discussion of the characteristics of these quantities should shed more light on the origin of fractal diffusion coefficients with respect to the *complete* dynamics of a deterministic dynamical system (see Section 3.3). This may enable a more general characterization of the deterministic dynamics in the class of periodic piecewise linear maps which has been denoted as class \mathcal{P} in Section 2.1.

3.1 Principles of numerics: Iteration method and computer simulations

The first numerical method to get access to time-dependent quantities is based on techniques developed in Chapter 2, i.e., especially on the transition matrix method of Section 2.3.1. This method has been slightly varied. The key idea is to take a close look at the Frobenius-Perron matrix equation Eq.(2.18) again. For applying the first passage method, this equation has been solved previously via solving the eigenvalue problem of the topological transition matrix and performing spectral decomposition of the Frobenius-Perron operator into its eigenmodes. This provided analytical solutions for the diffusion coefficient in some special cases and has also been employed as a basis for numerical computations.

However, numerically there is a much simpler way: If there exists a topological transition matrix $T(a)$ at slope a for a chain of boxes of class \mathcal{P} , the Frobenius-Perron matrix equation (2.18) can be written as¹

$$\rho_n = \frac{1}{a^n} T^n(a) \rho_0 \quad , \quad (3.1)$$

i.e., the equation gets simply solved via iteration of topological transition matrices. This enables the computation of the full time-dependent probability density vector, or the probability density, respectively, $\rho_n \equiv \rho_n(x)$ and all dynamical quantities defined by averages over this density. The method shall therefore be called *iteration method* and may be best described as being semi-analytical, since it employs no statistical sampling or other kinds of numerical approximations. Similar methods, although based on stochastic transition matrices, have already been developed by Li [Li76] and Fujisaka and Grossmann [Fuj82].

There are several advantages of this iteration method in comparison to the numerical eigenvalue method of the previous chapter:

- It is technically quite trivial, and it is more save in numerical implementations than the eigenvalue method, because it does not involve the solution of complex eigenvalue problems.
- The computation of full probability densities and respective averages gives for the first time access to time-dependent dynamical systems quantities, which was not provided by the eigenvalue method before.
- The parameter-dependent diffusion coefficient $D(a)$ can be obtained by the iteration method via the second moment of the probability density and gives values with an excellent precision, as will be discussed later. Moreover, the method requires much less computing time than the eigenvalue method.

The only disadvantage of the iteration method is that it provides only probability

¹Again, as in Chapter 2 for simplicity an index a for the slope has been neglected here.

density averages and no ensemble averages, although the time-dependent statistical dynamical quantities of interest here, especially the velocity autocorrelation function and the mean square displacement, are correctly defined only via ensemble averages. Therefore, certain approximations for these functions via probability densities will be introduced such that time-dependent quantities can be computed via probability density averages, which get equal to the original ensemble averages in the limit of time to infinity. Whether these approximations represent the dynamical behaviour of the original quantities under consideration qualitatively and quantitatively reasonably well, has to be checked in detail.

To produce ensemble averages, which are at least by definition correct, *computer simulations* have been performed. As a second independent method to compute time-dependent dynamical quantities, they will serve for checking the validity of the approximations introduced on the basis of probability density averages. To a certain degree, this will also go *vice versa*, since doing computer simulations in supposedly “simple” dynamical systems as class \mathcal{P} -maps is to a certain degree questionable in itself: For example, for Bernoulli maps it is well-known that computer simulations give completely wrong results because of shifting orbits straight into the range of numerical roundoff-errors after a few iterations [Ott93, Pei92]. Furthermore, fundamental miscalculations may occur in maps where the existence of a natural measure, and of a respective invariant probability density, are not in advance clear [Boy84, Gor88, Boy90].² Thus, performing computer simulations in class \mathcal{P} -maps does not guarantee reliable results from a fundamental dynamical systems theory point of view (see also Refs. [Bec93, Ott93, Sch89]). Apart from these considerations, there is of course the question about conventional numerical errors of statistical quantities, where computer simulations can be expected to be significantly behind iteration method solutions.

Thus, the goal of simulations here is basically two-fold: First, to confirm the results of the iteration method, and second, to verify the usefulness of computer simulations themselves by matching the respective results to the iteration method solutions. Strictly speaking: neither computer simulations nor the iteration method do guarantee correct results, at least not for time-dependent dynamical quantities, because of fundamental problems of different kinds. However, if the results of these two independent methods match to a sufficiently high degree, this could be regarded as a hint that both methods work, and that they lead to results which are in certain limits correct.

²The notations *natural* and *physical* measure are synonymous and are used often in the physics literature [Ott93, Lev89]. Mathematicians prefer to talk about *Kolmogorov* and *Sinai-Ruelle-Bowen (SRB)* measures [Eck85, dM93, Las94]. All these measures are related to each other and are usually supposed to exist for performing computer simulations. In fact, if the dynamical system is suitably “nice”, all these measures are identical [Boy90].

Another feature of computer simulations is that they are remarkably simple to perform for class \mathcal{P} -maps. They may be programmed even by non-specialists without too much effort and may run in principle (apart from numerical precision problems) on personal computers or even pocket calculators. Thus, one may wonder whether the precision of computer simulations is sufficient to see anything of a fractal structure in so-computed diffusion coefficients. Moreover, there is no restriction to Markov partition values of the slope anymore by simulations so that non-Markovian values can be checked as well, at least in the limits of the numerical precision available.

3.2 Time-dependent statistical dynamical quantities: results

The two numerical methods described above have been applied in detail to the dynamical system map \mathcal{L} . For the following computations, the coordinate system of the chain of boxes has been shifted about $L/2$ in the x -coordinate and about $1/2$ in the y -coordinate, in comparison to how it has been used in Chapter 2. Thus, at odd chainlength L the origin of the coordinate system is exactly in the center of the 0th box. An initial density of particles $\rho_0(x)$ has been chosen, which is uniform in the 0th box, $\rho_0(x) = 1$, $-1/2 < x \leq 1/2$. Since map \mathcal{L} is periodic, it suffices to consider this initial density for probability density averages as well as for ensemble averages. The chainlength has always been determined such that the dynamics of the map does not get affected by any boundary conditions. The three Markov partition series defined in Section 2.3.2 have been employed again, and Markov partitions and topological transition matrices have been computed numerically by the procedures outlined in Section 2.3. All computations have been performed in double precision.

Although it does not seem to be very common anymore to give statistical error estimates for numerically computed quantities in dynamical systems theory, at least not for one-dimensional dynamical systems of the type considered here (see almost all references cited), it shall be tried to give some error estimates in the following. It should be clear that any quantitative error estimates consist only of statistical errors, which have been calculated via parameter variation.³ As has been discussed in the previous section, this does not exclude hidden systematical

³For the iteration method, the only error-producing variable is basically the initial condition of the Markov partition generating orbit, which has been computed up to a precision of 10^{-8} . For computer simulations, the parameters varied are the number of particles, their initial conditions, the grid size used to compute probability density averages over particles, the iteration time for the particles and the slope of the map.

errors induced by applying the computer to chaotic dynamical systems. More details will be given below.

3.2.1 Probability densities

Solutions for probability densities have been obtained in three different ways: Firstly, in applying the iteration method n iterations of $\rho_0(x)$ have been performed according to the Frobenius-Perron matrix equation Eq.(2.18), or Eq.(3.1), respectively, for given Markov partition value of the slope. Secondly, for computer simulations 500,000 particles have been distributed uniformly in the 0th box and iterated individually by applying the equations of map \mathcal{L} n times. Thirdly, the diffusion equation Eq.(2.9) has been solved analytically with respect to the initial density defined above, with the diffusion coefficient being fixed by the respective numerically computed parameter-dependent diffusion coefficient.

As an example, Fig. 3.1 shows the probability density results for the slope $a \simeq 3.0971$, which defines a Markov partition of fifteen parts per box, based on a seven times iterated generating orbit. In Fig. 3.1 (a), the probability density of the complete dynamical system map \mathcal{L} has been computed at three different times. The iteration method densities may be considered as exact, since no significant numerical error could be estimated for the graphs presented here. They behave qualitatively, i.e., on a large scale, very much like Gaussian functions and match more quantitatively very well to the Gaussian solutions of the diffusion equation, given by the dashed lines, apart from a pronounced periodic fine structure. As can be seen in both diagrams, the fine structure gets weaker in the wings of the distribution, where the iteration method probability densities approach the solutions of the diffusion equation increasingly better. The behaviour in the wings has been magnified in Fig. 3.1 (c). One observes first details of the fine structure with clouds of dots around the straight lines, which again represent results of computer simulations.

Fig. 3.1 (d) finally proves that the periodic fine structure, which can be seen in magnification (c), is indeed due to the internal dynamics of the single boxes of the chain: To obtain this plot, the box probability density for the reduced map Eq.(2.38) has been computed. The symmetry of the density with respect to $x = 0$ reflects the central symmetry of the box map, and the piecewise constant parts are due to the map being piecewise constant. The symbols with error bars give results from computer simulations. They match quite well to the iteration method results, which again appear without significant errors. In fact, box probability density solutions can, to a certain extent, also be calculated analytically, as will be shown in Section 5.4. In Chapter 5, much more mathematical and other details about box probability densities for map \mathcal{L} and their relevance for diffusion coefficients will be provided.

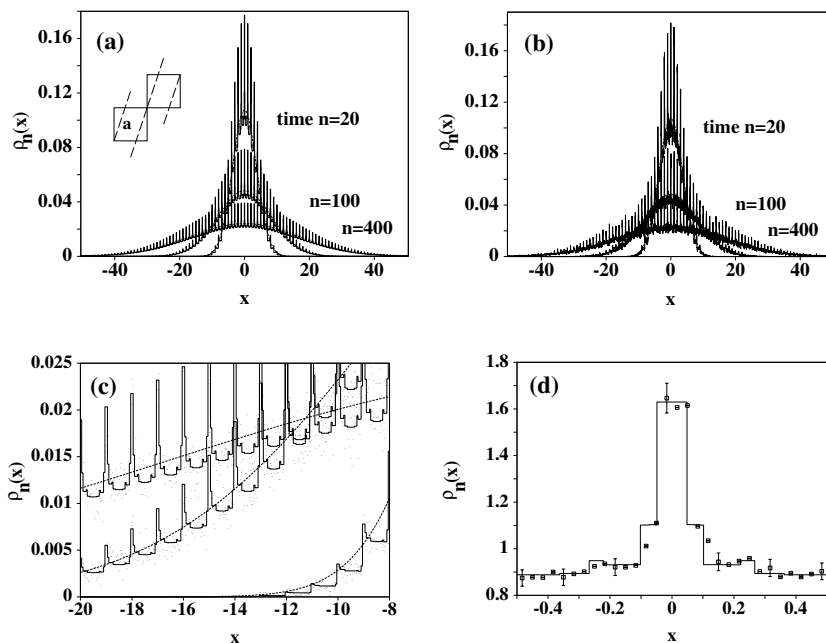


FIGURE 3.1. Example of a probability density for map \mathcal{L} , here slope $a \simeq 3.0971$: Results in diagram (a) provided by the iteration method (see text), in diagram (b) and (c) by the iteration method as well as by computer simulations, and in diagram (d) only by computer simulations. The dashed lines in diagrams (a), (b) and (d) represent analytical solutions of the diffusion equation Eq.(2.9).

In comparison, Fig. 3.1 (b) shows probability densities obtained from computer simulations. Again, the dashed lines give the respective solutions of the diffusion equation. One realizes that, in fact, it is possible to get qualitative correct probability densities from computer simulations which even contain some fine structure. Statistical errors are difficult to obtain for these results, but could roughly be estimated as up to 15% in the peak, and up to 100% in the wings. Computer simulation results for probability densities of other chains of maps have already been presented in Refs. [Fuj82, Gro83a], but no fine structure has been described in these references.

In summary, the probability density results show that the deterministic dynamics of map \mathcal{L} takes place on two different scales: Firstly, on a large scale which is related to the full chain of boxes and is characterized by diffusive behaviour in agreement to the statistical diffusion equation, indicated by Gaussian probability distributions. And secondly, there appears a fine structure which reflects the in-

ternal deterministic box dynamics of the dynamical systems and which shows up periodically continued in the full probability density. Analogous numerical results have been found for a large number of other Markov partition values of the slope. Moreover, supposedly non-Markovian slopes⁴ have been checked by computer simulations, and Gaussian curves have been observed as well. These results may offer answers to some problems raised in the previous chapter: With respect to Gaussian probability densities on a large scale, it has been obtained numerical evidence that map \mathcal{L} is diffusive for any Markov partition value of the slope as well as for any non-Markovian value. And the problems about spectral decomposition and diagonalization of topological transition matrices may be caused by the detailed interplay between box probability step function and large-scale Gaussian probability distribution, since, on a fine scale, the eigenmodes of non-trivial topological transition matrices seem to mix in a way which is different to that of a large-scale Gaussian, and therefore make simple analytical solutions of the Frobenius-Perron equation not possible anymore.

Analogous results for probability densities have been obtained for another class \mathcal{P} -map (see Chapter 4). This may motivate the following, more general conjecture:

Conjecture 3.1 (Central limit theorem) *The probability density of uniquely ergodic class \mathcal{P} -maps obeys a central limit theorem on a large scale.*

A similar conjecture has been mentioned in Ref. [Gas92a]. There exists a rich mathematical literature about proofs of central limit theorems for one-dimensional maps (see, e.g., Refs. [Hof82, Ish86, Ish89] and references therein), however, usually maps of an interval onto itself have been considered, which are not identical to the periodic chain of boxes introduced as class \mathcal{P} .

3.2.2 Probability density averages and ensemble averages

Since the iteration method gives access to the full probability density, the moments of this function are the fundamental quantities for this method to obtain more information about the time-dependent behaviour of the dynamical system under consideration.

The k th moment of the probability density $\rho_n(x)$ is defined by

$$\langle x_a^k(n) \rangle := \int dx \rho_n(x) x^k(n) \quad . \quad (3.2)$$

⁴Slopes which do not provide any Markov partition seem to appear, among others, at all non-integer rational numbers above slope $a = 2$ [Gro95a].

Thus, for $k = 2$ the *second moment* can be obtained by the probability density average

$$\langle x_a^2(n) \rangle := \int dx \rho_n(x) x^2(n) \quad (3.3)$$

and may be used to model the ensemble average of the *mean square displacement*

$$msd_a(n) := \frac{1}{N} \sum_{i=1}^N (x_i(n) - x_i(0))^2 \quad , \quad (3.4)$$

where the average has been taken over N single particles, represented by points on the real line.

Fig. 3.2 (a) shows some examples of numerical results obtained for these two quantities by iteration method and computer simulations. One first observes that the simulation results for the second moment match usually with statistical errors less than 1% to the iteration method results, which again contain negligible numerical errors. Since in the following the second moment will be taken in replacement of the mean square displacement for computing diffusion coefficients in case of the iteration method, the results should be compared to the mean square displacement values obtained from computer simulations, as presented in the small inset. One observes quantitative deviations at $n = 0$, which occur since the second moment of the initial density is not equal to zero, and slight qualitative deviations in the initial region for times $n \leq 3$. For larger times, all graphs behave very soon linearly, as can be expected for diffusive motion, and the respective slopes of second moment and mean square displacement, which are decisive for computing time-dependent diffusion coefficients, agree even quantitatively very well.

Fig. 3.2 (b) shows the *curtosis* of three probability densities, which is related to the fourth moment of a probability density according to

$$cu_a(n) := \frac{\langle x^4(n) \rangle}{\langle x^2(n) \rangle^2} - 3 \quad . \quad (3.5)$$

For Gaussian functions, the curtosis is exactly equal to zero. If the maximum of a function is less than the one of a Gaussian, its curtosis is less than zero, and if it is greater, its curtosis is greater than zero [Sac84, Mar71]. For maps of class \mathcal{P} , the curtosis provides not only a necessary, but also a sufficient condition to prove that their probability densities are approaching Gaussians: According to a theorem of statistical mathematics [Har87], it can be shown that the curtosis and the *skewness*, which is proportional to the third moment, being equal to zero is a sufficient condition to check for a Gaussian distribution. Since class \mathcal{P} -maps are per definitionem without any drift, the first and the third moments of their probability densities are zero. Thus, the skewness is also equal to zero, and it suffices to show that the curtosis vanishes for applying the theorem.

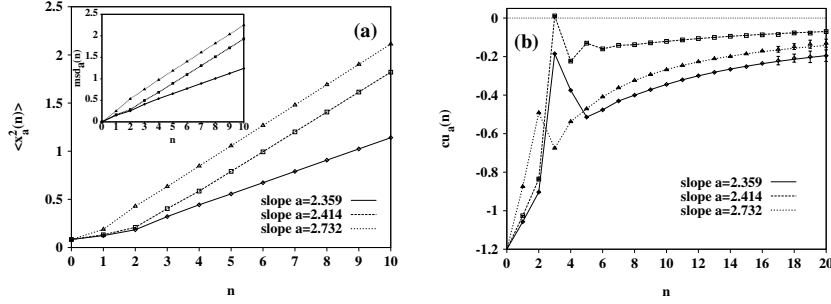


FIGURE 3.2. Moments of probability densities and mean square displacements for three different Markov partition values of the slope of map \mathcal{L} : Diagram (a) shows the second moments of three probability densities, cf. Eq.(3.3). The inset of (a) gives the respective mean square displacements, cf. Eq.(3.4), and diagram (b) presents the kurtosis of the same three probability densities, cf. Eq.(3.5). Semi-analytical iteration method results (see text) are represented by lines, computer simulation results by symbols with error bars of statistical errors, if exceeding the size of the symbols. The inset in (a) consists only of simulation results.

Fig. 3.2 (b) thus provides quantitative evidence that the respective probability densities of map \mathcal{L} are indeed very close to Gaussian distributions, and that they are getting monotonically more close to them with larger times n . As for the second moment, the initial values at time $n = 0$ are determined by the analytical results for the initial density being uniform in the center box. There is again an excellent quantitative agreement between simulation and iteration method results, although the precision of the simulation data is soon getting worse for larger times. Besides, one notes some pronounced “wiggles” in the graphs at small times, which especially in case of $a \simeq 2.414$ seem to start periodically, but decay very fast. Such wiggles can also be observed in Fig. 3.3 (a), which gives three results for time-dependent diffusion coefficients, computed in different ways for one value of the slope. As labeled in the diagram, the curve with the diamonds has been obtained from simulation data via the ensemble average

$$D_a^{sim}(n) := \frac{msd_a(n) - msd_a(n-1)}{2}, \quad (3.6)$$

which in the limit of time to infinity leads to the exact *Einstein formula* for the diffusion coefficient

$$D(a) \equiv D_a(\infty) = \lim_{n \rightarrow \infty} \frac{msd_a(n)}{2n}. \quad (3.7)$$

Analogously, but nevertheless in an approximation, a second time-dependent diffusion coefficient has been computed from iteration method results, i.e., via prob-

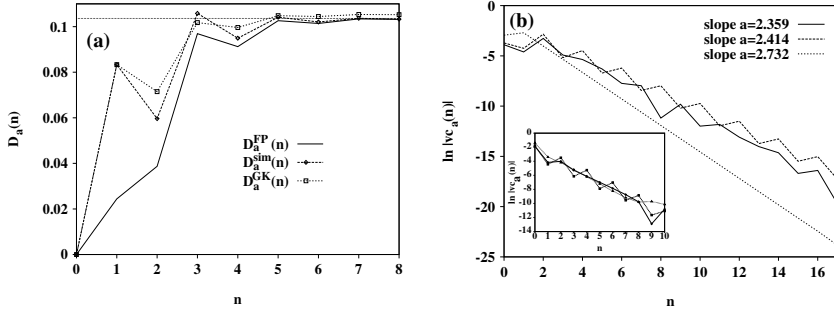


FIGURE 3.3. Two time-dependent statistical dynamical quantities for up to three different Markov partition values of the slope of map \mathcal{L} : Diagram (a) shows the time-dependent diffusion coefficient for the slope $a \simeq 2.414$, computed by three different methods. Diagram (b) contains velocity autocorrelation functions for three different slopes, computed via the iteration method as an approximative solution in the main diagram, and obtained from computer simulations in the small inset (see text).

ability density averages by solving the Frobenius-Perron equation according to

$$D_a^{FP}(n) := \frac{\langle x^2(n) \rangle - \langle x^2(n-1) \rangle}{2} . \quad (3.8)$$

The result is given by the bold line without symbols in Fig. 3.3 (a). Thus, the time-dependent diffusion coefficient is determined by the slope of the mean square displacement and by the slope of the second moment in these two formulas. In the limit time n to infinity, the probability density average formula for diffusion leads again to an Einstein formula

$$D(a) \equiv D_a(\infty) = \lim_{n \rightarrow \infty} \frac{\langle x_a^2(n) \rangle}{2n} , \quad (3.9)$$

which gives correct values for the time-independent diffusion coefficient by neglecting any correlations in the long-time limit [Sch89]. As a third method, the Green-Kubo formula of diffusion can be employed [Gas92a],

$$D_a^{GK}(n) := \frac{vc_a(0)}{2} + \sum_{i=1}^n vc_a(i) . \quad (3.10)$$

$vc_a(n)$ stands for the velocity autocorrelation function of the map,

$$vc_a(n) := \frac{1}{N} \sum_{i=1}^N v_i(n)v_i(0) , \quad (3.11)$$

where the correlation function is defined via an ensemble average over N particles with velocities $v_i(n)$. The horizontal line in Fig. 3.3 (a) marks the exact value of the diffusion coefficient $D(2.414)$ in the limit of time to infinity, computed by analytical methods.

In other words, the different graphs in Fig. 3.3 (a) are based on correct diffusion coefficient formulas in case of the Green-Kubo formula Eq.(3.10) and in case of the ensemble average Einstein formula Eq.(3.6). However, both formulas could only be evaluated by computer simulation results, the precision of which is somehow questionable from a fundamental point of view (cf. 3.1), disregarding a statistical numerical error of less than the size of the symbols (usually up to 1%). On the other hand, Eq.(3.8) defines an approximation of the correct ensemble average Einstein formula via probability density averages. Results for these averages can be obtained with negligible numerical errors from the iteration method, but now the quality of the approximation is not *per se* clear. Nevertheless, Fig. 3.3 (a) shows that all these different solutions agree reasonably well, at least qualitatively. For the first few iterations, the iteration method solution is clearly apart from the other two curves, but it is soon getting closer to them, and for values above time $n > 5$ it is almost indistinguishable from the ensemble average Einstein values. On the other hand, the two simulation results agree qualitatively quite well, but for larger times n one can see that the Green-Kubo result stays slightly above the precise long-time value of the diffusion coefficient. This quantitative deviation seems to be due to numerical problems beyond the range of simple statistical errors, as is well-known in the literature, since no refined methods have been employed here for computing velocity autocorrelation functions.⁵

In contrast to these problems, the two Einstein formula results converge quantitatively quite well, and they approach the exact diffusion coefficient value extremely fast: The iteration method applied here leads to values for $D(a)$ being exact up to an order of 10^{-7} , which is about three orders of magnitude better than achieved by solving eigenvalue problems numerically. Its error with respect to convergence in time n is, after maximally fifteen iterations, negligible compared to the error produced by other quantities, i.e., especially by the precision of the initial condition

⁵In fact, for other Markov partition values of the slope (e.g., $a \simeq 2.359$ and $a \simeq 2.732$) the difference between the numerical Green-Kubo results and the precise values of the diffusion coefficients in the long-time limit is even considerably worse, and there is no convergence to the exact values at all. This may be avoided, e.g., by averaging further over multiple ensembles of initial conditions, by employing time-translational invariance of the system [Woo71], or by using the Wiener-Khinchin theorem [Rei87, Eck85, Wag92]. Thus, although objections have been raised about the validity of the Green-Kubo formula, with respect to the results obtained here there is no reason to assume that something is fundamentally wrong with this approach in the case of chaotic dynamical systems, as has recently been discussed by several authors in the literature, see Refs. [Eva90b, Kub92, Suh94, Bia94, Dor95a], and references therein.

of the Markov partition generating orbit. Moreover, by restricting the iteration method solely to the computation of time-independent diffusion coefficients, the computing time needed for iterating large transition matrices up to a size of 1,300 x 1,300 is about 2 CPU seconds for each diffusion coefficient value (on IBM RS-6000), which is again about two orders of magnitude better than provided by the eigenvalue solutions before.⁶

The computer simulations provide at their best parameter-dependent diffusion coefficients with a precision of about 10^{-2} after up to twenty iteration steps.⁷ Thus, it can be expected that parameter-dependent diffusion coefficients computed by simulations do not show many details of respective curves, except certain oscillations, and they may not give much evidence for a profound fractal structure, see, e.g., the results presented in Ref. [Tse94].

Apart from such quantitative considerations, one finds again pronounced wiggles in the time-dependent diffusion coefficient shown in Fig. 3.3 (a), which occur at a certain period. One should compare these oscillations and their period to the respective curtosis result for this value of the slope in Fig. 3.2 (b). Again, the strength of these wiggles ceases with larger times. It should be noted that such wiggles show up as well in the approximative solution via probability densities, which confirms the quality of this approximation even on a fine scale, at least qualitatively.

Finally, numerical results for the velocity autocorrelation function shall be discussed. They are shown in the semi-logarithmic plots of Fig. 3.3 (b), where the logarithms of absolute values have been plotted versus the time n . Two versions of the velocity autocorrelation function have been computed for the three values of the slope already considered in Fig. 3.2: the correct definition in Eq.(3.11), which can be extracted from computer simulations, and an approximation, defined by

$$vc_a^{FP}(n) := D_a^{FP}(n+1) - D_a^{FP}(n) \quad , \quad (3.12)$$

where $D_a^{FP}(n)$ is the probability density average diffusion coefficient of Eq.(3.8). To obtain this approximation, the Green-Kubo formula has been inverted, i.e., Eq.(3.10) has been differentiated with respect to the discrete time n , and n has been chosen such that this velocity autocorrelation function is well-defined at $n=0$. The purpose of this procedure is to obtain an approximation $vc_a^{FP}(n)$ for the correct velocity autocorrelation function $vc_a(n)$, which can be computed solely via probability density averages and, this way, is accessible to solutions of the Frobenius-Perron equation by the iteration method.

The brief discussion of the Green-Kubo formula showed that computer simulation

⁶It has been taken advantage of the fact that the topological transition matrices are here usually very sparse.

⁷The same efficiency and precision has been obtained for non-Markovian slopes.

results for the ensemble average velocity autocorrelation function on the level performed here are quantitatively not very reliable. On the other hand, it is not clear in advance whether the alternative, i.e., probability density approximation of Eq.(3.12), leads to reasonable solutions. Nevertheless, the results for both versions in Fig. 3.3 (b) agree qualitatively well, apart from slight deviations at the first iteration $n = 1$, although their quantitative values are quite different. This confirms the qualitative validity of simulations to compute these quantities. The peculiar character of velocity autocorrelation functions shows up rather at larger times, i.e., generally for $n > 10$ in computer simulations and for $n > 20$ in the iteration method, where strong numerical precision problems set in, see, e.g., the inset in Fig. 3.3 (b). The velocity autocorrelation functions thus provide a lower boundary for the number of iterations which can be performed in both methods before certain numerical roundoff errors must be expected to show up. On a fine scale, one observes again certain wiggles which seem to be persistent, i.e., the strength of which does not decrease with larger times in this plot. These wiggles show up very clearly in the iteration method results for at least two values of the slope,⁸ and one also encounters them to a certain degree in the simulation results. Graphs of time-dependent statistical dynamical quantities analogous to the ones illustrated by the examples in Fig. 3.2 and Fig. 3.3 have been found not only for a large variety of other Markov partition values of the slope of map \mathcal{L} , but also for another class \mathcal{P} -map (see Chapter 4). Moreover, non-Markovian slopes have been checked by computer simulations, with similar results in the limits of precision accessible by simulations. This leads to the following conjecture:

Conjecture 3.2 (decay of velocity autocorrelation functions) *The velocity autocorrelation function of uniquely ergodic class \mathcal{P} -maps decays exponentially on a large scale.*

The exponents of the velocity autocorrelation functions have been found to vary in a range of -0.2 to 2.5 for map \mathcal{L} and do not appear to be of a universal value. In simple cases, plain exponential velocity autocorrelation functions have already been computed analytically for certain class \mathcal{P} -maps [Gas92a], and a similar conjecture as the one above has already been given in the same reference. The question about a proper behaviour of correlation functions is of very fundamental physical interest, as has been shown in discussions about the occurrence of long-time tails in various types of dynamical systems in statistical physics [Dor75, Dor77, Lee88, Viv83, Mac83a, Bun85], and is intimately connected to the problem of the existence of transport coefficients. Thus, the conjecture above

⁸The semi-logarithmic plot of absolute values cancels wiggles in certain cases, see the following section.

can also be interpreted as a conjecture that there are no long-time tails in this class of dynamical systems.

3.3 Fractal diffusion coefficients, time-dependent dynamical quantities, and stability of dynamical systems

An important feature of the time-dependent quantities discussed above, which has been pointed out, but which has not yet been explained, is the occurrence of certain wiggles in the curtosis, in the time-dependent diffusion coefficient and in the velocity autocorrelation function. As an example, these wiggles will be analyzed for the Markov partition values of the slope considered above: For the slope $a \simeq 2.414$, pronounced wiggles have been observed for all three dynamical quantities mentioned above, and in all these quantities the wiggles seem to appear with a period of two. For $a \simeq 2.359$, the curtosis shows some non-monotonicities at the beginning, and the velocity autocorrelation function provides wiggles which seem to occur with a certain periodic, although more complex structure than for $a \simeq 2.414$. And for $a \simeq 2.732$, one obtains again slight wiggles in the curtosis, but seemingly nothing in the velocity autocorrelation function. However, it should be mentioned that wiggles occur clearly in the original correlation function for this slope before applying the logarithm to absolute values. Thus, these oscillations get “smoothed out” in the semi-logarithmic plot.⁹

Now, these values of the slope just correspond to the first members of the “turnstile dynamics” series α , β and γ , which are marked in the graph of the fractal diffusion coefficient of Fig. 2.12. Thus, $a \simeq 2.414$ is the first value of series γ , the series with diffusion coefficients being close to local maxima, $a \simeq 2.359$ is the first value of series β which identifies the local minima just in front of series γ -values, and $a \simeq 2.732$ is the first value of series α which labels the series of local minima of the diffusion coefficient curve approaching $a = 3$. To get an idea about the origin of the wiggles in the time-dependent quantities, one may consider again the respective pairs of boxes of these three values of the slope, as drawn in Fig. 2.12. If one takes a look at the orbit of the critical point of $a \simeq 2.414$, one can see that this orbit performs a jump at the first iteration and some internal box motion at its second iteration, and that it gets back to its initial condition after the second iteration again, although shifted into the

⁹The time-dependent diffusion coefficients for $a \simeq 2.359$ and $a \simeq 2.732$, which have not been shown in the diagrams here, have been investigated as well. Again, wiggles have been observed with similar regularities as described for the respective correlation functions.

adjacent box. Since other orbits close to this orbit behave similarly, this may qualitatively explain the period two of the wiggles in the dynamical quantities of slope $a \simeq 2.414$ and as well their “persistence”, as shown in Fig. 3.3 (b), since this dynamical process can continue infinitely often. The situation is a bit different for slope $a \simeq 2.359$, as can be seen in the respective pair of boxes. Here, after a jump at the first iteration, the orbit gets reflected two times in the adjacent box before getting mapped exactly to the right boundary of this adjacent box. It means that the orbits of an initial density being uniform in the left escape region, i.e., where particles perform a jump to the right at the next iteration, get mapped such that the density of this region covers the next box to the right uniformly again after three iteration steps. This may explain the more complicated periodicity of the respective wiggles in the time-dependent quantities on the one hand, and that these wiggles are less pronounced than for the slope $a \simeq 2.414$ on the other hand. Finally, the critical point for $a \simeq 2.732$ gets mapped with a jump to the right at its first iteration, and, as before for slope $a \simeq 2.359$, a uniform probability density of the left escape region produces a full coverage of the next box to the right after the second iteration. This may explain that the wiggles in the respective dynamical quantities are even less pronounced than before.

The same approach has been applied to a number of other members of the three series in the initial region, and other values of the slope have been checked as well. There seems to be a general tendency that pronounced wiggles, indicating strong dynamical correlations, occur at local maxima of the parameter-dependent diffusion coefficient curve and that at local minima, wiggles and correlations are less pronounced. This behaviour shows up quite clearly for slopes below $a = 3$, but it is increasingly difficult to verify for higher values of the slope. These very qualitative explanations in the spirit of the turnstile dynamics of the previous chapter do not hold for any more detailed descriptions and give only a first glance of the complete dynamics of the system. In detail, of course *all* single orbits would have to be taken into account and not only iterated critical points or escape regions, since quantities like velocity autocorrelation functions are especially sensitive to all microscopic details, as has already been experienced in kinetic theory calculations thirty years ago [Dor75, Dor77].

Nevertheless, these considerations give strong evidence that the wiggles in the time-dependent dynamical quantities analyzed before are due to strong spatio-temporal correlations, induced basically by the periodic coupling of the chain of boxes. Thus, it may be concluded that the structure of the fractal diffusion coefficient $D(a)$ of map \mathcal{L} is to its full extent, i.e., with respect to its dynamical origin in time, produced by such long-range correlations. This may also explain why the picture of a simple random walk does not hold anymore in detail, as has already been remarked at several occasions in Chapter 2, since for values of the slope considerably above $a = 2$ intrinsic correlations get more pronounced and

are not negligible anymore. It should be noted that a “surprisingly rich structure” of the velocity autocorrelation function has already been observed in the periodic Lorentz gas at different densities via computer simulations [Mac83c]. It may be conjectured that this fine structure is due to the deterministic dynamics of the Lorentz gas in a similar way as outlined above.

Thus, there is a straight line of certain phenomena from probability densities over time-dependent statistical dynamical quantities to deterministic diffusion coefficients of map \mathcal{L} : All these quantities behave “nicely diffusive” in a statistical sense on a large scale, but they reveal certain “wiggles” or “oscillations” on a fine scale, which clearly indicates that the diffusion process was generated by a *deterministic* dynamical system. The occurrence of such fine structures on smaller scales may be assumed to be typical for deterministic diffusion in periodic dynamical systems and may be responsible for the difficulties to obtain analytical solutions to a more broad extent.

At last, some question about the stability of the dynamical system map \mathcal{L} with respect to certain perturbations, and the relevance of these questions to problems of physical interest shall be briefly discussed.

1. shadowing:

The shadowing property guarantees a certain stability for the orbits of a dynamical system with respect to dynamical perturbations, like noise imposed on the system, or numerical roundoff errors.¹⁰ According to a simple counterexample, it may be conjectured that map \mathcal{L} does not possess the shadowing property for any value of the slope.¹¹ Thus, although the numerical results presented above seem to be reasonable, they probably cannot be justified by existence of shadowing.

2. noise and phase transitions:

An interesting question is how the fractal diffusion coefficient of map \mathcal{L} behaves by applying random noise to the map, i.e., how much the fractal structure persists, and when it gets smoothed out.¹² Since by increasing the strength of the noise there must occur a transition between the process of purely deterministic dif-

¹⁰For a definition of the shadowing property see Refs. [Guc90, Pei92]. Shadowing has been proven to exist for a large variety of dynamical systems: see, e.g., Refs. [Bow75, Guc90, Lev89] for hyperbolic dynamical systems, Refs. [Gre90, Ham87, Ham88] for non-hyperbolic dynamical systems, and Refs. [Cov88, Nus88] for various other types.

¹¹This example is due to Prof. H.E. Nusse; respective valuable discussions with her are gratefully acknowledged. The basic idea is that for any value of the slope orbits can be found which get mapped onto unstable fixed points, situated at integer values. By perturbing these orbits slightly, one obtains at once totally different, strongly diverging orbits nearby which contradict the shadowing property. An analytical proof might be carried out along these lines.

¹²This question was raised by Prof. J. Kurths; discussions with him are gratefully acknowledged.

fusion, without any external perturbations, and stochastic diffusion, determined by external random noise, a phase transition of map \mathcal{L} might be expected which could show up by computing the diffusion coefficient at certain values of the slope by varying the strength of the noise.

Evidence for phase transitions has already been obtained for one-dimensional climbing sine maps by imposing Gaussian random noise on the map and computing diffusion coefficients with respect to varying the control parameter [Gei82]; they have also been found in a variety of other simple dynamical systems at different circumstances [Bec93].

3. structural stability:

Another important question regarding perturbations of map \mathcal{L} is the property of structural stability, i.e., whether a map is stable with respect to certain linear topological transformations of its functional form.¹³ This question might be related to the problem whether slight perturbations in the periodic continuation of the chain of boxes, e.g., produced by replacing several boxes of the chain by boxes with slightly different functional forms of the box map, affect the occurrence of fractal diffusion coefficients. However, the property of structural stability is connected to the shadowing property, and since map \mathcal{L} does not seem to be shadowing, it may be conjectured that it is not structurally stable.

4. noise and diffusion coefficients:

In recent literature, a surprising suppression of deterministic diffusion by noise has been discovered in climbing-sine maps [Rei94], which have often been used to model Josephson junctions [Gei85]. Similar phenomena may be expected to occur in dynamical systems like map \mathcal{L} as well: If one perturbs the system by applying random noise, this may have an impact on single orbits like varying the slope of the map a little bit. However, if one starts with map \mathcal{L} , e.g., at the local maximum of the diffusion coefficient at the value of the slope $a = 3$, varying the slope is in any case identical to a decrease of the diffusion coefficient. Thus, a suppression of diffusion by noise may be related to oscillations in the parameter-dependent diffusion coefficient or, in case of class \mathcal{P} -maps, to the existence of fractal diffusion coefficients.

¹³see Refs. [Lev89, Ott93] for some introductions, Ref. [Guc90] for a general discussion, and Ref. [dM93] for mathematical details in case of one-dimensional maps

3.4 Conclusions

(1) A new numerical procedure, denoted as iteration method, has been developed for investigating deterministic diffusion in class \mathcal{P} -maps. It is based on the use of Markov partitions with respective topological transition matrices and enables the computation of time-dependent probability densities by solving the Frobenius-Perron equation. This method gives not only access to certain time-dependent dynamical statistical quantities, but it provides also a simple, efficient, and very precise way to compute parameter-dependent diffusion coefficients.

(2) Simple straightforward computer simulations have been performed for map \mathcal{L} . Via comparison to iteration method results these simulations have been confirmed to produce reasonable data in the limits of numerical precision. However, the simulations have not been sufficiently precise for producing any detailed fractal structure of diffusion coefficient curves.

(3) A procedure to approximate ensemble averages of dynamical quantities via probability density averages has been introduced. It has been checked to provide reasonable qualitative and quantitative results.

(4) Gaussian probability densities with strong periodic fine structures have been obtained for map \mathcal{L} . While the large-scale behaviour of these probability densities proves numerically that the macroscopic dynamics obeys the statistical diffusion equation, and thus probably a central limit theorem, the fine structure of these densities has been shown to be induced by the periodic scattering mechanism of the dynamical system and thus is related directly to the microscopic deterministic dynamics of the system.

(5) Second and fourth moments of the probability density, time-dependent diffusion coefficients, and velocity autocorrelation functions have been computed for map \mathcal{L} in various ways. Again, they turned out to be “behaved nicely” on a large scale in the sense that they showed all characteristics of a statistical diffusion process. Especially, no numerical evidence for long-time tails in the velocity autocorrelation functions has been obtained.

(6) Certain oscillations in these time-dependent quantities have been observed on a fine scale. They have been related qualitatively to the coupling mechanism of the periodic scatterers of the dynamical system. These oscillations indicate microscopic spatio-temporal correlations, which may be considered as the dynamical origin for the fractal structure of the parameter-dependent diffusion coefficient. Such fine structures of time-dependent quantities are assumed to be typical for deterministic diffusion in dynamical systems.

(7) Certain stability properties of map \mathcal{L} have been discussed, and they have been partly related to the occurrence of fractal diffusion coefficients and to their time-dependent origin.

4

Crisis in deterministic diffusion

In the previous two chapters, only one special map of the so-called class \mathcal{P} of piecewise linear maps, introduced as map \mathcal{L} in Section 2.1, has been studied in detail. Nevertheless, main results have been claimed to be typical for other class \mathcal{P} -maps as well, especially the existence of a parameter-dependent fractal diffusion coefficient, and the occurrence of certain features in the probability density and in other time-dependent dynamical quantities. To obtain these results, methods have been developed which enabled analytical calculations (via first passage and transition matrix method, see Chapter 2) and fast and reliable numerical computations of parameter-dependent diffusion coefficients and of time-dependent dynamical quantities (iteration method, see Chapter 3). Moreover, two approaches have been suggested to achieve a qualitative and, to a certain degree, a quantitative understanding of the origin of the fractal diffusion coefficient of map \mathcal{L} (plus-minus method and turnstile dynamics, see Chapter 2).

In this chapter, a new map of class \mathcal{P} will be introduced (see Section 4.1) to which the methods mentioned above shall be applied (see Sections 4.2 to 4.3). This map will serve as a touchstone whether the arsenal of methods developed to deal with deterministic diffusion works satisfactorily for other class \mathcal{P} -maps as well. The most important point is to check whether the main results obtained for map \mathcal{L} can, in a similar way, be recovered for this second map. The choice of the map has been motivated by a phenomenon which was recently reported in the literature as a “crisis in chaotic scattering” (see Section 4.1).¹ Thus, apart from making a first step to check the universality of the characteristics of deterministic diffusion obtained before, one may expect to gain more insight into the problem whether certain features of microscopic chaotic scattering are of any relevance for the process of macroscopic deterministic transport. This may be important not only from a fundamental physical point of view, but also for the purpose of bringing the aspects of deterministic diffusion more close to physical reality, since the chaotic scattering phenomenon to be discussed in the following has also been found in more realistic dynamical systems.²

¹I am obliged to Prof. C. Grebogi for some helpful discussions about this subject, and for his continuous interest in the problem treated in this chapter.

²A summary of this chapter is intended to be published as another letter in the style of Ref. [Kla95b].

4.1 Simple models for crises in chaotic scattering

The phenomenon of a crisis in chaotic scattering has first been reported by Lai et al. for a two-dimensional open Hamiltonian dynamical system. The brief discussion here follows his presentations in Refs. [Lai93, Lai94]. In the model, which has essentially been introduced by Troll and Smilansky [Tro89, Tro91], a point particle is scattered by an infinite one-dimensional array of two-dimensional nonoverlapping elastic scatterers. These scatterers are placed at constant intervals along the y axis, and each scatterer is represented by a circular attractive potential that becomes negligible small at a certain distance. As the dynamical variables of the system, the angular momentum of the particle and an angle related to the scattering angle have been chosen. The dynamics of the model can be changed by switching the particle energy as a control parameter.

For high enough energies, one observes the existence of two topologically and dynamically isolated chaotic invariant sets in the phase space of the particle. These sets represent the values of the dynamical variables for which the particle does not escape out of the system. By decreasing the energy, one gets to a certain critical energy value where the two formerly disconnected invariant sets just “touch” each other. At this point, both chaotic sets get linked dynamically, and by decreasing the energy further, an uncountable number of such links between both sets is created. Thus, a *crisis in chaotic scattering* can, roughly speaking, be defined in this scattering model as the *merging of two topologically and dynamically isolated invariant sets* of the dynamical variables. This phenomenon leads to certain major changes in characteristic dynamical systems quantities, as will be explained below, and can be understood by referring to certain microscopic orbits of the scattered particle: For low enough energies, one encounters a kind of “channeling”, i.e., particles keep going upwards or downwards in the array of scatterers without turning around. These two different directions in the movement of the particles are related to the existence of the two invariant sets mentioned above. At the critical energy value, so-called “orbiting collisions” set in, where a particle can circulate in the potential for an infinite number of times. This means that a particle can also be scattered backwards, i.e., it can be turned around and can go up-downwards, which is the physical counterpart of the two formerly invariant sets being dynamically connected. The phenomenon of orbiting collisions is a special property of attractive-repulsive potentials, if they are sufficiently high nonlinear, and has already been discussed earlier in the context of transport theory and the Boltzmann equation (see Ref. [Kla92] and further references therein).

In Refs. [Lai93, Lai94], a piecewise linear one-dimensional map has been proposed as a simple model which also shows a crisis in chaotic scattering. This map is given in Fig. 4.1 (a) to (d). The control parameter of the system is here the absolute value of the height between the horizontal line drawn in the figures

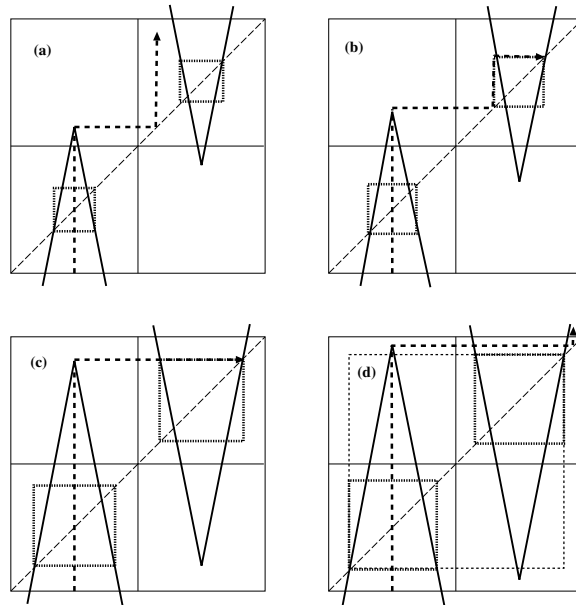


FIGURE 4.1. A one-dimensional model for a crisis in chaotic scattering (after Lai et al., see text). Diagram (a) shows the model before crisis, (b) at the beginning of the crisis, (c) to the end of the crisis, (d) after the crisis.

and the respective extrema of the two branches of the map. It is varied without changing the slope of the map. With respect to the crisis scenario, the decrease of the energy in the two-dimensional system corresponds here to an increase of the height. In Fig. 4.1 (a), the situation before crisis is illustrated. If one starts with an initial distribution of particles which uniformly covers the interval of the small box drawn to the left, one observes that these particles either stay in this box for infinite time, forming a Cantor set as a fractal repeller, or they leave the box and asymptote monotonically to infinity. The important fact is that they *never* enter the other small box of the antisymmetric counterpart of this map to the right at these parameter values, as one can check by considering single orbits, e.g., the orbit of the critical point shown in the figure. The same is true *vice versa* for the right small box so that the two small boxes contain two topologically and dynamically isolated chaotic invariant sets, as in case of the two-dimensional system described above, and the dynamics of the particles is again comparable to a “channeling” movement.

Fig. 4.1 (b) shows the map for the critical value of the control parameter, where the crisis occurs. This is exactly where the two formerly invariant sets touch each other dynamically via a first heteroclinic tangency: escape out of one box, i.e., the

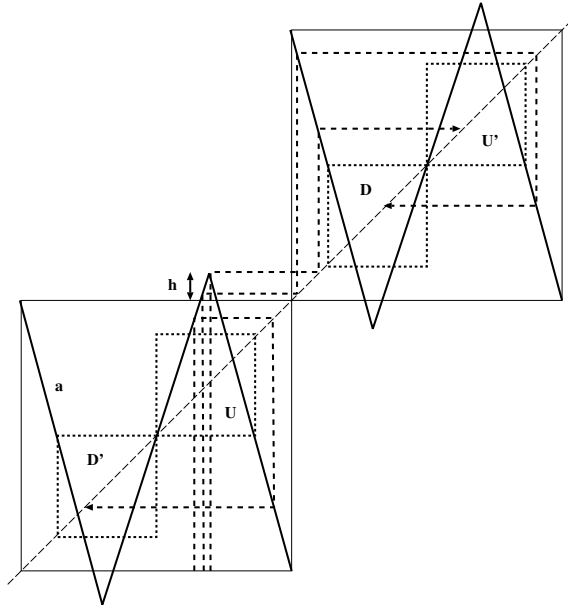


FIGURE 4.2. A diffusive one-dimensional “crisis” model, denoted as map \mathcal{S} , cf. Fig. 4.1 (a).

orbit of the critical point, can go directly into the other box and gets mapped to a fixed point. Thus, a merging of the two formerly invariant sets takes place. Dynamically, this is the first time when backscattering occurs. Fig. 4.1 (c) illustrates the last stage of this merging procedure, where escape out of one box hits just the upper boundary of the other box after one iteration, forming a last heteroclinic tangency. Finally, in Fig. 4.1 (d) the merging of invariant sets is complete, and one new large invariant set exists, which includes both formerly isolated invariant sets. Escape out of this large set again asymptotes to infinity. In Refs. [Lai93, Lai94], the parameter-dependent fractal dimensions of the invariant sets have been computed. The result shows a constant value before the crisis sets in, an increase of the dimension after the crisis value and a constant value again after the merging is complete.

In Fig. 4.2, it has been tried to model this scenario by a map of class \mathcal{P} by periodically continuing the original map of Fig. 4.1 in a slightly modified form. The map of Fig. 4.2 will be referred to as map \mathcal{S} , defined by

$$M_a(x) = \left\{ \begin{array}{ll} -ax + 1 & , \quad 0 < x \leq \frac{1}{4} + \frac{1}{4a} \\ ax + \frac{1}{2}(1-a) & , \quad \frac{1}{4} + \frac{1}{4a} < x \leq \frac{3}{4} - \frac{1}{4a} \\ -ax + a & , \quad \frac{3}{4} - \frac{1}{4a} < x \leq 1 \end{array} \right\} , \quad a \geq 3 \quad , \quad (4.1)$$

and by Eqs.(2.5), (2.6) and (2.7). The control parameter is here the absolute value a of the uniform slope of the map. By varying the slope, one varies the extrema as well. Intuitively, it can be expected that the crisis mechanism does not rely on keeping the slope constant. Thus, the height h , i.e., the absolute value of the distance between a box boundary of the map and the extremum which exceeds this box boundary,

$$h = \frac{a-3}{4} \quad , \quad (4.2)$$

is here a linear function of a . For values $h > 0$, diffusion sets in.³ Fig. 4.2 should be compared to the situation in Fig. 4.1 (a) before crisis. The respective candidates for isolated invariant sets in the new map have been marked again by small boxes and have been labeled U, D, U', D' . The boxes U and D correspond to the two boxes shown in case of the former non-periodic one-dimensional map of Fig. 4.1 (a). However, by following the three different trajectories included in Fig. 4.2, one observes that for map \mathcal{S} these sets are in no way isolated from each other after onset of diffusion. The other way around, it is clear that a proper diffusion coefficient can only be defined if there exist *no* disconnected invariant sets in the dynamical system at any parameter value, since otherwise the system would not be uniquely ergodic and the diffusion coefficient would at least not be uniquely defined in the complete dynamical system. Thus, the existence of a diffusion coefficient seems to be contradictory to the rigorous conditions for a crisis in chaotic scattering. Nevertheless, there are still “remains” for the “crisis inducing invariant sets” of the map of Fig. 4.1 in map \mathcal{S} , and one may conjecture that they have a certain impact on diffusion in this new dynamical system by varying the control parameter. Fig. 4.2 is already close to the “crisis value” of map \mathcal{S} , which is the slope $a \simeq 3.562$, or the height $h \simeq 0.140$, respectively, where particles of the small box U can get directly into the next small box D after one iteration. Similar considerations apply to other “sawtooth-like” one-dimensional models so that the fundamental scenario outlined here does not depend on the functional form of the special map.

Thus, as the basic problem of this chapter it may be posed the question whether a “crisis in chaotic scattering in its degenerated form”, as it occurs for map \mathcal{S} , i.e., modeled by a collision of different intrinsic scattering regions of the map, plays a role for the dynamics in a simple diffusive dynamical system. This question may be answered by investigating whether a microscopic “crisis-like” dynamical mechanism shows up in some way in the behaviour of macroscopic quantities like the parameter-dependent diffusion coefficient $D(a)$.

³According to Conjecture 2.2, it can be assumed that for $h > 0$ a parameter-dependent diffusion coefficient exists for map \mathcal{S} .

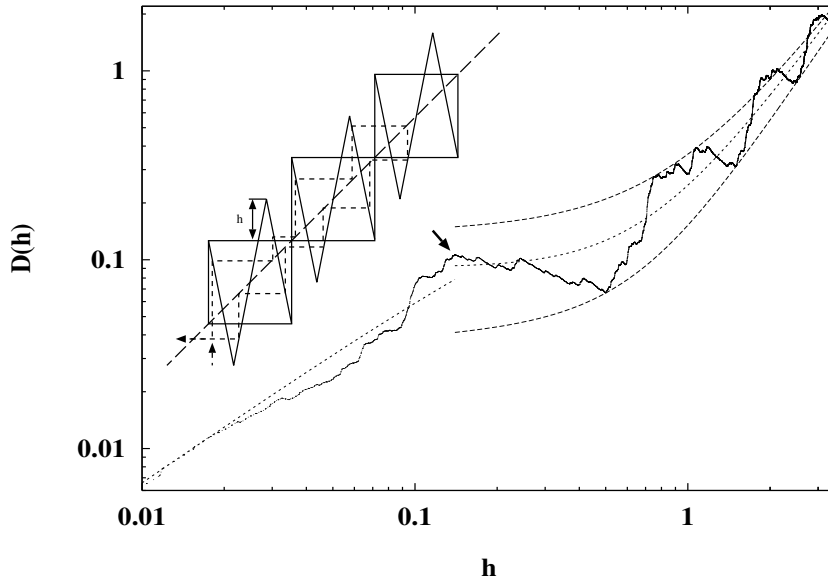


FIGURE 4.3. Double logarithmic plot of the diffusion coefficient $D(h)$ for map \mathcal{S} with respect to the height h . 14,271 single data points (from a total number of 38,889) have been plotted. Two random walk solutions (dotted lines) and two curves which connect certain diffusion coefficient values close to local extrema (dashed lines, see text) have been included.

4.2 Parameter-dependent diffusion coefficients and random walks

The parameter-dependent diffusion coefficient $D(a)$ for map \mathcal{S} has been computed by employing the methods presented in the previous chapters: Analytically, this diffusion coefficient has been obtained at certain integer values of the slope via first passage and transition matrix method analogously to the calculations performed for map \mathcal{L} in Chapter 2. Numerically, the iteration method of Chapter 3 has been applied, based on the choice of four different Markov partition series.

The resulting diffusion coefficient curve for map \mathcal{S} is shown in Fig. 4.3. Here, a double logarithmic scale has been used, and the diffusion coefficient has been plotted with respect to the height h which is related to the slope a according to Eq.(4.2). Four additional curves have been included in this figure, two of them passing through the extrema of the original $D(h)$ -curve above a certain value of the height, and two curves providing a kind of “mean value” for the parameter-dependent diffusion coefficient in certain ranges of the height. It should be noted

that the parameter-dependent diffusion coefficient of this new class \mathcal{P} -map shows again a very complex, supposedly fractal structure. Details of this structure shall not be in the center of the discussion in this section, but will be considered later. Instead, it shall be tried to understand the large-scale behaviour of this diffusion coefficient, as will be explained in the following.

For the two dashed curves which envelope the diffusion coefficient above $h = 0.1$, analytical solutions have been employed: For integer values of the height, one obtains

$$D(h) = \frac{2h^3 + 3h^2 + h}{12h + 9} \rightarrow \frac{h^2}{6} \quad (h \gg 1) \quad , \quad h = k \quad , \quad k \in N \quad , \quad (4.3)$$

which has been plotted as a function of h in the diagram and gives the upper curve. For the lower curve, the diffusion coefficient has been fitted with this functional form at $h = (2k + 1)/2$ and $h = (4k + 3)/4$, $k \in N_0$. Thus, these two curves give roughly the upper and lower limits in which the parameter-dependent diffusion coefficient oscillates back and forth, and they also demonstrate a certain large-scale behaviour of the exact diffusion coefficient, without taking any fine structure into account. The remaining two curves are based on two simple random walk models. To compute the diffusion coefficient via random walks, one starts again with the Einstein formula

$$D(h) = \lim_{n \rightarrow \infty} \frac{[\Delta x^2(n)]}{2n} \quad , \quad (4.4)$$

where

$$[\Delta x^2(n)] := \frac{1}{N} \sum_{i=1}^N (x_n^i - x_0^i)^2 \quad (4.5)$$

denotes the ensemble average of the mean square displacement over N particles with individual position x_n^i at discrete time n .

Since for a random walk there is no ‘‘history’’ for the dynamics of the particles, the Einstein formula reduces, as a first approximation, to

$$D(h) = \lim_{n \rightarrow \infty} \frac{1}{2} [\Delta x^2] \quad (4.6)$$

with

$$\Delta x = x_n - x_{n-1} = M_h(x) - x \quad , \quad x_n = M_h(x_{n-1}) \quad , \quad M_h(x) \equiv M_a(x) \quad , \quad (4.7)$$

i.e., the dynamics is characterized by only one iteration step. In the limit of time to infinity, the ensemble average approaches a probability density average [Sch89],

$$[\Delta x^2] \approx \langle \Delta x^2 \rangle \quad , \quad \langle \dots \rangle := \int dx \rho_n(x) \dots \quad . \quad (4.8)$$

Since the dynamical system under consideration is periodic, it suffices to consider only one box of the chain of boxes so that the integral above can be taken in the limits between zero and one. This leads to a random walk diffusion coefficient formula of

$$D_{rw}(h) \approx \frac{1}{2} \int_0^1 dx \rho^*(x) (M_n(x) - x)^2 \quad (n \rightarrow \infty) \quad , \quad (4.9)$$

where $\rho^*(x)$ stands for the invariant probability density in one box, which is determined by iterating a reduced map $M_h(x) \bmod 1$ (see Section 5.4).

The equation above may serve as the starting point for two versions of a random walk: First, one may consider map S for values of the slope where the height is very small, i.e., where the map exceeds only slightly its box boundaries, $h \ll 1$, see also Ref. [Sch82]. As a second approximation, one may assume the box probability density to be uniform,

$$\rho^*(x) \approx 1 \quad , \quad (4.10)$$

which of course is not rigorously true. In fact, the box probability density will be shown to be a step function which varies with varying the slope, see Section 5.4. Finally, as a third approximation for small heights one may assume that it is only important whether a particle leaves a box, performing a jump to another box and thus contributing to large-scale diffusion, or whether it stays in a box. With this assumption, the distance Δx may be approximated to

$$\Delta x \approx \left\{ \begin{array}{ll} 0 & , \quad 0 \leq M_h(x) \leq 1 \\ 1 & , \quad M_h(x) < 0 \quad \text{or} \quad M_h(x) > 1 \end{array} \right\} \quad (4.11)$$

which leads to

$$D_{rw1}(h) = \int_{x_1}^{x_2} dx = \Delta x_{escape} \quad , \quad (4.12)$$

where the central symmetry of the map has been employed and x_1 and x_2 are defined by $M_h(x_i) = 0$, $i = 1, 2$ for $x_i < 1/2$. These points represent the boundary points of the left escape region of the map, where particles can leave the box and go to the left. Thus, the diffusion coefficient of this random walk approximation is completely determined by the size of the interval of one escape region Δx_{escape} , and since for small heights the interval is very small, this version of a random walk will be referred to as *small escape random walk*. For map S , one obtains

$$D_{rw1}(h) = \frac{2h}{4h+3} \rightarrow \frac{2}{3}h \quad (h \rightarrow 0) \quad , \quad (4.13)$$

which provides the dotted curve plotted in Fig. 4.3 for small values of h .

A second random walk approximation can be deduced from Eq. (4.9) for large

values of the height h , see, e.g., Ref. [Ott93], and may therefore be denoted as *high turnstile random walk*, where the term turnstile refers to the union of escape regions of a box map (see the following section): Again, the box probability density may be assumed to be uniform, as in Eq.(4.10). However, for large heights the distance of the jump a particle performs by leaving a box becomes very important, since it is proportional to the height. Without any further approximation to Δx , the random walk diffusion coefficient can thus be calculated to

$$D_{rw2}(h) = \int_0^{1/2} dx (M_h(x) - x)^2 \rightarrow \frac{h^2}{6} \quad (h \rightarrow \infty) \quad . \quad (4.14)$$

The exact analytical formula for smaller heights is a rational function of high degree and shall be omitted here, since it is quite long. The graph of the full solution is shown in Fig. 4.3 as a dotted line, which has been drawn for values of h above $h = 0.1$.

The same approximations can be worked out for the parameter-dependent diffusion coefficient of map \mathcal{L} , which has been discussed extensively in the previous chapters, but not with respect to the height h as an order parameter. The first random walk model gives the curve already shown in previous plots with respect to the slope a , see Fig. 2.12, and reads for the height h , $h = (a - 2)/2$,

$$D_{rw1}(h) = \frac{h}{2(h+1)} \rightarrow \frac{h}{2} \quad (h \rightarrow 0) \quad . \quad (4.15)$$

The second random walk model gives the formula

$$D_{rw2}(h) = \frac{(2h+1)^2}{24} \rightarrow \frac{h^2}{6} \quad (h \rightarrow \infty) \quad . \quad (4.16)$$

These results have been plotted double-logarithmically in Fig. 4.4, together with the exact values of the parameter-dependent diffusion coefficient already presented in Fig. 2.10 and, as in Figure 4.3, with the respective graphs which connect the extrema at odd and even integer values of the slope, which are obtained from Eqs. (2.28) and (2.32) for the respective values of $D(a)$ with $h = (a - 2)/2$,

$$D(h) = \frac{h(2h+1)}{12} \rightarrow \frac{h^2}{6} \quad (h \rightarrow 0) \quad , \quad h = k \quad , \quad k \in N_0 \quad (4.17)$$

and

$$D(h) = \frac{(2h+3)(2h+1)}{24} \rightarrow \frac{h^2}{6} \quad (h \rightarrow 0) \quad , \quad h = \frac{2k+1}{2} \quad , \quad k \in N_0 \quad . \quad (4.18)$$

Thus, for both maps the random walk curves plotted in the figures represent the large-scale behaviour of the respective exact diffusion coefficients quite well.

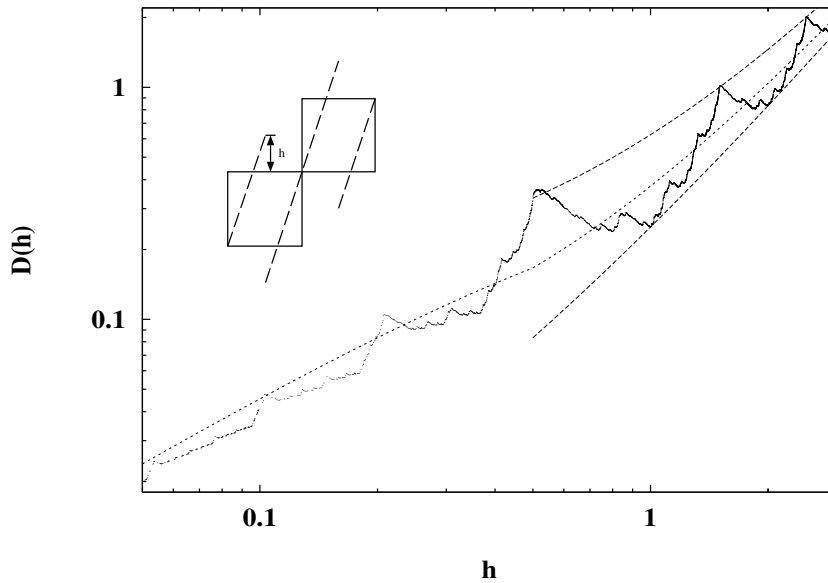


FIGURE 4.4. Double logarithmic plot of the diffusion coefficient $D(h)$ for map \mathcal{L} with respect to the height h . 7,908 single data points have been plotted. Two random walk solutions (dotted lines) and curves which connect certain diffusion coefficient values close to local extrema (dashed lines, see text) have been included.

Nevertheless, these random walks indicate with their different functional forms certain different large-scale characteristics of the respective maps: For map \mathcal{S} , which has been introduced as a model related to some critical chaotic scattering processes, one can distinguish three different large-scale regimes. The first one is represented quite well by the “small escape” random walk model and may be considered as a kind of initial region, where diffusion just sets in. Here, the diffusion coefficient behaves linearly for small heights. It follows a kind of “plateau regime”, at least in the double logarithmic plot, for values of the height from $h = 0.1$ up to $h = 1$, where diffusion seems to cease and the diffusion coefficient does not increase linearly anymore. Above $h = 1$, and increasingly better with larger heights, the diffusion coefficient grows quadratically in the height.

In contrast to this qualitative characterization for map \mathcal{S} , the picture for map \mathcal{L} allows a distinction of only two different regimes: Again, an initial region can be separated which has already been described in detail in Section 2.4, and for larger values of the height, a “high turnstile”-region shows up. For the initial region at small heights, the large-scale diffusion coefficient again behaves linearly, and for large heights, the diffusion coefficient grows quadratically. However, in case of

map \mathcal{L} a broad transition region between these two regimes, as it occurs for map \mathcal{S} , is clearly missing. Instead, the transition seems to take place abruptly. If the transition point should be labeled by any value of the height, Figure 4.4 suggests $h \simeq 0.75$, which corresponds to the slope $a \simeq 3$. It should be noted that in previous discussions the region around $a = 3$ has already been observed to be peculiar, especially because of the so-called “overhang” right above $a = 3$ (see Section 2.4 for a more detailed discussion). For map \mathcal{S} , the supposed first transition point which separates at least the regions described qualitatively by the two different random walk models has been marked by a black arrow and just corresponds to the “degenerated crisis point” defined in the previous section. This may be taken as a first hint that something like a rudimentary “crisis in chaotic scattering” indeed shows up in deterministic diffusion.

To summarize at this point, in both maps at least two different regions of deterministic diffusion can be distinguished. These regions can be described qualitatively by two different random walk models. In both cases, the lower region may be considered as a kind of initial region after the onset of diffusion. The characteristic behaviour of this region terminates abruptly at certain points, which are determined by special dynamical processes.

Apart from such qualitative considerations, the analytical random walk solutions, as well as the analytical results for the diffusion coefficient at integer values of the slope for both maps, reveal certain algebraic laws: For both maps, the diffusion coefficient decreases linearly in the height for small values, although with different factors, see Eqs.(4.13) and (4.15). In the limit of large heights, all solutions, i.e., the exact analytical values of the diffusion coefficient formulas, see Eqs.(4.3), (4.17), and (4.18), as well as the two high turnstile random walk models, see Eqs.(4.14) and (4.16), lead to an increase of the diffusion coefficient which is quadratic in the height with a factor of $1/6$ in front. This may be regarded as first numerical and analytical evidence for the following conjecture:

Conjecture 4.1 (Universal laws for diffusion coefficients of class \mathcal{P} -maps)

For diffusive class \mathcal{P} -maps, the parameter-dependent diffusion coefficient decreases linearly in the limit of small heights, and it grows quadratically for large heights with a universal factor of $1/6$.

Single parts of this conjecture have already been reported in the literature: In Ref. [Fuj82], a linear decrease of the diffusion coefficient for small heights has been suspected for different class \mathcal{P} -maps. Also, certain series of diffusion coefficient values have been computed analytically for these maps which already led to quadratic functions with a factor of $1/6$ in the limit of large heights. However, no conclusion about a respective universal behaviour has been drawn. In Ref. [Che95], another class \mathcal{P} -map has been discussed analytically via cycle expansion methods, and linear as well as quadratic limits have been found and conjectured

to be universal, however, here without noting the universality of the factor $1/6$ in the quadratic limit. In both cases, parameter-dependent diffusion coefficients could only be computed at special values of the slope, or with certain additional approximations. For map \mathcal{L} and map \mathcal{S} , the limits of small and large heights are clearly obtained with respect to the numerical results presented for the full range of parameter values in Figs. 4.3 and 4.4. Conjecture 4.1 follows here also with respect to the two analytical random walk approximations, which have been shown to describe the behaviour of the parameter-dependent diffusion coefficients quite well on a large scale, even above and below the purely linear and quadratic limiting cases, and which are expected to be generally applicable to any class \mathcal{P} -map. Nevertheless, despite such strong evidence for this conjecture, a rigorous proof of this large-scale universality remains to be done.

The reason why the factors of $1/6$ are not universal for small heights may be found in the different functional forms of the box maps. The specific character of the map can be assumed to be more decisive for weak diffusion, whereas in the limit of large heights, the detailed structure of the box map is not that important anymore for large-scale diffusion. It should be noted that similar results are not obtained with respect to the slope as the parameter for the diffusion coefficient. Thus, the height is clearly the correct order parameter to describe this kind of universal behaviour.

Similar results in the limit of large control parameters have also been found for certain two-dimensional maps, i.e., standard- and sawtooth maps, where again quadratic laws for diffusion coefficients have been derived, although with different coefficients [Ott93, Mei92, Rec80, Rec81, Car81b, Car81a, Ant81].

The discussion of applying random walk models for understanding deterministic diffusion coefficients shall be concluded by a brief remark concerning random walks at integer slopes. In Section 2.3, it has been mentioned that exact diffusion coefficient results for the slopes $a = 3$ and $a = 4$ of map \mathcal{L} can also be obtained from simple random walk models. The case of $a = 4$ can straightforward be verified by Eq. (4.15), which has been derived from the small escape random walk model, by taking into account the relation between height h and slope a given above this equation. However, for slope $a = 3$ this equation clearly leads to a wrong result. Neither does the other high turnstile random walk model give the correct answer. Nevertheless, it is possible to obtain the correct value for the diffusion coefficient at $a = 3$ from a small escape random walk model by *shifting the box* for which the random walk is defined by $\Delta x = 1/2$ to the right and by $\Delta y = 1/2$ to the top *without shifting the map*. Considering the escape of particles out of that newly defined box and applying the method of the small escape random walk again to this case in fact leads to the correct diffusion coefficient value at slope $a = 3$.

Both small escape random walk approaches with different definitions of “boxes”

can be performed at any integer slope $a \in \mathbb{N}$, $a \geq 2$, for map \mathcal{L} by taking into account that, e.g., for $a = 4$ and the boxes chosen appropriately particles can jump over a distance of $\Delta x = 1$ and $\Delta x = 2$, respectively, and dividing the escape region according to these jumps of different lengths. Following this procedure, the exact values of the diffusion coefficient can be reproduced via random walks at all integer slopes, and thus one obtains the oscillations of first order. However, it should be noted that to get this result on the basis of random walks the boxes had to be chosen differently for odd and even integer slopes. Thus, the random walk results clearly depend on the choice of a suitable reference system. In other words, it can be stated that the oscillations of the parameter-dependent diffusion coefficient of map \mathcal{L} at integer slopes, and likewise of map \mathcal{S} , are *not* understood by *one consistent, well-defined* random walk model. The other way around, one may conclude that these oscillations represent rather a characteristic feature of deterministic diffusion in such dynamical systems than a random walk approach.

4.3 Understanding the structure of fractal diffusion coefficients

In the previous section, the large-scale behaviour of fractal diffusion coefficients has been investigated via random walk models, and some general laws have been found. However, any intricate fine structure of the parameter-dependent diffusion coefficients has not been taken into account so far. In Section 2.4, a more detailed understanding of the structure of the fractal diffusion coefficient of map \mathcal{L} has already been obtained by certain systematic qualitative and quantitative approaches. Similar methods shall now be applied to the supposedly again fractal diffusion coefficient of map \mathcal{S} , which is shown in Fig. 4.5 with respect to the absolute value of the slope a of the map.

4.3.1 Counting wiggles and plus-minus dynamics

Following the discussion at the beginning of Section 2.4, one can start with counting the number of “wiggles” in certain regions of the slope. Referring to Fig. 4.5, one first observes an oscillation of the diffusion coefficient curve “in 0th order” with respect to odd integer slopes. Although the situation is not as clear as for map \mathcal{L} , it could be said that strong local minima occur at odd integer slopes of $a = 5, 9, 13$, whereas local maxima seem to occur at odd integers of $a = 7, 11, 15$. If one goes into more detail, one can try to estimate the number of next largest wiggles, i.e., “wiggles of first order”. One may find one pronounced wiggle in the region $3 \leq a \leq 5$, but for the next regions above $a = 5$, the choice of wiggles

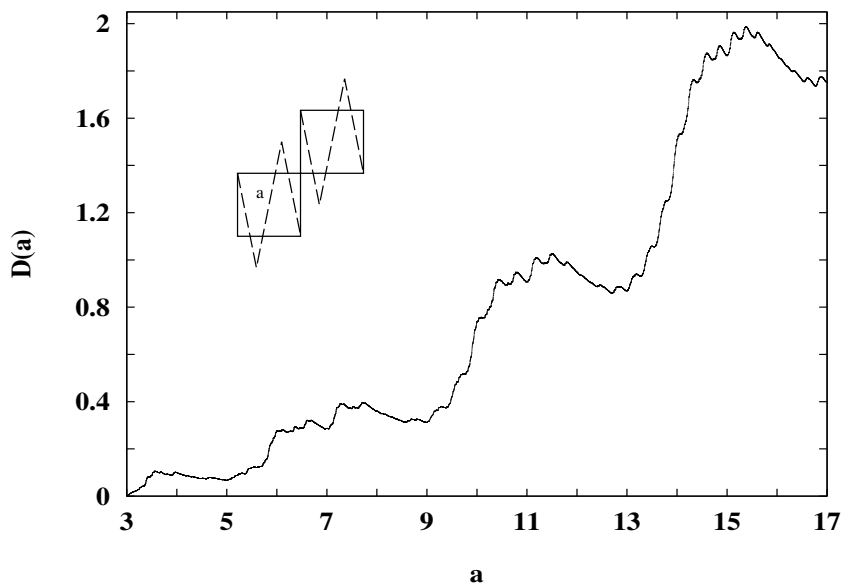


FIGURE 4.5. Parameter-dependent diffusion coefficient for map \mathcal{S} with respect to the slope a . The graph consists of 13,376 single data points (from a total number of 38,889).

of first order is quite ambiguous, i.e., about two in $5 \leq a \leq 7$ and about three in $7 \leq a \leq 9$. Nevertheless, for higher values of the slope the diffusion coefficient curve of Fig. 4.5 becomes more regular again, and one may estimate five wiggles of first order in $9 \leq a \leq 11$, six in $11 \leq a \leq 13$, seven in $13 \leq a \leq 15$, ... To continue this wiggle-counting on finer scales again is not very promising. Thus, the challenge is to explain the origin of wiggles of 0th order, the regularity of wiggles of first order for values of the slope above $a = 9$ and the strong deviations for slopes below this value.

As in Section 2.4, the qualitative *plus-minus method* shall be employed, which is illustrated in Fig. 4.6. The definitions of “plus” and “minus” regions of the box maps are not as straightforward for map \mathcal{S} as for map \mathcal{L} , since map \mathcal{S} possesses a more complicated box map structure. In Fig. 4.6 (a), regions of the box maps have been labeled with a “plus” sign if respective orbits either leave a box and jump to the right at the next iteration or remain in a box. The same way, a “minus” has been given if orbits of the respective regions jump to the left or remain in their original box. Thus, the left half of any box is marked with a minus, and the right half of any box with a plus. Following the definitions given in Section 2.4, the escape of particles out of the lower left box shown in Fig. 4.6 (a), which goes

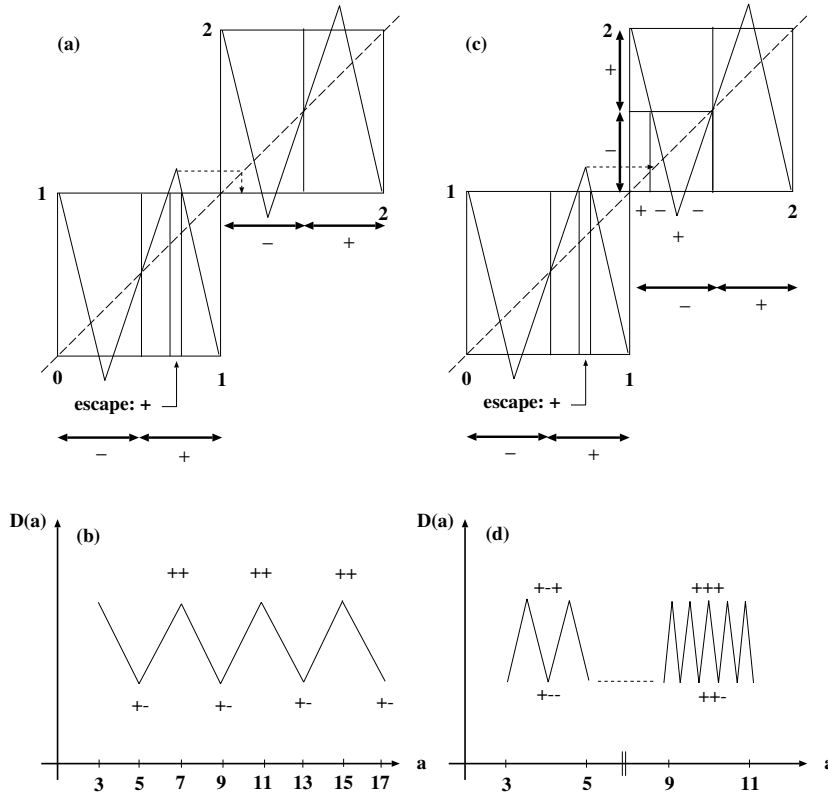


FIGURE 4.6. Sketch of the qualitative “plus-minus” method, applied to map \mathcal{S} (see text).

immediately to the right, will be considered. Since the slope is related linearly to the height of the maximum of the box map, cf. Eq. (4.2), increasing the value of the slope causes more particles from the escape region, as a plus region, to be mapped straight into the minus region of the box to the right of the initial box. This is supposedly bad for a fast diffusion process. However, by increasing the slope above a value of $a = 5$, particles close to the critical point, i.e., close to the maximum of the map, get for the first time a chance to be mapped into the plus region of the right adjacent box after one iteration, which should enhance diffusion. This procedure may be followed for further increasing the value of the slope and leads to the qualitative “diffusion coefficient curve” shown in Fig. 4.6 (b), which gives the result for wiggles of 0th order and corresponds roughly to the oscillations in the actual $D(a)$ -curve of Fig. 4.5 over the full range of the slope. Fig. 4.6 (c) sketches the refinement of this approach to obtain wiggles of first order with

respect to the dynamics of two iterations: The new subintervals introduced refer to particles of the escape region being mapped to another plus or minus region at the second iteration. Their origin depends on the structure of the box map. If one restricts oneself to the escape of particles of the escape region close to the critical point, one can see that increasing the slope creates different plus-minus sequences, which are good or bad for strong diffusion, as is illustrated in Fig. 4.6 (d) for some values of the slope. A better understanding may be achieved by noting that increasing the slope causes the orbit of the critical point to travel along the graph of the next right box map from the upper left to the lower right at the second iteration, thus exploring all the different plus and minus parts the graph of the box map goes through. As a result, one obtains wiggles of first order which do not match at all to the number of wiggles counted in the regions of the slope below $a = 9$, but this changes immediately above this value, where there is perfect coincidence again between the plus-minus method of first order, and the number of wiggles counted for first order.

Now, in certain respects a variation of the plus-minus method of first order may be introduced which refers to the conjecture in the context of a crisis in chaotic scattering that the “small boxes”, discussed in Section 4.1 and included in Fig. 4.7 (a), may play a role for deterministic diffusion. Fig. 4.7 (a) shows a magnification of the region below $a = 7$ with a picture of map \mathcal{S} , where certain points have been labeled by numbers and symbols. One notices that these points appear on the diffusion coefficient curve in diagram (a), and that they are all close to certain local maxima and minima of the curve. The idea is again that the orbit of the critical point, represented by a dashed line and a small circle in the figure, respectively, travels along the graph of the adjacent box map at the second iteration by increasing the slope, thus exploring different scattering regions of this map. Tentatively, and in contrast to the simple plus-minus method, escape regions which are related to the local minimum of the box map, thus moving orbits to the left, may generally be assumed to decrease diffusion, and *vice versa*. Moreover, the small boxes which belong to these escape regions, because they “shuffle” orbits with a high probability into the corresponding escape regions (cf. Section 4.1, or the following section) may be considered as well to be good or bad for diffusion, respectively. Diamonds refer to the boundaries of the “small boxes”, i.e., of the formerly “invariant sets” of the one-dimensional crisis model of Fig. 4.1, triangles are situated at the boundaries of the respective escape regions of map \mathcal{S} , and the values of the slope when the orbit of the critical point hits such a symbol at its second iteration are marked respectively on the diffusion coefficient curve. It appears as if, by considering small boxes as new mechanisms and estimating the effect of the escape regions differently from the previous plus-minus method, certain features of the structure of the diffusion coefficient curve can be understood in this region of the slope reasonably well, in contrast to the results of the simple

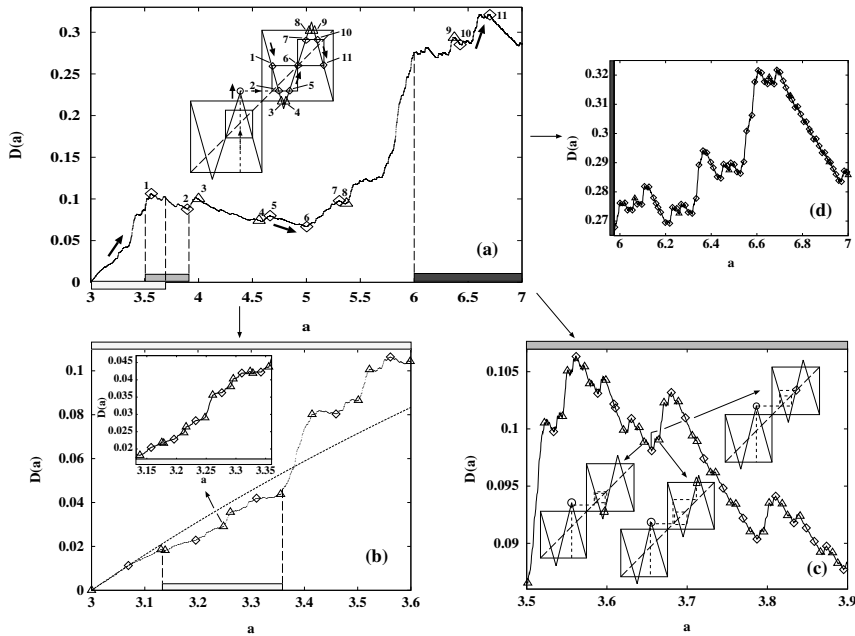


FIGURE 4.7. Application of “turnstile dynamics” to map \mathcal{S} . In diagram (a) and (b), 10,268 and 1,322 single data points have been plotted, respectively, in (c) and (d) 623 and 4,182 data points, connected with lines.

plus-minus method before. On the other hand, not all significant wiggles in Fig. 4.7 (a) can be identified by this method. For higher values of the slope, the results are even getting worse, and thus in fact the range of application of this procedure is very limited.

One may summarize at this stage that the plus-minus method, in cooperation with “wiggles counting”, corresponds to a very qualitative distinction of two different regions of the slope in map \mathcal{S} : a broad region below $a = 9$, where these two qualitative approaches do not work at all, and a region of higher values of the slope above $a = 9$, where the diffusion coefficient curve suddenly seems to behave quite regularly, which corresponds to obtaining satisfactorily results by the plus-minus method and by the “wiggles counting” procedure. On the other hand, including the small boxes in such a dynamical description, which are relevant for a crisis in chaotic scattering, and thus modifying the simple plus-minus approach seems to provide an understanding just in the region where the other two simple methods fail.

These qualitative conclusions may be compared to the results obtained by plotting

the diffusion coefficient curve of map S with respect to the height h in Fig. 4.3, and to the respective discussion of different regimes in this curve: The region where the plus-minus method and wiggle counting work corresponds roughly to the “high turnstile” limit of the respective random walk model, where diffusion increases quadratically with the height h . The “plateau region” of Fig. 4.3, on the contrary, matches quite precisely to the range where the small boxes seem to be important, i.e., below $a = 9$, or $h < 1.5$. The “crisis value” $a \simeq 3.562$ defines an “initial region” in Fig. 4.7, where no structure corresponding to the map illustrated in the figure can be found, and which matches to the “small escape” random walk region in Fig. 4.3. This again leads to a distinction between three different regions of the slope, i.e., an initial region, which has not been characterized further yet, a transition region, where certain details of the map are important, and a limiting region, which seems to be remarkably regular and smooth in its fine structure.

4.3.2 Turnstile dynamics

The discussion in this section will provide an extension of the turnstile dynamics introduced in Section 2.4, and may start with several definitions:

Turnstiles of map S are defined again, as in Section 2.4, as the “coupling regions” of the single boxes of the chain, where points of one unit interval get mapped outside that particular interval into another interval. *Critical orbit* may stand as an abbreviation for the orbit of the critical point, produced by applying the map to the critical point n times. Finally, the small boxes referred to in the previous section may be denoted as *collimators*, since if a particle gets mapped into such a collimator, there is a high probability that, after some iterations, it gets mapped into the respective turnstile which belongs to the collimator, leaving the corresponding unit interval, or box, by a jump into another unit interval. Thus, it could be said that these small boxes “focus” orbits into their respective turnstiles.

The basic idea of turnstile dynamics is again to consider the *coupling* of single turnstiles, and the proposition is that this turnstile coupling is crucial for transport of particles. A *simple* version of turnstile dynamics has been employed for map \mathcal{L} , where only the mechanism of a direct coupling between different turnstiles has been considered. Here, an *extended* version is obviously needed, since not only the mapping from one turnstile to another turns out to be important, but as well the mapping from a turnstile to a collimator. A *qualitative* version of turnstile dynamics has been introduced by plus-minus dynamics, and as a quantitative version an approach may be denoted which allows to identify extrema of diffusion coefficient curves via single points. Such a quantitative approach is the *method of critical orbits*, which has already been used for map \mathcal{L} and has been introduced as well in Fig. 4.7 (a). For this method, important dynamical mechanisms like collimators and turnstiles get exemplified by single orbits, which usually refer to

certain Markov partition series and can be computed numerically.

The goal of turnstile dynamics is to increase the understanding of the fractal structure of the parameter-dependent diffusion coefficient $D(a)$ for class \mathcal{P} -maps by establishing a relation between certain dynamical processes and the structure of these curves. This can be achieved qualitatively by explaining the number of wiggles in certain regions, and on certain scales, or quantitatively by identifying extrema up to a certain order by single points on the basis of turnstile mechanisms like the ones mentioned before. This goal is different to the one, e.g., of the random walk models employed above, which do only refer to certain features of the large-scale functional form of the respective diffusion coefficient curves.

Fig. 4.7 shows results of quantitative turnstile dynamics for map \mathcal{S} by employing the method of critical orbits: Diagram (a) has already been explained before and introduces the respective symbols which can be found in the diagrams (b) to (d). In these new magnifications, certain diffusion coefficient values have been marked with symbols. These symbols correspond to values of the slope, where the critical point, after a certain number of iterations, gets mapped to a point which defines a collimator, or another turnstile, without knowing any details about the precise form of the orbit (i.e., whether a particle stays in two boxes, travels through a series of boxes, etc.). One observes that in diagram (b), there are certain sequences of “turnstile” and “collimator” values which seem to separate self-similar regions, and that turnstile values can usually be found at the “kinks” of this curve, whereas single collimator symbols appear regularly between pairs of turnstile symbols and are situated at slight local extrema. This simple structure persists even on finer scales, as is demonstrated in the inset, which provides evidence for a self-similar structure resembling a devil’s staircase [Ott93, Pei92]. The dashed line in the diagram corresponds again to the respective “small escape” random walk solution. However, one notices that this special structure gets increasingly deformed with higher values of the slope. This is shown in diagram (c). Still, one encounters series of three symbols, consisting of two turnstile values and one collimator point, but now the collimator values clearly dominate, i.e., they occur at pronounced local extrema, whereas any turnstile value marks smaller extrema. Some other details should be noted: Firstly, there is a drastic change in the self-similar structure, since now there occur pairs of turnstile values in certain regions. Secondly, not all symbols are situated at local extrema anymore. And thirdly, even symbols which identify local extrema usually do not hit the precise extrema anymore, which is especially true for turnstile values. Thus, it may be said that diagrams (b) and (c) show a transition from a simple region, dominated by turnstile points, to a significantly more complex region dominated by collimator points. Diagram (d) finally shows a region of higher values of the slope, where collimator points seem to mark almost any extremum, except a few cases, where still turnstile values are encountered. One may also notice that now pairs of collimator points determine

the structure of the curve, in contrast to the three-point series in the diagrams (b) and (c).

In Figure 4.8, magnifications are presented for higher values of the slope. Collimator points still identify, to a certain extent, local extrema, although an increasing number of them does not match anymore to any extremum. No simple self-similar structures comparable to the ones observed in Fig. 4.7 exist anymore. Nevertheless, these curves appear to be self-similar in more complex ways. The results also demonstrate that collimator values indeed have something to do with local extrema, at least for sufficiently high values of the slope, and that these extrema can be identified by collimator points even on very fine scales. Apart from this, one observes that the “smoothness” of the diffusion coefficient curves is basically a matter of the scale, since by zooming in, even previously “smooth” curves become riddled again.

A brief remark regarding fractal dimensions of these curves shall be included here: The magnifications of Figs. 4.7 and 4.8 may lead to conjecture that, like for map \mathcal{L} , the parameter-dependent diffusion coefficient of map \mathcal{S} , as shown over its full range of computed values in Fig. 4.5, is multifractal. Moreover, the discussions above of the two transitions which show up in these diagrams in certain ways suggest that these supposedly different fractal dimensions may have their origin in different deterministic dynamical behaviour in these parameter regions. However, this is difficult to prove numerically (cf. the remarks in Section 2.4) and remains to be shown in detail.

The most important results of this section shall be briefly summarized: An analysis via methods of turnstile dynamics reveals that an interesting transition occurs at the crisis point $a \simeq 3.562$. This transition is characterized by a change in the turnstile dynamics mechanism. Below the crisis point, *turnstile* points seem to be dominant, whereas above the crisis point, they get more and more suppressed, and *collimator* points become more and more important. Furthermore, the self-similar structure of the diffusion coefficient curve changes significantly, i.e., it gets modified from a simple “smooth” structure to a wiggled, more complex one. And at last, one should remark that this transition takes place just at a strong local maximum of the curve. This maximum is precisely identified by the crisis point.

One may conclude that a dynamical mechanism like the one described by a crisis in chaotic scattering is indeed of importance for deterministic diffusion in the maps investigated here. The suspected crisis point is on a large scale characterized by the transition between the two random walk models discussed above, but this does not lead to a well-defined parameter value for the crisis point. More quantitatively, a crisis point may be defined via turnstile dynamics: although one cannot speak about a collision of invariant sets anymore, it seems as if a *collision of turnstiles*, or rather of *turnstile basins*, takes place. In case of map \mathcal{S} , the term turnstile basin is synonymous to collimator. The idea is that orbits of turnstile basins of a

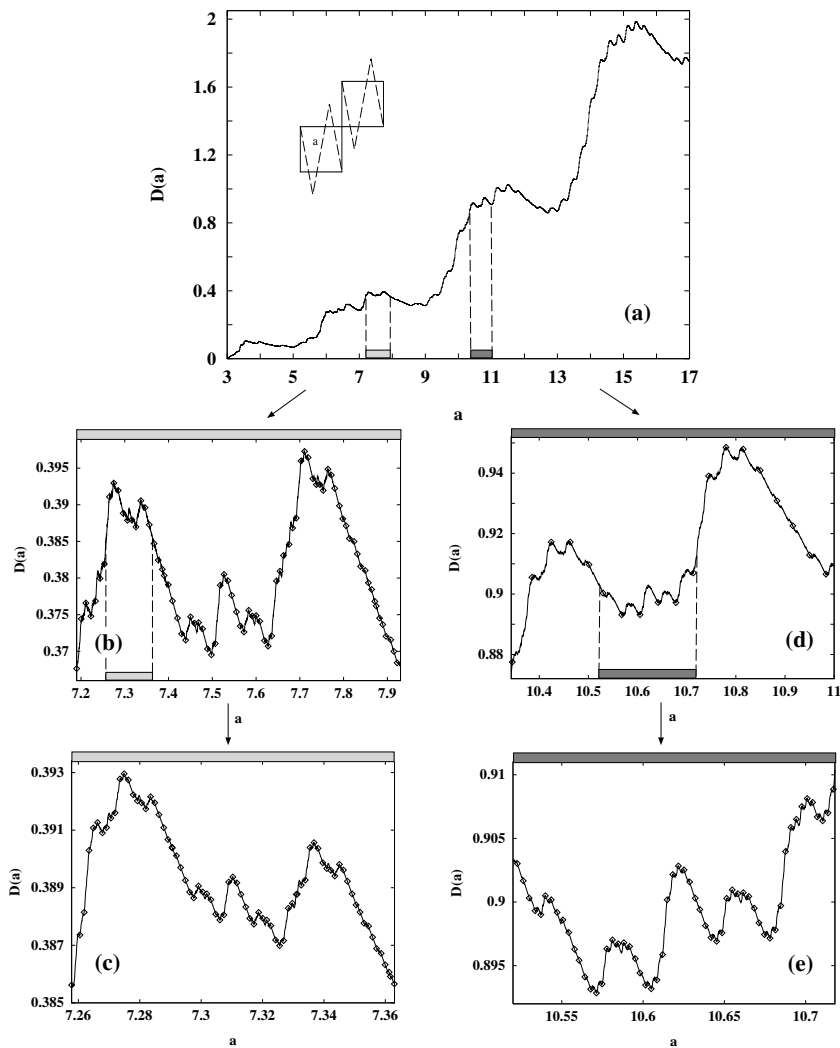


FIGURE 4.8. Further magnifications of the diffusion coefficient of map S and application of turnstile dynamics. In diagram (a), 13,376 single data points have been plotted, in (b) 4,793, in (c) 1,098, in (d) 3,913, and in (e) 1,175, all connected with lines.

box get mapped to their respective turnstile parts with a very high probability after some iterations. Thus, if the value of the slope, or of the height, respectively, is such that the critical point of an upward turnstile gets mapped after one itera-

tion to the collimator of a downwarding turnstile for the first time, a crisis occurs. For map \mathcal{S} , this gives the crisis point $a \simeq 3.562$. For map \mathcal{L} , the situation seems to be more complicated in a sense, since this map does not possess a collimator mechanism. Here, a turnstile basin may be defined by the plus and minus regions of one box introduced in Section 2.4. This would lead to the identification of the slope $a = 3$ as the respective crisis point.

Since the dynamical mechanism of the observed transition in the deterministic diffusion coefficient seems to be related to the one of a crisis in chaotic scattering, and taking into account that the scenario takes place here in a diffusive dynamical system, the process described above may be described as a *crisis in deterministic diffusion*. It should be noted that, according to the first passage method outlined in Section 2.2, the diffusion coefficient is related linearly to the Kolmogorov-Sinai entropy of the dynamical system, see Eqs.(2.16) and (2.12). In Ref. [Bec93], phase transitions in dynamical systems have been classified with respect to significant changes in fundamental dynamical systems quantities, as fractal dimensions, Lyapunov exponents, and entropies. Following this classification, a crisis in deterministic diffusion may be regarded as an *external dynamical phase transition* of the system: The transition occurs by variation of an *external* order parameter, i.e., the slope, or the height, respectively, and the transition shows up in respective *dynamical* quantities, i.e., parameter-dependent diffusion coefficients, or KS-entropies, respectively.⁴

It may be suspected that such phase transitions are quite common not only in simple deterministic dynamical systems of the type discussed here, but even in higher-dimensional, and maybe more realistic models: For example, in Refs. [Kna87, Nob95],⁵ two-dimensional dynamical systems have been considered which are in certain respects related to the two-dimensional model by Lai introduced at the beginning. For these models, an energy threshold has been shown to exist above which the diffusion coefficient behaves linearly in the energy, whereas below no diffusion coefficient can be defined. It may be conjectured that this energy threshold is linked dynamically to a process like a crisis as described above, but this remains to be investigated. Furthermore, it shall be mentioned that dynamical processes like orbiting collisions have also been discussed in many-particle systems of low densities, where particles interact via Lennard-Jones potentials with each other, and certain relations between these collisions and the behaviour of transport coefficients have been pointed out [Kla92]. Thus, physically a direct connection may be suspected between certain microscopic chaotic scattering pro-

⁴Apart from this fundamental phase transition, other dynamical phase transitions seem to be possible in class \mathcal{P} -maps which depend in more detail on the special properties of the map; see, e.g., the second transition in map \mathcal{S} for larger values of the height, which does not occur for map \mathcal{L} .

⁵The author thanks Prof. E. Schöll for drawing his attention to these references.

cesses, like orbiting collisions, over a crisis in dynamical systems to a certain behaviour in transport coefficients, like parameter-dependent diffusion coefficients, which finally may show up macroscopically in form of dynamical phase transitions.

4.4 Conclusions

(1) The methods developed for map \mathcal{L} to compute fractal diffusion coefficients and to understand their complex structures have been successfully applied to a new map, called map \mathcal{S} . The main results obtained for map \mathcal{L} which have been claimed to be more generally characteristic for class \mathcal{P} -maps, i.e., the fractality of parameter-dependent diffusion coefficients and certain features of the deterministic dynamics of the system, have been encountered in map \mathcal{S} as well.

(2) Simple random walk models have been derived and discussed for map \mathcal{L} and map \mathcal{S} . In the limiting cases of high and small values of the height, they lead to certain functional forms, i.e., to a linear law for small heights, and to a law quadratic in the height with a factor of $1/6$ for large heights. These laws are suspected to be universal for class \mathcal{P} -maps. Further evidence for this universality is also obtained from exact analytical as well as numerical results for the parameter-dependent diffusion coefficient.

(3) Certain transitions have been observed in the fractal parameter-dependent diffusion coefficients of map \mathcal{L} and map \mathcal{S} . On a large scale, they can be described by random walk models. For map \mathcal{S} , two transitions have been found, whereas for map \mathcal{L} , only one transition occurs. These transitions appear to be induced by different microscopic dynamical scattering processes.

(4) Map \mathcal{S} was chosen as a diffusive version of a one-dimensional map which shows a crisis in chaotic scattering. Although the mechanism which originally produced the crisis is in certain respects degenerated in map \mathcal{S} , the microscopic dynamics of this system is still quite analogous to the one of a crisis in chaotic scattering. One of the transition points in the parameter-dependent diffusion coefficient of map \mathcal{S} , and the single transition observed in map \mathcal{L} , could be related to the crisis mechanism. This macroscopic appearance of a crisis has been denoted as a crisis in deterministic diffusion. The phenomenon seems to be responsible for an external dynamical phase transition, which is conjectured to be quite common in deterministic diffusive dynamical systems.

5

Fractal Functions for Fractal Diffusion Coefficients

In Section 2.4, it has been mentioned as a striking observation that some of the magnifications of the fractal diffusion coefficient of map \mathcal{L} resemble very much certain analytical fractal functions. Such fractal functions, defined by functional equations, have been encountered in the literature just by working on dynamical systems which are quite analogous to the ones considered here [Tas93a, Tas94, Tas95]. This suggests that it might be possible to obtain fractal diffusion coefficients not only by computing them pointwise, as it has been done before, but that there is a more fundamental relation of fractal diffusion coefficients to analytical fractal functions over a broad range of parameter values.

The problem of this chapter is thus to investigate whether such a relation can be actually established. For this purpose, a more formal analytical approach is required to compute deterministic diffusion coefficients in the class \mathcal{P} of maps under consideration, which is beyond the range of procedures developed in the framework of the first passage method of the previous chapters.

In Section 5.1, the formal background of this approach, based on the Green-Kubo formula of diffusion, will be outlined. In Section 5.2, these tools will be applied for gradually computing deterministic diffusion coefficients for map \mathcal{L} in a series of increasingly better numerical and analytical approximations. Finally, the two main ingredients of this new method to compute parameter-dependent diffusion coefficients, i.e., some newly-defined parameter-dependent fractal functions (see Section 5.3) and parameter-dependent probability densities on the unit interval (see Section 5.4) will be analyzed in more detail for a certain range of the parameter.¹

¹The work of this chapter has been initiated by a hint of Prof. P. Gaspard, Brussels, during a conversation at the SIAM conference on Dynamical Systems in Snowbird, USA, May 1995. Prof. Gaspard also assisted with further hints in the course of the calculations. The actual work got started during a subsequent stay at the IPST, College Park, USA, June 1995, in collaboration with Prof. J.R. Dorfman, who especially developed the idea of deriving the recursion relation for fractal functions Eq.(5.9).

5.1 Construction of jump-velocity functions

For convenience, some definitions shall be repeated which have already been introduced in previous chapters. They will be needed here more extensively.

Again, a map of class \mathcal{P}

$$M_a : R \rightarrow R, \quad x_n \mapsto M_a(x_n) = x_{n+1}, \quad a > 0, \quad x_n \in R, \quad n \in N_0, \quad (5.1)$$

cf. Eq.(2.5) or Section 2.1.3, respectively, shall be considered modeling an *old* chain of boxes, i.e., a periodic one-dimensional map with a lift of degree one,

$$M_a(x_n + 1) = M_a(x_n) + 1, \quad (5.2)$$

in which a diffusion process shall be possible, cf. Conjecture 2.2.

Let the corresponding “reduced map” be

$$\tilde{M}_a(\tilde{x}) := M_a(\tilde{x}) \pmod{1}, \quad (5.3)$$

cf. Eq.(2.38), with $\tilde{x} := x - [x]$ being the fractional part of x , $\tilde{x} \in [0, 1)$, where $[x]$ denotes the largest integer less than x . This map governs the internal box dynamics according to [Sch89, Gro82, Fuj82]

$$\tilde{x}_{n+1} = \tilde{M}_a(\tilde{x}_n), \quad \tilde{x}_n = \tilde{M}_a^n(\tilde{x}), \quad \tilde{x} \equiv \tilde{x}_0. \quad (5.4)$$

The goal is to calculate $D(a)$ by means of the Green-Kubo formula

$$D(a) = \left\langle j_a(\tilde{x}_0) \sum_{n=0}^{\infty} j_a(\tilde{x}_n) \right\rangle - \frac{1}{2} \langle j_a^2(\tilde{x}_0) \rangle, \quad (5.5)$$

cf. Eq.(3.10),² where the average

$$\langle \dots \rangle := \int_0^1 d\tilde{x} \tilde{\rho}_a(\tilde{x}) \dots \quad (5.6)$$

has to be taken over the invariant probability density on the unit interval $\tilde{\rho}_a(\tilde{x})$, which is determined by the reduced map $\tilde{M}_a(\tilde{x})$ and its corresponding Frobenius-Perron equation, cf. Eq. (2.10).

The “jump-velocity” $j_a(x_n) := [x_{n+1}] - [x_n]$ takes only integer values and can be interpreted as denoting how many boxes of the chain a particle has traversed after

²In comparison to the Green-Kubo formula Eq.(3.10) used in Chapter 3, here a separation between *internal* and *external* box motion has been performed in advance. It can be shown that in the limit of time n to infinity the contributions of any internal box motion vanish.

one iteration if it starts at initial condition \tilde{x} .

Because of the lift condition given by Eq.(5.2), it makes no difference whether the jump-velocity is calculated for the dynamics ruled by the full map or by the reduced map:

$$\begin{aligned}
 j_a(x_n) &= [M_a(x_n)] - [x_n] \\
 &= [M_a(\tilde{x}_n + [x_n])] - [\tilde{x}_n + [x_n]] \\
 &= [M_a(\tilde{x}_n)] \\
 &= j_a(\tilde{x}_n) \quad .
 \end{aligned} \tag{5.7}$$

In evaluating the Green-Kubo formula for class \mathcal{P} -maps, one encounters two main problems: (1) summing up the jump-velocities in the first term of Eq.(5.5), and (2) computing the invariant probability density $\tilde{\rho}_a(\tilde{x})$.

To deal with the first problem, one defines a ‘‘jump-velocity function’’

$$J_a^n(\tilde{x}) := \sum_{k=0}^n j_a(\tilde{x}_k) \tag{5.8}$$

for which the following recursion relation can be derived:

$$\begin{aligned}
 J_a^n(\tilde{x}) &= \sum_{k=0}^n j_a(\tilde{M}_a^k(\tilde{x})) \\
 &= j_a(\tilde{x}) + \sum_{k=1}^n j_a(\tilde{M}_a^k(\tilde{x})) \\
 &= j_a(\tilde{x}) + J_a^{n-1}(\tilde{M}_a(\tilde{x})) \quad .
 \end{aligned} \tag{5.9}$$

This function is highly irregular, since it gives the integer value of the displacement of a particle starting at any initial position \tilde{x} :

$$\begin{aligned}
 J_a^n(\tilde{x}) &= j_a(\tilde{x}_0) + j_a(\tilde{x}_1) + \dots + j_a(\tilde{x}_n) \\
 &= [x_1] - [x_0] + [x_2] - [x_1] + \dots + [x_{n+1}] - [x_n] \\
 &= [x_{n+1}] \quad .
 \end{aligned} \tag{5.10}$$

For evaluating the Green-Kubo formula, it is suitable to define a more well-behaved function $T_a^n(\tilde{x})$ by

$$J_a^n(\tilde{x}) =: \frac{d}{d\tilde{x}} T_a^n(\tilde{x}) \tag{5.11}$$

which satisfies the recursion relation

$$T_a^n(\tilde{x}) = t_a(\tilde{x}) + b_a(\tilde{x}) T_a^{n-1}(\tilde{M}_a(\tilde{x})) \quad . \tag{5.12}$$

Here, $t_a(\tilde{x})$ is given by

$$\frac{d}{d\tilde{x}}t_a(\tilde{x}) = j_a(\tilde{x}) \quad , \quad t_a(\tilde{x}) = \tilde{x} j_a(\tilde{x}) + c_a(\tilde{x}) \quad , \quad (5.13)$$

with $c_a(\tilde{x})$ taken to be constant in each of the subintervals of the unit interval where the jump-velocity $j_a(\tilde{x})$ has a given value. This constant is fixed by the condition that $T_a(\tilde{x})$ be continuous on the unit interval, and that $T_a(0) = T_a(1) = 0$. For piecewise linear maps, the coefficient $b_a(\tilde{x})$ is equal to $\pm 1/a$.³

As an example, diffusion in the well-known map \mathcal{L} (cf. Section 2.1.3)

$$M_a(x) = \left\{ \begin{array}{ll} ax & , \quad 0 \leq x < \frac{1}{2} \\ ax + 1 - a & , \quad \frac{1}{2} \leq x < 1 \end{array} \right\} \quad , \quad a \geq 2 \quad , \quad (5.14)$$

will be considered, here with the slope a restricted to the range $2 \leq a \leq 4$.

In this case, the jump-velocities are given by

$$j_a(\tilde{x}) = \left\{ \begin{array}{ll} 0 & , \quad 0 \leq \tilde{x} < 1/a \\ 1 & , \quad 1/a \leq \tilde{x} < 1/2 \\ -1 & , \quad 1/2 \leq \tilde{x} < 1 - 1/a \\ 0 & , \quad 1 - 1/a \leq \tilde{x} < 1 \end{array} \right\} \quad , \quad 2 \leq a \leq 4 \quad . \quad (5.15)$$

The jump-velocity function is determined by the functional equation

$$J_a^n(\tilde{x}) = \left\{ \begin{array}{ll} J_a^{n-1}(a\tilde{x}) & , \quad 0 \leq \tilde{x} < 1/a \\ 1 + J_a^{n-1}(a\tilde{x} - 1) & , \quad 1/a \leq \tilde{x} < 1/2 \\ -1 + J_a^{n-1}(a\tilde{x} + 2 - a) & , \quad 1/2 \leq \tilde{x} < 1 - 1/a \\ J_a^{n-1}(a\tilde{x} + 1 - a) & , \quad 1 - 1/a \leq \tilde{x} < 1 \end{array} \right\} \quad , \quad 2 \leq a \leq 4 \quad , \quad (5.16)$$

and, according to the rules given above, can be integrated to

$$T_a^n(\tilde{x}) = \left\{ \begin{array}{ll} \frac{1}{a} T_a^{n-1}(a\tilde{x}) & , \quad 0 \leq \tilde{x} < 1/a \\ \frac{1}{a} T_a^{n-1}(a\tilde{x} - 1) + \tilde{x} - 1/a & , \quad 1/a \leq \tilde{x} < 1/2 \\ \frac{1}{a} T_a^{n-1}(a\tilde{x} + 2 - a) - \tilde{x} + 1 - 1/a & , \quad 1/2 \leq \tilde{x} < 1 - 1/a \\ \frac{1}{a} T_a^{n-1}(a\tilde{x} + 1 - a) & , \quad 1 - 1/a \leq \tilde{x} < 1 \end{array} \right\} \quad , \quad (5.17)$$

$$2 \leq a \leq 4 \quad .$$

In Section 5.3 it will be shown that the functions $T_a(\tilde{x}) = \lim_{n \rightarrow \infty} T_a^n(\tilde{x})$ of Eq.(5.17) exist, and they will be discussed there in more detail, supported by numerical results.

Functions like $T_a(\tilde{x})$ have been introduced in Refs. [Tas93a, Tas94, Tas95] and may be called *generalized Takagi functions*. In special cases, they have been shown to be fractal [Tas93a, Tas94, Tas95].

³Possible problems at discontinuity points of the map $\tilde{M}_a(\tilde{x})$ as well as more rigorous mathematical questions regarding differentiation and integration of these functions will not be taken into account.

5.2 Approximation procedures for fractal diffusion coefficients

In the previous section, the problem of summing up jump-velocities has been transformed into computing generalized Takagi functions $T_a(\tilde{x})$. This makes it already possible to calculate diffusion coefficients $D(a)$ in simple cases, i.e., for integer slopes.

For such values of the slope, the invariant probability density is uniform over the unit interval, $\tilde{\rho}_a(\tilde{x}) = 1$, which facilitates the calculations significantly. As an example, the slope $a = 3$ will be considered. According to Eqs.(5.15), (5.17), and the Green-Kubo formula Eq.(5.5), the diffusion coefficient can be computed straightforward to

$$D(3) = 2T_3\left(\frac{1}{2}\right) - 2T_3\left(\frac{1}{3}\right) - \frac{1}{6} = \frac{1}{3} \quad , \quad (5.18)$$

where, apart from the fact that $T_a(\tilde{x})$ is symmetric, the fact has been used that for any fixed point, and any (eventually) periodic orbit, $T_a(\tilde{x})$ can in principle be calculated exactly by iterating the generalized Takagi function on this orbit. By generalizing this procedure, the previous exact diffusion coefficient formulas Eqs. (2.28) and (2.32) can be recovered.

However, for arbitrary slope a the invariant probability density will not be uniform and has to be calculated by more rigorous methods. This “second main problem”, i.e., solving the Frobenius-Perron equation, will be faced explicitly in Section 5.4, where detailed numerical results for $\tilde{\rho}_a(\tilde{x})$ will be presented.

A final problem remains to be solved: Because of the integration in the Green-Kubo formula, the probability densities are “entangled” with the generalized Takagi functions. This makes exact analytical calculations generally quite time-consuming (see Section 5.4). Nevertheless, it shall be demonstrated that, following this approach, a number of increasingly refined analytical and numerical approximations for $D(a)$ can be obtained.

In the simplest case, one may assume a uniform box probability density for all values of the slope, which is rigorously true only for integer slopes, as mentioned above. With this *first approximation*, the second term in the Green-Kubo formula can be evaluated to

$$\langle j_a^2(\tilde{x}_0) \rangle = \int_{1/a}^{1-1/a} d\tilde{x} \tilde{\rho}_a(\tilde{x}) \approx \frac{a-2}{a} \quad , \quad (5.19)$$

and the first term reduces to

$$\sum_{n=0}^{\infty} \langle j_a(\tilde{x}_0) j_a(\tilde{x}_n) \rangle \approx \int_{1/a}^{1/2} d\tilde{x} T_a'(\tilde{x}) - \int_{1/2}^{1-1/a} d\tilde{x} T_a'(\tilde{x}) = 2T_a\left(\frac{1}{2}\right) - 2T_a\left(\frac{1}{a}\right) \quad . \quad (5.20)$$

According to Eq.(5.17), these two special values of $T_a(\tilde{x})$ turn out to be

$$T_a\left(\frac{1}{a}\right) = \frac{1}{a} T_a(1) = 0 ; T_a\left(\frac{1}{2}\right) = \frac{1}{2} + \frac{1}{a} T_a\left(\frac{a}{2} - 1\right) - \frac{1}{a} = \frac{a-2}{2a} + \frac{1}{a} T_a(h) \quad (5.21)$$

with $h := a/2 - 1$ being the height between the maximum of the map and the boundary of the box at $\tilde{x} = 1/2$.

As shown by its index, $T_a(\tilde{x})$ also depends on the slope a . However, as a *second approximation* one may assume that, in a given interval of the slope, $T_a(\tilde{x})$ changes “not too discontinuously” by changing the slope, i.e., that $T_a(\tilde{x})$ can be approximated by a generalized Takagi function at fixed slope a , e.g., in this case by $T_a(\tilde{x})$ at $a = 3$.

Thus, one obtains

$$D^I(a) = \frac{a-2}{2a} + \frac{2}{a} T_3(h) \quad , \quad 2 \leq a \leq 4 \quad . \quad (5.22)$$

This provides a first rough approximation of the exact diffusion coefficient, which might be called analytical, because the function $T_3(h)$ is defined by the functional equation Eq.(5.17). The first term gives precisely the solution of a simple random walk model for slope a close to 2, cf. to Eq.(4.15) in Section 4.2. Note that Eq. (5.22) reproduces the exact values of $D(a)$ at $a = 2, 3, 4$.

The result is shown in Fig. 5.1.⁴ Diagram (a) presents $D^I(a)$ in comparison to the exact curve. Especially for $a \leq 3$, the approximation mimics certain regions of the actual $D(a)$ -curve reasonably well, although one might be surprised that just above $a = 3$, where the two approximations involved might be expected to work well, both curves are qualitatively and quantitatively significantly apart.

In Diagrams (b) and (c), two further approximation results are shown. Here, the same calculation has been done as before, but now assuming a probability density which is not necessarily uniform over the whole unit interval, or averaging the exact probability density for map $\tilde{M}_a(\tilde{x})$ in the escape region, respectively. The term escape region refers to the subinterval where the graph of the map exceeds its box boundaries and the particles can “jump” from one box to the other, cf.

⁴In diagrams (a) to (c), each single curve consists of at least 2,000 data points, in case of the exact curve connected with lines. The inset shows around 500 data points for each curve.

The exact diffusion coefficients have been computed via the transition matrix method, see Section 2.3, all approximation results are based on numerical methods to be explained in Sections 5.3 and 5.4. Numerical errors should always be neglectable, cf. Sections 2.4, 5.3, and 5.4.

The number of points is the same for the “pseudo-derivative” plots in diagram (d) to (g), however, here a numerical error could not be estimated.

It should be noted that in diagram (d), (f), and (g) the points are not homogeneously distributed with respect to their values of the slope so that certain structures, e.g., the ones just above $a = 2$ and $a = 3$, become more pronounced than others.

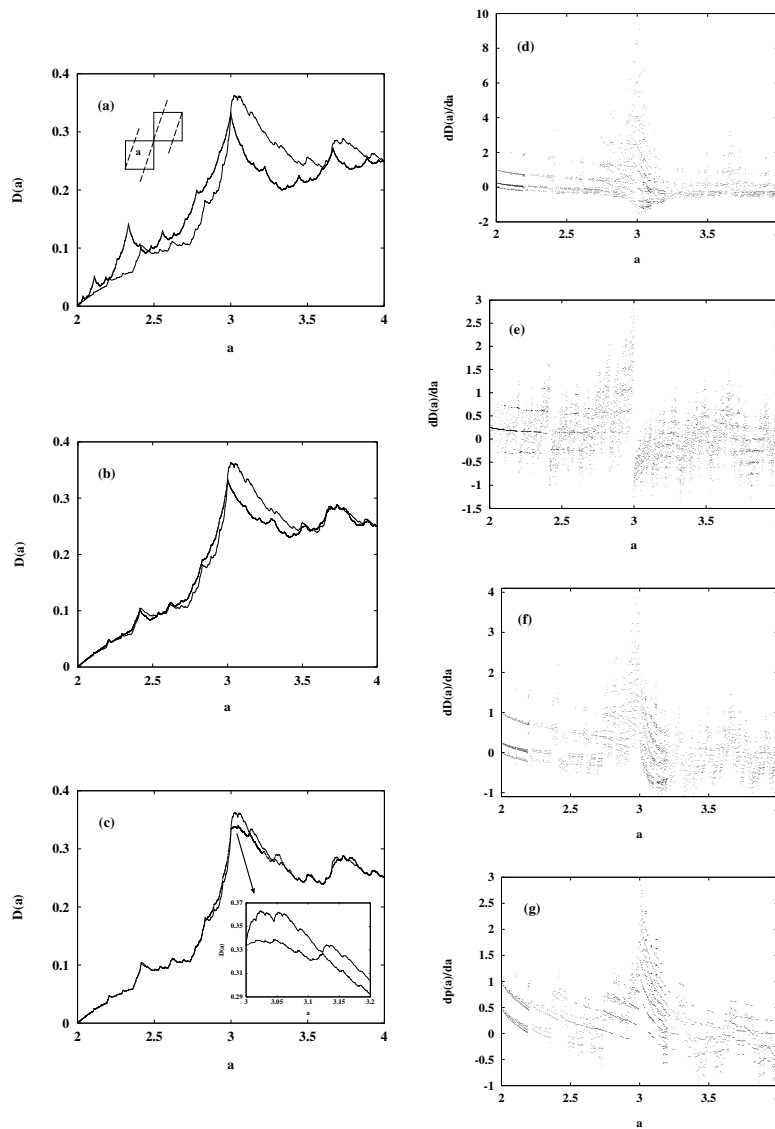


FIGURE 5.1. Comparison of approximations with exact results. Left column: diffusion coefficient $D(a)$; the exact curve in diagram (a) to (c) is given by the bold black line. Right column, diagram (d) to (f): “pseudo-derivatives” $dD(a)/da$ of the diffusion coefficient; diagram (d) gives exact results, diagram (e) and (f) contain approximations. Right column, diagram (g): “pseudo-derivative” $dp(a)/da$ of the escape probability, see text.

Section 2.4. The escape probability $p_{esc}(a)$ is then given by

$$p_{esc}^{II,III}(a) := \int_{1/a}^{1-1/a} d\tilde{x} \tilde{\rho}_a^{II,III}(\tilde{x}) \quad , \quad 2 \leq a \leq 4 \quad , \quad (5.23)$$

and with these assumptions one obtains

$$D^{II,III}(a) = \frac{p_{esc}^{II,III}(a)}{2} + \frac{2p_{esc}^{II,III}(a)}{a-2} T_a(h) \quad , \quad 2 \leq a \leq 4 \quad . \quad (5.24)$$

Diagram (b) contains the result of what could be called a semi-numerical approximation. It is based on a model probability density, i.e., a map has been chosen that replaces the original map under consideration, Eq.(5.14), such that a parameter-dependent probability density can be computed analytically, being uniform in the escape region and providing a simple functional form for $p_{esc}^{II}(a)$. No further approximation has been applied to $T_a(h)$, instead, its exact values have been computed numerically.

Over wide regions this second approximation is getting more close to the exact $D(a)$ than the first one, however, above $a = 3$ the approximation results still deviate clearly from the correct values. Diagram (e) to the right shows the “pseudo-derivative” $\Delta D^{II}(a)/\Delta a$, $\Delta a \ll 1$, and should be compared to diagram (d) in the upper right edge which gives the “pseudo-derivative” of the exact diffusion coefficient.⁵ With respect to the pseudo-derivative results this approximation is still far apart from the exact solution.

Finally, diagram (c) employs Eq.(5.24) with the exact escape probability $p_{esc}(a) \equiv p_{esc}^{III}(a)$ and, as before, with the exact generalized Takagi functions. Both quantities have been computed numerically. Note that the result is still approximate, because $\tilde{\rho}_a(\tilde{x}) \equiv \tilde{\rho}_a^{III}(\tilde{x})$ has simply been averaged in the escape region without weighting $T_a(\tilde{x})$ appropriately.

⁵In Ref. [Ers93], it has been proved that, for class \mathcal{P} -maps, parameter-dependent invariant probability densities are continuous, but nowhere differentiable with respect to their parameter values. Since the diffusion coefficient $D(a)$ is based on integrations over these probability densities, it is mathematically not in advance clear whether the derivative $dD(a)/da$ is well-defined. However, as has already been mentioned in Section 2.4, numerical results indicate that a “pseudo-derivative” $\Delta D(a)/\Delta a$, $a \ll 1$, i.e., a kind of “mean value” of ΔD over “tiny” regions of Δa approaching zero, makes some sense. With respect to such mathematical problems, it cannot totally be ruled out that the structures of $\Delta D(a)/\Delta a$, presented in diagram (d) to (g), are numerically artificial. On the other hand, taking a close look at the $D(a)$ -curve and matching it to its “pseudo-derivatives”, it might as well be conjectured that these plots represent actual properties of the fractal diffusion coefficient under consideration, and that such “banded structures” are especially characteristic for curves which contain some self-similarity.

Without being able to a final conclusion about this issue at this stage, these “pseudo-derivative curves” should be regarded as a matter of further discussion.

For $a \leq 3$, this third approximation $D^{III}(a)$ matches to the exact curve very well almost everywhere. For $a > 3$, the largest deviations can still be found in the region just above $a = 3$, which is given in the blowup and might be best described as an “overhang” of the exact diffusion coefficient (cf. Section 2.4). Although this phenomenon could not be caught satisfactorily by any of the approximations I to III, the third approach produces at least a slight cusp for the first time.

The pseudo-derivative of this third approximation is shown in diagram (f). It gives an overall behaviour which is not too far apart from the exact results in diagram (d), at least up to values around $a = 3$. Diagram (g) below demonstrates that indeed the numerically computed exact escape probability is essentially responsible for this coincidence.

The approximation procedures presented here work as well for any higher value of the slope and give simple formulas for the full $D(a)$ –curve in terms of generalized Takagi functions. It should be possible to extend this approach without great modifications to any other map of class \mathcal{P} .

5.3 Fractal generalized Takagi functions

In Section 5.1, generalized Takagi functions $T_a(\tilde{x})$ have been introduced, and it has been shown that they play an important role for evaluating the parameter-dependent diffusion coefficient $D(a)$ in terms of the Green-Kubo formula. Therefore, knowing details about the structure of these functions may be helpful to achieve a better understanding of the nature of the fractal diffusion coefficient $D(a)$.

To calculate the functions $T_a(\tilde{x})$, numerical methods have to be used. They can be developed by starting with the recursion relation Eq.(5.12),

$$T_a^n(\tilde{x}) = t_a(\tilde{x}) + b_a(\tilde{x}) T_a^{n-1}(\tilde{M}_a(\tilde{x})) \quad , \quad 0 \leq \tilde{x} \leq 1 \quad , \quad n \in N_0 \quad , \quad (5.25)$$

where formally $T_a^{-1}(\tilde{x}) \equiv 0$ can be assumed, which gives the correct values of $T_a^0(\tilde{x})$ at the next iteration.

Here, as an example, the generalized Takagi function Eq.(5.17) will be discussed. As has already been noticed in Ref. [Tas93a], constructing functions like $T_a(\tilde{x})$ by evaluating Eq.(5.25), or (5.17), respectively, time step by time step resembles creating the well-known Koch curve: one gets a series of graphs $T_a^n(\tilde{x})$ which rapidly converges to $T_a(\tilde{x})$, revealing self-similar structures on an increasingly refined scale.

This observation can directly be exploited for numerical calculations, based on the following scheme: Iterating Eq.(5.17) in form of Eq.(5.25) $(n + 1)$ -times, one

obtains

$$\begin{aligned}
T_a^n(\tilde{x}) &= t_a(\tilde{x}) + \frac{1}{a} [t_a(\tilde{M}_a(\tilde{x})) + \frac{1}{a} T_a^{n-2}(\tilde{M}_a^2(\tilde{x}))] \\
&= \dots = t_a(\tilde{x}) + \frac{1}{a} t_a(\tilde{M}_a(\tilde{x})) + \dots + \frac{1}{a^n} t_a(\tilde{M}_a^n(\tilde{x})) + \frac{1}{a^{n+1}} T^{-1}(\tilde{M}_a^{n+1}(\tilde{x})) \\
&= \sum_{k=0}^n \frac{1}{a^k} t_a(\tilde{M}_a^k(\tilde{x})) \tag{5.26}
\end{aligned}$$

with

$$t_a(\tilde{x}) = \left\{ \begin{array}{ll} 0 & , \quad 0 \leq \tilde{x} < 1/a \\ \tilde{x} - 1/a & , \quad 1/a \leq \tilde{x} < 1/2 \\ -\tilde{x} + 1 - 1/a & , \quad 1/2 \leq \tilde{x} < 1 - 1/a \\ 0 & , \quad 1 - 1/a \leq \tilde{x} < 1 \end{array} \right\} , \quad 2 \leq a \leq 4 \quad , \tag{5.27}$$

so that $|t_a(\tilde{M}_a^k(\tilde{x}))| < (a-2)/(2a)$ for all $\tilde{x} \in [0, 1)$.

In the limit $n \rightarrow \infty$, this ensures that $T_a(\tilde{x})$, defined by Eq. (5.17), is convergent and thus is well-defined by applying criteria of convergence to the series of Eq.(5.26).⁶

If one wants to stop the iteration procedure at a certain time step n , one can estimate a largest error of $T_a^n(\tilde{x})$ with respect to the exact $T_a(\tilde{x})$ by

$$\begin{aligned}
\Delta T_a^n(\tilde{x}) &:= |T_a(\tilde{x}) - T_a^n(\tilde{x})| \leq |T_a(\tilde{x})| - |T_a^n(\tilde{x})| \\
&\leq \left(\sum_{k=0}^{\infty} \left| \frac{1}{a} \right|^k - \sum_{k=0}^n \left| \frac{1}{a} \right|^k \right) \frac{a-2}{2a} \approx \frac{a-2}{2a^n} \quad . \tag{5.28}
\end{aligned}$$

For example, after $n = 10$ iterations the error gets less than $5 \cdot 10^{-5}$ for any slope $2 \leq a \leq 4$.

Based on these results, a numerical procedure to evaluate $T_a(\tilde{x})$ can be implemented in a straightforward way. All one has to do is to start with any \tilde{x} and summing up the terms $t_a(\tilde{x})$ on the iterated orbit $\tilde{x}_{n+1} = \tilde{M}_a^n(\tilde{x}_0)$ for n sufficiently large.

Some plots of $T_a(\tilde{x})$, Eq.(5.17), can be found in Fig. 5.2. Diagram (a) shows a three-dimensional surface plot, and (b) gives a contour plot of this surface.⁷ The regular occurrence of peaks and valleys and the change of this structure with changing the slope should be compared to the exact results of $D(a)$ in Fig. 5.1. It is striking that the occurrence of the troublesome ‘‘overhang’’ regions corresponds

⁶Generalizations of this proof to larger classes of maps might be possible, however, they seem to depend on the properties of each specific $t_a(\tilde{x})$, which are difficult to formalize.

⁷These graphs consist of 22 functions $T_a(\tilde{x})$ at fixed slopes a , each evaluated at 200 different values of \tilde{x} .

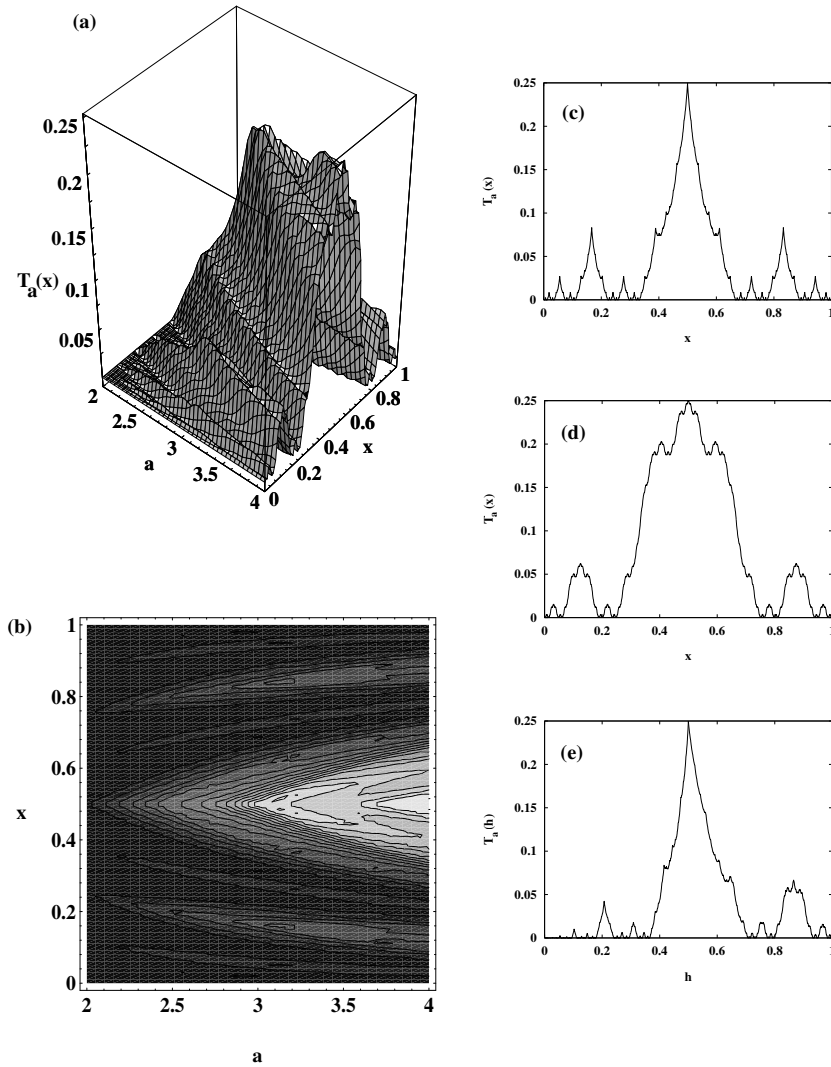


FIGURE 5.2. Generalized Takagi functions $T_a(x)$, example: surface plot (a), contour plot (b), and three slices of (a) at certain parameter values, see text.

to the onset of a bifurcation-like behaviour in the contour plot (b). Diagrams (c) to (e) provide cuts of the generalized Takagi surface parallel to the x -axis at $a = 3$ and $a = 4$, and along the diagonal from $(a, x) = (2, 0)$ to $(4, 1)$.⁸ It should be noted that the graphs in diagrams (c) and (e) directly appear in the approximations $D^I(a)$ and $D^{II}(a)$ in Fig. 5.1 (a) and (b).

The structures in these diagrams can be understood by referring to certain orbits: The main local maxima, separated by points of zero value in diagram (c) to (e), are related to backward iterations of the critical points at $x_c = 1/2$ by $x_{-n} = \tilde{M}_a^{-n}(\tilde{x}_c)$, $n \in N_0$. this leads to the functional form $\tilde{x}(a) \sim 1/a^k$, $k \in N$ to be observed in contour plot (b). Via backward iteration of the “boundary points” $\tilde{x}_b = 0$, one obtains all the local minima $T_a(\tilde{x}) = 0$ with the same functional form as for the maxima in diagram (b). Any additional “fine structure” in the plots seems to be essentially due to further backward iteration of these points. The respective orbits are selected by the property that they hit parts of the reduced map which have been created by applying the modulus to the original map, see Eq.(5.3). For example, the so-called bifurcation-like structure is supposedly generated by the new “non-uniqueness overlap” of the two inner branches of $\tilde{M}_a(\tilde{x})$ above $a = 3$, which makes inversion of the dynamics more difficult and the dynamics itself more rich and complex.

The most important result here is that the parameter-dependent generalized Takagi functions $T_a(\tilde{x})$ are fractal functions with self-similar structures. In fact, they obey a simple scaling law: height and width of similar structures, as shown in diagram (c) and (d), scale with precisely the slope a , which is due to the factor $1/a$ in front of the functions $T_a(\tilde{x})$ in Eq.(5.17).

5.4 Computation of invariant probability densities on the unit interval

To get exact values for the diffusion coefficient $D(a)$ via the Green-Kubo formula Eq.(5.5), one needs the precise invariant probability densities $\tilde{\rho}_a(\tilde{x})$ on the unit interval.

One can find a rich mathematical literature about existence and uniqueness theorems of these densities for various classes of one-dimensional maps, and about procedures to compute them, see, e.g., Refs. [Gas92a, Tas93a, Tas94, Tas95, Ers93, dM93, Las94, Las73, Li78, Li76, Boy79, Gas92c, Gas92b, Ant93, Tas93b, Ant92].

However, for the class of maps under consideration a procedure shall be presented

⁸Based on the iteration procedure outlined above, the numerical error of these graphs is negligible.

which employs the transition matrix method outlined in Section 2.3 and which can analytically be applied in simple cases. It is based on the following Corollary:

Corollary 5.1 (Invariant probability densities for maps with uniform slope)

Let $\tilde{M}_a : [0, 1) \rightarrow [0, 1)$, $\tilde{x}_n \mapsto \tilde{M}_a(\tilde{x}_n) = \tilde{x}_{n+1}$, $a \in \mathbb{R}$, $n \in \mathbb{N}_0$ a discrete one-dimensional piecewise linear expansive map with uniform slope a . If, for given slope a , the map is uniquely ergodic and if a Markov partition exists, then

- (i) the largest eigenvalue χ_{\max} of the topological transition matrix $T(a)$ corresponding to $\tilde{M}_a(\tilde{x})$ is equal to the slope a .
(ii) the invariant probability density $\tilde{\rho}_a(\tilde{x})$ is determined by the “largest” eigenvector $\tilde{\rho}_a^{\max}$ corresponding to χ_{\max} , $\tilde{\rho}_a = c \tilde{\rho}_a^{\max}$, where the constant c is fixed by a normalization condition: $\int_0^1 d\tilde{x} \tilde{\rho}_a(\tilde{x}) \equiv 1$.

This corollary can be obtained from a more general theorem which is valid for piecewise uniform maps and will be proven elsewhere.⁹ The corollary ensures that, for any Markov partition value of the slope (see Section 2.3.2) the invariant probability density on the unit interval is well-defined. Furthermore, it might be interpreted as a proof that all these invariant probability densities are step functions of the type of the following example, as has already been discussed numerically in Section 3.2.1, and as has also been shown in Ref. [Ers93].

As an example of the application of this corollary, and as an example of the calculation of a non-trivial diffusion coefficient $D(a)$, one of the simplest Markov partitions in the range $2 \leq a \leq 4$ shall be considered, see Fig. 5.3. The calculation can be carried out in different steps:

(1) Existence of Markov partitions:

The slope a is determined by the Markov condition that $\varepsilon := a/2 - 1$, $0 \leq \varepsilon \leq 1/2$, gets mapped onto $\tilde{x} = 1/2$ after one iteration, and therefore to ε again after two iterations:

$$\tilde{M}_a(\varepsilon) = a\varepsilon = \frac{1}{2} \quad \Rightarrow \quad a = 1 + \sqrt{2} \simeq 2.414 \quad . \quad (5.29)$$

(2) Construction of topological transition matrices:

The Markov partition of the reduced map can be constructed according to the procedure outlined in Section 2.3.2 and leads to the following topological transition matrix $T(a)$, cf. Fig. 5.3:

$$T(2.414) = \begin{pmatrix} 1 & 1 & 1 & 0 \\ 1 & 0 & 1 & 0 \\ 0 & 1 & 0 & 1 \\ 0 & 1 & 1 & 1 \end{pmatrix} . \quad (5.30)$$

⁹It will be included as an appendix in a publication, which is based on this chapter.

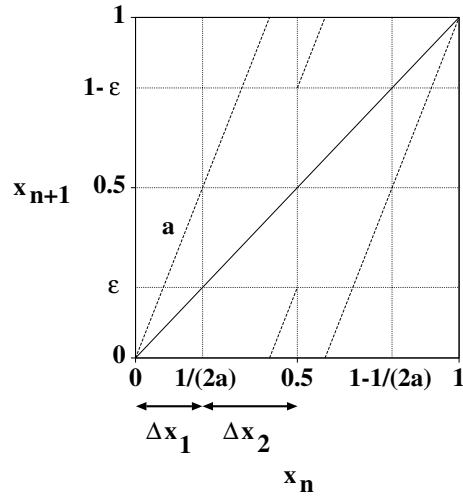


FIGURE 5.3. Computation of invariant probability densities and of non-trivial diffusion coefficients: example, slope $a \simeq 2.414$.

It should be noted that this matrix is not symmetric.

(3) Calculation of the largest eigenvector:

With part (i) of Corollary 5.1, solving the eigenvalue problem of the matrix $T(a)$ reduces to computing the eigenvector to χ_{max} , $\tilde{\rho}_{2.414}^{max} := (\rho_1, \rho_2, \rho_3, \rho_4)^*$. This calculation can be further simplified by taking the symmetry of the map into account, $\rho_1 = \rho_4$, $\rho_2 = \rho_3$, which, in this case, leads to

$$\tilde{\rho}_{2.414}^{max} = c \begin{pmatrix} \rho_1 \\ 1 \\ 1 \\ \rho_1 \end{pmatrix} \quad \text{with} \quad \rho_1 = \frac{1+a}{a} = \sqrt{2} \quad . \quad (5.31)$$

(4) Normalization of $\tilde{\rho}_a^{max}$:

Applying the normalization condition given in part (ii) of the corollary to the probability density vector $\tilde{\rho}_a^{max}$, it reads

$$c \sum_{k=1}^4 \rho_k \Delta \tilde{x}_k \equiv 1 \quad , \quad (5.32)$$

where $\Delta \tilde{x}_k$ stands for the size of the subinterval of the k th Markov partition cell, see Fig. 5.3. One obtains

$$c = \frac{a}{2(a-1)} \quad \text{and} \quad \rho_1^{max} = \frac{a}{\sqrt{2}(a-1)} \quad , \quad \rho_2^{max} = \frac{a}{2(a-1)} \quad . \quad (5.33)$$

Now, the Green-Kubo formula Eq.(5.5) can be evaluated explicitly to get the diffusion coefficient $D(a)$: The second term of this equation gives

$$\langle j_a^2(\tilde{x}_0) \rangle = \frac{a-2}{2(a-1)} \quad , \quad (5.34)$$

the first term reduces to

$$\left\langle j_a(\tilde{x}_0) \sum_{n=0}^{\infty} j_a(\tilde{x}_n) \right\rangle = \rho_2^{max} [2T_a(\frac{1}{2}) - 2T_a(\frac{1}{a})] \quad . \quad (5.35)$$

Employing Eq.(5.17), these two values for $T_a(\tilde{x})$ can be computed to

$$\begin{aligned} T_a(\frac{1}{a}) &= \frac{1}{a} T_a(1) = 0 \quad ; \\ T_a(\frac{1}{2}) &= \frac{1}{a} T_a(\tilde{M}_a(\frac{1}{2})) + \frac{1}{2} - \frac{1}{a} \\ &\quad \tilde{M}_a(\frac{1}{2}) = \varepsilon = \frac{1}{2a} \quad , \quad T_a(\frac{1}{2a}) = \frac{1}{a} T_a(\frac{1}{2}) \\ \Rightarrow T_a(\frac{1}{2}) &= \frac{a(a-2)}{2(a^2-1)} \quad , \end{aligned} \quad (5.36)$$

which finally results in $D(2.414) = (\sqrt{2} - 1)/4 \simeq 0.1036$.

Although these calculations can in principle be performed for any Markov partition value of the slope, they soon get quite tedious, since the size of the partitions and, hence, of the corresponding transition matrices increases rapidly. Therefore, numerical solutions are desirable.

Instead of solving eigenvalue problems, it is more convenient to apply the iteration method, as described in Section 3.1 for whole chains of maps. Results produced by this method are given in Fig. 5.4. Diagram (a) shows a three-dimensional surface plot of the parameter-dependent invariant probability densities, diagram (b) provides a density plot for this surface.¹⁰ The kinks which appear in the surface plot and which form such a symmetric pattern in the density plot are due to the discontinuity of the map Eq.(5.14) at $\tilde{x} = 1/2$ in its reduced form (see also Ref. [Ers93]): The functional form of the $(n+1)$ -th line is determined by forward iteration of the critical points according to $\tilde{x}_n = \tilde{M}_a^n(\tilde{x}_c)$, $\tilde{x}_{c1} = a/2 - 1$ and $\tilde{x}_{c2} = 2 - a/2$, respectively. The parameter-dependent probability densities themselves are simple step functions. This can be seen in diagram (d) and (e) in which cuts of the surface parallel to the \tilde{x} -axis are presented.¹¹ Diagram (c) finally contains the results of the escape probability $p_{esc}(a)$, defined in Eq.(5.23), at various

¹⁰These graphs are based on 102 functions $\tilde{\rho}_a(\tilde{x})$ at fixed slopes a , each evaluated at 100 different values of \tilde{x} .

¹¹For a numerical error, see the discussion of the iteration method in Section 2.4.

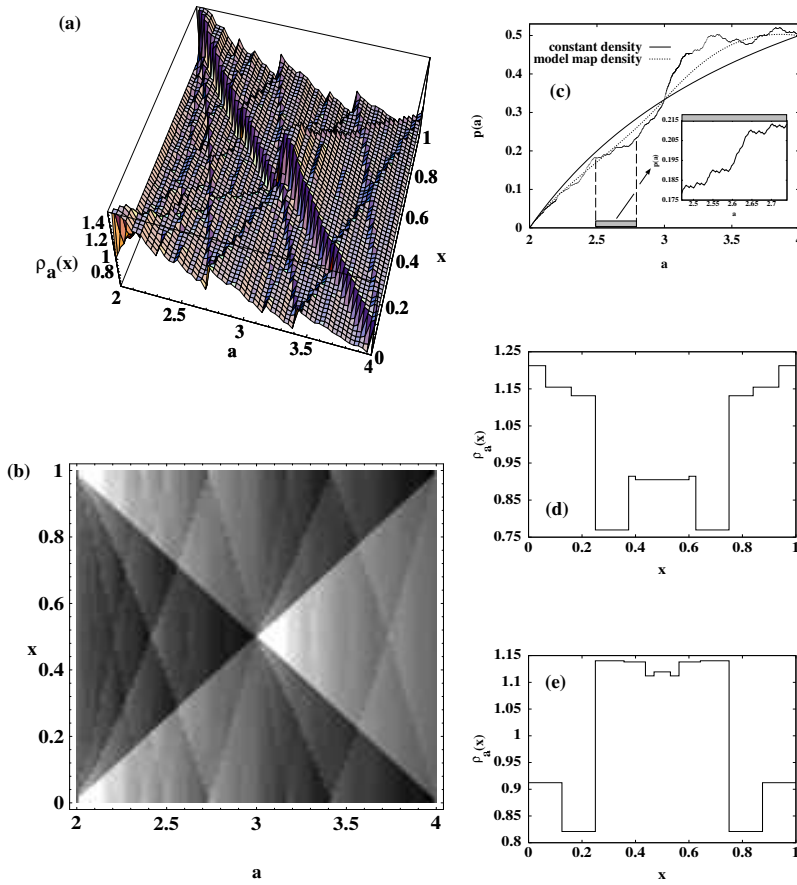


FIGURE 5.4. Invariant probability densities $\tilde{\rho}_a(\tilde{x})$ on the unit interval, example: surface plot (a), density plot (b), escape probability (c) and two slices of (a) parallel to the x -axis: Diagram (d) at $a \simeq 2.5$, Diagram (e) at $a \simeq 3.5$.

levels of approximation. The dashed curve corresponds to a uniform probability density $\tilde{\rho}_a(\tilde{x}) = 1$ as employed in the approximation $D^I(a)$, the full line is based on the integrated piecewise uniform probability density of the simple model map mentioned before, which has been calculated and used for approximation $D^{II}(a)$, and the dots refer to exact results, as obtained from the full correct probability densities computed numerically.¹² From this diagram, it can also be inferred why

¹²In diagram (c), 2,381 single data points are shown, the inset contains 200 points, connected with lines.

the approximations $D^{I,II}(a)$ in Fig. 5.1 are less than the exact values of $D(a)$ for $a < 3$, and greater than $D(a)$ for $a > 3$. The inset reveals self-similar structures of $p_{esc}(a)$ so that it might be assumed that this exact curve, like the exact diffusion coefficient $D(a)$, is again fractal.¹³

All these numerical results are closely related to the propositions made in Ref. [Ers93] and, in a sense, can be taken as illustrations of them, although in this reference no fractal structures have been assumed, or found.¹⁴

5.5 Conclusions

(1) Another method to compute fractal diffusion coefficients for simple one-dimensional maps has been presented. Numerically and analytically, it provides a convenient alternative to the procedures outlined before. Mathematically, it might even be considered as being more rigorous, because it lacks any “external” definition of diffusion coefficients as, e.g., in case of the transition matrix method.

(2) This method, based on the Green-Kubo formula, leads to a distinction between generalized Takagi functions, linked to the dynamics of the system, and invariant probability densities, linked to its equilibrium states. Therefore, understanding the fractality of the diffusion coefficients traces back to a more detailed understanding of these two functions as the main components of this approach.

(3) Such an analysis, performed for an example, reveals the generalized Takagi functions to be self-similar and fractal. Although the invariant probability densities are simple step functions, their corresponding escape probabilities, by which the densities are built into the calculation of the diffusion coefficients, also turn out to be self-similar and fractal.

(4) A first approximation of the Green-Kubo formula establishes a direct connection between fractal generalized Takagi functions and parameter-dependent diffusion coefficients and, hence analytically, ensures the fractality of the parameter-dependent diffusion coefficient.

(5) Two more refined approximations provide an opportunity to see how the details of the fractal diffusion coefficient gradually emerge by taking the generalized Takagi functions and the invariant probability densities into account increasingly better. If one wants to follow this distinction, the so-called overhangs can basically be characterized as a density effect, since first features seem to appear just after building in the probability densities more properly.

¹³According to Ref. [Ers93], this curve is continuous, but nowhere differentiable.

¹⁴The author is indebted to Dr. A. Pikovsky for pointing out this reference.

(6) Moreover, it seems that in this picture the exact fine structure of the curve is due to a complicated coupling between jump-velocities and invariant probability densities. This coupling turns out to be especially pronounced in certain regions of the curve, e.g., again in the overhang regions.

(7) The remarkable “banded structure” in the pseudo-derivative plots of the exact diffusion coefficients is linked to the respective behaviour of the exact escape probability. Thus, in this picture it can again be described as a density effect.

(8) The structure of invariant probability densities and generalized Takagi functions can be related to the occurrence of certain orbits, especially to iterations of the critical points. It is remarkable that the invariant probability densities are determined by forward iterations of these points, whereas the generalized Takagi functions are shaped by backward iterations in time, which leads, in a way, to a separation of the direction of time in form of these two different functions. The fractal diffusion coefficient, in reverse, consists of both histories by integration of both functions over the complete set of their parameter values.

6

Concluding remarks

In this work, a simple one-dimensional model for deterministic diffusion has been studied. The main goal was to compute the parameter-dependent diffusion coefficient of this system. By various analytical and numerical methods, based on chaotic dynamical systems theory and transport theory of statistical mechanics, many interesting features of the resulting diffusion coefficient curves have been revealed, and first approaches have been developed to understand the complex nature of these curves in more detail.

In the following section, the most important results shall be briefly summarized. The last section provides an outlook to further problems, where the methods developed here may be successfully applied as well, and where similar results can be expected.

6.1 Summary of main results

(A) In two one-dimensional piecewise linear chaotic maps with a periodic distribution of identical scatterers, parameter-dependent *diffusion coefficients* have been discovered which show an unambiguously *fractal structure*. These results appear to be the first examples of dynamical systems with fractal diffusion coefficients. It is suspected that such curves are quite typical for periodic deterministic dynamical systems with diffusive dynamics.

(B) A variety of *new methods* to compute deterministic diffusion coefficients analytically and numerically has been developed: Based on the statistical first passage method and on a solution of the Frobenius-Perron equation by employing Markov partitions and topological transition matrices, the largest eigenmodes of the Frobenius-Perron operator could be calculated by solving eigenvalue problems, and the diffusion coefficient could be related to certain eigenvalues of this operator. This *first* method has for the first time been applied analytically and numerically for computing parameter-dependent diffusion coefficients. Another numerical method has been invented to obtain complete solutions of the Frobenius-Perron equation. This *second* method turned out to be very simple, efficient, and precise for computing fractal diffusion coefficients as well as for evaluating certain time-dependent dynamical quantities. It has been confirmed that computer

simulations, as a well-known conventional *third* method, provide reasonable numerical results for computing diffusion coefficients and other time-dependent dynamical quantities. Finally, a new analytical approach to compute fractal diffusion coefficients, based on the Green-Kubo formula and on the definition of certain fractal functions, has been performed. This *fourth* method has to a large extent also been implemented numerically.

(C) A detailed *analysis of deterministic diffusion* in simple dynamical systems has been performed: The eigenmodes of the Frobenius-Perron operator turned out to be formally identical to the ones of the diffusion equation on a large scale, with a remarkable periodic fine structure on a small scale. The probability densities of the dynamical systems have been revealed to be Gaussians with a periodic fine structure. And the time-dependent curtosity, the time-dependent diffusion coefficients, as well as the velocity autocorrelation functions showed a statistical diffusive behaviour on a large scale, with certain oscillations on a small scale. Thus, in all these quantities different behaviour on two different scales has been found: On a large scale, one encounters functions equal to the solutions of the simple diffusion equation of statistical physics. This guarantees the existence of diffusion coefficients as macroscopic quantities in the dynamical systems under consideration. On a small scale, the chaotic deterministic dynamics is intimately connected to the special features of the microscopic scattering mechanisms. This produces a periodic fine structure in the dynamical quantities which is due to the periodic distribution of the scatterers. It is conjectured that this fine structure is typical for periodic deterministic dynamical systems with diffusive dynamics. Moreover, the fine structure of time-dependent dynamical quantities could be related to oscillations in the parameter-dependent fractal diffusion coefficients and may thus be considered as the dynamical origin of the fractality of the diffusion coefficient curves.

(D) Some approaches to achieve a better physical *understanding of the structure of fractal diffusion coefficients* have been developed: In certain regions of these curves, and on certain scales, the number of local extrema could be related qualitatively to the special microscopic coupling mechanism between different scatterers, which changes with changing the parameter value of the diffusion coefficient. Employing this idea in more detail, local extrema could be identified by single points in the framework of “turnstile dynamics”, which established a quantitative relation between microscopic orbits and the structure of macroscopic diffusion coefficients. By applying these methods, a surprising phenomenon has been discovered in the diffusion coefficient curves, i.e., the existence of so-called overhang parameter regions, where diffusion gets unexpectedly enhanced in a quite spectacular way. By support of two simple analytical random walk models, which describe the large-scale functional form of the numerically obtained diffusion coefficient curves, two simple laws have been found, which represent

limiting cases for the large-scale behaviour of the diffusion coefficient as functions of its parameter value. This behaviour is linear in the parameter right after the onset of diffusion, but approaches a quadratic law with a factor of $1/6$ for high parameter values. Evidence for the occurrence of phase transitions has been obtained not only by these random walk models, but also by turnstile dynamics analyses. In one of the maps under investigation, only one phase transition has been observed, in the other map even another phase transition at larger values of the parameter is suspected. The phase transition at lower parameter values, which has been observed in both systems, has been interpreted as a crisis in deterministic diffusion, in analogy to similar phenomena which occur in other dynamical systems. Such a crisis can be defined by a collision of certain scattering regions with increasing the parameter value and may be characterized dynamically as a transition from a simple and regular dynamics to a more complicated one. Another picture about the creation of fractal diffusion coefficients has been provided by splitting the dynamics of the system into the parameter-dependent invariant probability density of a scatterer and a new type of fractal functions as generators of the movement of particles between these scatterers. Based on this approach, analytical and numerical approximation procedures have been introduced which relate the diffusion coefficient curves to fractal functions, defined via functional equations. This method enables a better understanding of certain features of the fractal diffusion coefficient curves, e.g., of overhang regions and of derivative plots of fractal diffusion coefficients, with respect to their dynamical origin.

(E) A number of general *conjectures*, based on either numerical or analytical evidence obtained from the two maps investigated here, has been given: They are claimed to be valid for a broad class of maps and deal with the existence of Markov partitions, with the existence of diffusion coefficients in a rigorous mathematical sense, with the validity of a central limit theorem for dynamical systems probability densities, with the absence of long-time tails in the velocity autocorrelation function, and with the existence of a crisis in deterministic diffusion as an external dynamical phase transition. These conjectures point mainly to a more rigorous mathematical foundation of the main results presented here and may motivate more mathematically oriented researchers in this field to work on these problems.

6.2 Outlook

In the introduction of this work, it has been announced that the author would be a bit “disobedient” to traditional physics by discussing an abstract model for deterministic diffusion, which at first sight may not have very much to do with physical reality. However, this model was at least “simple” enough for

performing a detailed theoretical analysis. As it has been shown in this work, one can indeed learn much from such simple models. Many very interesting features have been discovered, and one may wonder whether such phenomena can be encountered in any experiments. Thus, to become “more obedient” again, and as an attempt to bring the main results of this work, and the experience with the techniques developed in its course, more close to physical reality, a “road to reality” may be outlined in the following. It may give some hints to interested people where fractal diffusion coefficients are expected to show up, and it may point in a direction of possible applications of such phenomena.

Fractal diffusion coefficients have been found here in a very simple class of chaotic dynamical systems. However, the complexity of the systems can be increased systematically step by step while analyzing their diffusive dynamics by the methods presented in this work, as well as by employing other techniques [Cvi91a, Che95]. One may start with computing diffusion coefficients for slightly more difficult maps, being piecewise linear with piecewise uniform slope [Gro83b], where similar results are expected. As a next step, one can consider piecewise differentiable maps in which anomalous diffusion has been observed, trying to understand the origin of this phenomenon in more detail [Gei84, Wan93, Art93, Sto94]. This should serve as a preparation for a more general case, i.e., parameter-dependent diffusion in so-called climbing sine maps, which promise a very complicated scenario of normal and various kinds of anomalous diffusion [Sch82, Gro82]. These maps have often been used to model the physics of Josephson junctions, a well-known and widely used semiconductor device [Gei85]. Furthermore, the influence of noise on diffusion in such systems may be investigated, which is also a problem more related to applications, since noise is encountered in most physical experiments. Here, several kinds of noise-induced phase transitions can be expected [Rei94, Gei82].

Being familiar with diffusion in various types of one-dimensional dynamical systems, one can try to apply similar methods to the case of two-dimensional systems, especially to the periodic Lorentz gas, which has been the object of a great variety of recent investigations, see, e.g., Refs. [Gas94, Cvi91b] and references therein. It may be conjectured that this system also shows parameter-dependent fractal transport coefficients. In fact, molecular dynamics computer simulations reveal pronounced oscillations in the electric conductivity of a periodic Lorentz gas with respect to varying an external electric field [Mor87, Del95]. This may indicate an underlying fractal structure similar to the parameter-dependent diffusion coefficient curves obtained here. One should note that it has recently been possible to create Lorentz gas-like structures in certain semiconductors [Wei91, Wei95]. This seems to provide another opportunity to check the results of the deterministic theory of transport in experiments [Gei90, Fle95]. E.g., for this type of system Ohm’s law has been derived starting from the microscopic

dynamics by methods of dynamical systems theory [Che93a, Che93b]. Moreover, for the magnetoresistance of a one-dimensional conducting metallic ring complex structures have been observed experimentally with respect to varying the strength of an external magnetic field, which do not seem to be induced by well-known quantum effects [Umb84].¹ However, it remains to be investigated carefully whether these structures are of any deterministic nature.

Thus, it seems that there are many problems in statistical physics and dynamical systems theory for which evaluating macroscopic physical quantities explicitly with respect to their underlying microscopic deterministic dynamics can lead to surprising and highly interesting results. These results may not only be of fundamental theoretical, but also of quite practical interest,

¹The author thanks Profs. T.R. Kirkpatrick and J.R. Dorfman for pointing out this reference to him.

References

- [Als89a] L. Alsedà and J. Llibre, *Kneading theory of Lorenz maps*. in: Dynamical Systems and Ergodic Theory, volume 23 of Banach Center Publications, pages 83–89 (Polish Scientific Publishers, Warszawa, 1989).
- [Als89b] L. Alsedà, J. Llibre, M. Misiurewicz and C. Tresser, *Periods and entropy for Lorenz-like maps*. Ann. Inst. Fourier, Grenoble **39**, 929–952 (1989).
- [Als93] L. Alsedà, J. Llibre and M. Misiurewicz, *Combinatorial Dynamics and Entropy in Dimension One* (World Scientific, 1993).
- [Ant81] T.M. Antonsen and E. Ott, *Diffusion coefficient for ions in the presence of a coherent lower hybrid wave*. Phys. Fluids **24**, 1635–1640 (1981).
- [Ant92] I. Antoniou and S. Tasaki, *Generalized spectral decomposition of the β -adic baker's transformation and intrinsic irreversibility*. Physica A **190**, 303–329 (1992).
- [Ant93] I. Antoniou and S. Tasaki, *Spectral decomposition of the Renyi map*. J. Phys. A: Math. Gen. **26**, 73–94 (1993).
- [Art91] R. Artuso, *Diffusive dynamics and periodic orbits of dynamical systems*. Phys. Lett. A **160**, 528–530 (1991).
- [Art93] R. Artuso, G. Casati and R. Lombardi, *Periodic orbit theory of anomalous diffusion*. Phys. Rev. Lett. **71**, 62–64 (1993).
- [Art94] R. Artuso, *Recycling deterministic diffusion*. Physica D **76**, 1–7 (1994).
- [Bal94] N.J. Balmforth, E.A. Spiegel and C. Tresser, *Topological entropy of one-dimensional maps: approximations and bounds*. Phys. Rev. Lett. **72**, 80–83 (1994).
- [Bar93a] A. Baranyai, D.J. Evans and E.G.D. Cohen, *Field-dependent conductivity and diffusion in a two-dimensional Lorentz Gas*. J. Stat. Phys. **70**, 1085–1098 (1993).
- [Bar93b] M.F. Barnsley, *Fractals everywhere* (Academic Press, Boston, 2nd edition, 1993).

- [Bas94] E.L. Basor and K.E. Morrison, *The Fisher-Hartwig conjecture and Toeplitz eigenvalues*. *Lin. Alg. Appl.* **202**, 129–142 (1994).
- [Bea91] R.M. Beam and R.F. Warming, *The asymptotic spectra of banded Toeplitz and quasi-Toeplitz matrices*. Technical Memorandum 103900, NASA Ames Research Center, Moffett Field, California, 1991.
- [Bec93] Chr. Beck and F. Schlögl, *Thermodynamics of Chaotic Systems*, volume 4 of Cambridge nonlinear science series (Cambridge University Press, Cambridge, 1993).
- [Ber52] T.H. Berlin and M. Kac, *The spherical model of a ferromagnet*. *Phys. Rev. A* **86**, 821–835 (1952).
- [Bia94] M. Bianucci et al., *Chaos and linear response: analysis of the short, intermediate-, and long-time regime*. *Phys. Rev. E* **50**, 2630–2638 (1994).
- [Bow75] R. Bowen, *Equilibrium states and the ergodic theory of Anosov diffeomorphisms*, volume 470 of Lecture notes in mathematics (Springer-Verlag, Berlin, 1975).
- [Bow79] R. Bowen, *Invariant measures for Markov maps of the interval*. *Commun. Math. Phys.* **69**, 1–17 (1979).
- [Boy79] A. Boyarski and M. Scarowsky, *On a class of transformations which have unique absolutely continuous invariant measures*. *Trans. Am. Math. Soc.* **255**, 243–242 (1979).
- [Boy84] A. Boyarsky, *On the significance of absolutely continuous invariant measures*. *Physica D* **11**, 130–146 (1984).
- [Boy88] A. Boyarsky, *A matrix method for estimating the Lyapunov exponent of one-dimensional systems*. *J. Stat. Phys.* **50**, 213–229 (1988).
- [Boy90] A. Boyarsky, *Discontinuity of physical measures*. *Phys. Lett. A* **149**, 12–16 (1990).
- [Bre94] W. Breymann and J. Vollmer, *Pruning-induced phase transition observed by a scattering model*. *J. Stat. Phys.* **76**, 1439–1465 (1994).
- [Bru76] St.G. Brush, *The kind of motion we call heat*, volume 1/2 (North Holland, Amsterdam, 1976).

- [Bun85] L.A. Bunimovich, *Decay of correlations in dynamical systems with chaotic behaviour*. Sov. Phys. JETP **62**, 841–852 (1985).
- [Bye90] W. Byers, P. Góra and A. Boyarsky, *Maximal absolutely continuous invariant measures for piecewise linear Markov transformations*. Ergod. Th. and Dynam. Sys. **10**, 645–656 (1990).
- [Car81a] J.R. Cary and J.D. Meiss, *Rigorously diffusive deterministic map*. Phys. Rev. A **24**, 2664–2668 (1981).
- [Car81b] J.R. Cary, J.D. Meiss and A. Bhattacharjee, *Statistical characterization of periodic, area-preserving mappings*. Phys. Rev. A **23**, 2744–2746 (1981).
- [Che89] Q. Chen and J.D. Meiss, *Flux, resonances and the devil's staircase for the sawtooth map*. Nonlinearity **39**, 347–356 (1989).
- [Che90] Q. Chen et al., *Resonances and transport in the sawtooth map*. Physica D **46**, 217–240 (1990).
- [Che93a] N.L. Chernov, C.L. Eyink, J.L. Lebowitz and Ya.G. Sinai, *Derivation of Ohm's law in a deterministic mechanical model*. Phys. Rev. Lett. **70**, 2209–2212 (1993).
- [Che93b] N.L. Chernov, C.L. Eyink, J.L. Lebowitz and Ya.G. Sinai, *Steady-state electrical conduction in the periodic Lorentz gas*. Comm. Math. Phys. **154**, 569–601 (1993).
- [Che95] Ch.-Ch. Chen, *Diffusion coefficient of piecewise linear maps*. Phys. Rev. E **51**, 2815–2822 (1995).
- [Cla93] I. Claes and C. Van den Broeck, *Dispersion of particles in periodic media*. J. Stat. Phys. **70**, 1215–1231 (1993).
- [Coh93] E.G.D. Cohen, *Fifty years of kinetic theory*. Physica A **194**, 229–257 (1993).
- [Coh95] E.G.D. Cohen, *Transport coefficients and Lyapunov exponents*. Physica A **213**, 293–314 (1995).
- [Cor82] I.P. Cornfeld, S.V. Fomin and Ya.G. Sinai, *Ergodic Theory* (Springer, New York, 1982).
- [Cov88] E.M. Coven, I. Kan and J.A. Yorke, *Pseudo-orbit shadowing in the family of tent maps*. Trans. Am. Math. Soc. **308**, 227–241 (1988).

- [Cvi89] P. Cvitanović, *Universality in Chaos* (Adam Hilger, Bristol, 2nd edition, 1989), a reprint selection.
- [Cvi91a] P. Cvitanović, *Periodic orbits as the skeleton of classical and quantum chaos*. *Physica D* **51**, 138–151 (1991).
- [Cvi91b] P. Cvitanović, J.-P. Eckmann and P. Gaspard, *Transport properties of the Lorentz gas in terms of periodic orbits*. Niels Bohr Institute report (1991).
- [Cvi95] P. Cvitanović, *Classical and Quantum Chaos: A Cyclist Treatise*. lecture notes, preprint; available via WWW server (1995).
- [Dan89a] I. Dana, *Hamiltonian transport on unstable periodic orbits*. *Physica D* **39**, 205 (1989).
- [Dan89b] I. Dana, N.W. Murray and I.C. Percival, *Resonances and diffusion in periodic Hamiltonian maps*. *Phys. Rev. Lett.* **65**, 1693 (1989).
- [Dav79] P.J. Davis, *Circulant matrices* (Wiley Interscience Publ., New York, 1979).
- [Del95] Ch. Dellago, L. Glatz and H.A. Posch, *Lyapunov spectrum of the driven Lorentz gas*. *Phys. Rev. E* **52**, 4817–4826 (1995).
- [dM93] W. de Melo and S. van Strien, *One-dimensional dynamics*, volume 25 of *Ergebnisse der Mathematik und ihrer Grenzgebiete, 3.Folge* (Springer, Berlin, 1993).
- [Dor75] J.R. Dorfman, *Kinetic and hydrodynamic theory of time correlation functions*. in: E.G.D. Cohen, Hrsg., *Fundamental problems in statistical mechanics*, volume 3, pages 277–330 (North-Holland, Amsterdam, 1975).
- [Dor77] J.R. Dorfman and H. van Beijeren, *The Kinetic Theory of Gases*. in: B.J. Berne, Hrsg., *Statistical mechanics*, volume B, chapter 3, pages 65–179 (Plenum Press, New York, 1977).
- [Dor95a] J.R. Dorfman, *From molecular chaos to dynamical chaos*. lecture notes, Institute for Physical Science and Technology, College Park (1995).
- [Dor95b] J.R. Dorfman and P. Gaspard, *Chaotic scattering theory of transport and reaction-rate coefficients*. *Phys. Rev. E* **51**, 28–35 (1995).

- [Eck85] J.-P. Eckmann and D. Ruelle, *Ergodic theory of chaos and strange attractors*. Rev. Mod. Phys. **57**, 617–656 (1985).
- [Ein05] A. Einstein, *Über die von der molekularkinetischen Theorie der Wärme geforderte Bewegung von in ruhenden Flüssigkeiten suspendierten Teilchen*. Ann. d. Ph. **17**, 549–560 (1905).
- [Els85] Y. Elskens and R. Kapral, *Reversible dynamics and the macroscopic rate law for a solvable Kolmogorov system: the three Bakers' reaction*. J. Stat. Phys. **38**, 1027–1049 (1985).
- [Ers93] S.V. Ershov, *Is a perturbation theory for dynamical chaos possible?* Phys. Lett. A **177**, 180–185 (1993).
- [Eva90a] D.J. Evans, E.G.D. Cohen and G.P. Morriss, *Viscosity of a simple fluid from its maximal Lyapunov exponents*. Phys. Rev. A **42**, 5990–5997 (1990).
- [Eva90b] D.J. Evans and G.P. Morriss, *Statistical Mechanics of Nonequilibrium Liquids* Theoretical Chemistry. (Academic Press, London, 1990).
- [Fle95] R. Fleischmann et al., *Chaos und fraktale Energiespektren in Antidot-Gittern*. Physikalische Blätter **51**, 177–182 (1995).
- [Fri81] N. Friedman and A. Boyarsky, *Matrices and eigenfunctions induced by Markov maps*. Lin. Alg. Appl. **38**, 141–147 (1981).
- [Fuj82] H. Fujisaka and S. Grossmann, *Diffusion in discrete nonlinear dynamical systems*. Z. Physik B **48**, 261 (1982).
- [Gas90] P. Gaspard and G. Nicolis, *Transport properties, Lyapunov exponents, and entropy per unit time*. Phys. Rev. Lett. **65**, 1693–1696 (1990).
- [Gas92a] P. Gaspard, *Diffusion, effusion, and chaotic scattering*. J. Stat. Phys. **68**, 673–747 (1992).
- [Gas92b] P. Gaspard, *Diffusion in uniformly hyperbolic one-dimensional maps and Appell polynomials*. Phys. Lett. A **168**, 13–17 (1992).
- [Gas92c] P. Gaspard, *r-adic one-dimensional maps and the Euler summation formula*. J. Phys. A: math. Gen. **25**, L483–L485 (1992).
- [Gas92d] P. Gaspard and F. Baras, *Dynamical Chaos underlying diffusion in the Lorentz Gas*. in: M. Mareschal and B.L. Holian, Hrsg., *Microscopic simulations of complex hydrodynamic phenomena*, volume 292 of NATO ASI Series B: Physics, pages 301–322, Plenum Press, New York, 1992.

- [Gas93] P. Gaspard, *What is the role of chaotic scattering in irreversible processes?* Chaos **3**, 427–442 (1993).
- [Gas94] P. Gaspard and F. Baras, *Chaotic scattering and diffusion in the Lorentz gas.* Phys. Rev. E **51**, 5333–5352 (1994).
- [Gas95] P. Gaspard and J.R. Dorfman, *Chaotic scattering theory, thermodynamic formalism, and transport coefficients.* Phys. Rev. E **52**, 3525–3552 (1995).
- [Gei82] T. Geisel and J. Nierwetberg, *Onset of diffusion and universal scaling in chaotic systems.* Phys. Rev. Lett. **48**, 7–10 (1982).
- [Gei84] T. Geisel and S. Thomaе, *Anomalous diffusion in intermittent chaotic systems.* Phys. Rev. Lett. **52**, 1936–1939 (1984).
- [Gei85] T. Geisel, J. Nierwetberg and A. Zacherl, *Accelerated diffusion in Josephson junctions and related chaotic systems.* Phys. Rev. Lett. **54**, 616–619 (1985).
- [Gei90] T. Geisel et al., *Chaotic dynamics of ballistic electrons in lateral superlattices and magnetic fields.* Phys. Rev. Lett. **64**, 1581–1584 (1990).
- [Gle88] J. Gleick, *Chaos - Making a New Science* (Penguin, New York, 1988).
- [Gle93] P. Glendinning and C. Sparrow, *Prime and renormalisable kneading invariants and the dynamics of expanding Lorenz maps.* Physica D **62**, 22–50 (1993).
- [Gor88] P. Góra and A. Boyarsky, *Why computers like Lebesgue measure.* Comput. Math. Applic. **16**, 321–329 (1988).
- [Gor89] P. Góra and A. Boyarsky, *Approximating the invariant densities of transformations with infinitely many pieces on the interval.* Proc. Am. Math. Soc. **105**, 922–928 (1989).
- [Gor91] P. Góra and A. Boyarsky, *Computing the topological entropy of general one-dimensional maps.* Trans Am. Math. Soc. **323**, 39–49 (1991).
- [Gra88] P. Grassberger, *On symbolic dynamics of one-humped maps of the interval.* Z. Naturforsch. **43a**, 671–680 (1988).
- [Gre90] C. Grebogi et al., *Shadowing of physical trajectories in chaotic dynamics: containment and refinement.* Phys. Rev. Lett. **65**, 1527–1530 (1990).

- [Gro82] S. Grossmann and H. Fujisaka, *Chaos-induced diffusion in nonlinear discrete dynamics*. Phys. Rev. A **26**, 1179 (1982).
- [Gro83a] S. Grossmann and S. Thomaе, *Shape dependence of correlation times in chaos-induced diffusion*. Phys. Lett. A **97**, 263–267 (1983).
- [Gro83b] S. Grossmann and S. Thomaе, *Shape-dependence of correlation times in chaos-induced diffusion*. Phys. Lett. A **97**, 263–267 (1983).
- [Gro95a] J. Groeneveld. e-mail communications Utrecht-Berlin (1995).
- [Gro95b] S. Grossmann, *Wie entsteht eigentlich Turbulenz?* Physikalische Blätter **51**, 641–646 (1995).
- [Guc90] J. Guckenheimer and P. Holmes, *Nonlinear Oscillations, Dynamical Systems and Bifurcations of Vector Fields*, volume 42 of Applied mathematical sciences. (Springer, Berlin, 3rd edition, 1990).
- [Ham87] S.M. Hammel, J.A. Yorke and C. Grebogi, *Do numerical orbits of chaotic dynamical processes represent true orbits*. J. Complexity **3**, 136–145 (1987).
- [Ham88] S.M. Hammel, J.A. Yorke and C. Grebogi, *Numerical orbits of chaotic processes represent true orbits*. Bull. Am. Math. Soc. **2**, 465–469 (1988).
- [Har87] J. Hartung, *Lehr- und Handbuch der angewandten Statistik* (Oldenbourg, München, 6th edition, 1987).
- [Hes92a] S. Hess, *Einfache Flüssigkeiten*. in: W. Raith, Hrsg., *Vielteilchensysteme*, volume 5 of Lehrbuch der Experimentalphysik, chapter 3, pages 227–292 (de Gruyter, Berlin, 1992).
- [Hes92b] S. Hess, *Gase*. in: W. Raith, Hrsg., *Vielteilchensysteme*, volume 5 of Lehrbuch der Experimentalphysik, chapter 1, pages 1–96 (de Gruyter, Berlin, 1992).
- [Hof82] F. Hofbauer and G. Keller, *Equilibrium states for piecewise monotonic transformations*. Ergod. Th. and Dynam. Sys. **2**, 23–43 (1982).
- [Hoo91] W.G. Hoover, *Computational Statistical Mechanics*, volume 11 of Studies in Modern Thermodynamics (Elsevier, Amsterdam, 1991).
- [Hsu85] C.S. Hsu and M.C. Kim, *Construction of maps with generating partitions for entropy evaluation*. Phys. Rev. A **31**, 3253–3265 (1985).

- [Hub90] J.H. Hubbard and Sparrow C., *The classification of topologically expansive Lorenz maps*. Comm. Pure Appl. Math. **43**, 431–443 (1990).
- [Ish86] H. Ishitani, *A central limit theorem of mixed type for a class of one-dimensional transformations*. Hiroshima J. Math. **16**, 161–188 (1986).
- [Ish89] H. Ishitani, *Perron-Frobenius operator and central limit theorem*. World Sci. Adv. Ser. Dyn. Sys. **7**, 122–139 (1989).
- [Kat95] A. Katok and B. Hasselblatt, *Introduction to the Modern Theory of Dynamical Systems*, volume 54 of Encyclopedia of Mathematics and its Applications (Cambridge University Press, Cambridge, 1995).
- [Kla92] R. Klages, *Theoretische Analyse des Boltzmann-Stoßterms der kinetischen Theorie und Berechnung von Transportkoeffizienten*. diploma thesis, Berlin (1992).
- [Kla95a] R. Klages, *Existence of diffusion coefficients in chains of one-dimensional piecewise linear maps: scetch of a proof*. College Park (1995).
- [Kla95b] R. Klages and J.R. Dorfman, *Simple maps with fractal diffusion coefficients*. Phys. Rev. Lett. **74**, 387–390 (1995).
- [Kna87] A. Knauf, *Ergodic and topological properties of Coulombic periodic potentials*. Commun. Math. Phys. **110**, 89–112 (1987).
- [Kon89] X.-P. Kong and E.G.D. Cohen, *Anomalous diffusion in a lattice-gas wind-tree model*. Phys. Rev. B **40**, 4838–4845 (1989).
- [Kow54] G. Kowalewski, *Einführung in die Determinantentheorie* (de Gruyter, Berlin, 4th edition, 1954).
- [Kub92] R. Kubo, M. Toda and N. Hashitsume, *Statistical Physics*, volume 2 of Solid State Sciences (Springer, Berlin, 2 edition, 1992).
- [Lai93] Y.-Ch. Lai et al., *Crisis in chaotic scattering*. Phys. Rev. Lett. **71**, 2212–2215 (1993).
- [Lai94] Y.-Ch. Lai and C. Grebogi, *Crisis and enhancement of chaotic scattering*. Phys. Rev. E **49**, 3761–3770 (1994).
- [Las73] A. Lasota and J.A. Yorke, *On the existence of invariant measures for piecewise monotonic transformations*. Trans. Am. Math. Soc. **186**, 481–488 (1973).

- [Las94] A. Lasota and M.C. Mackey, *Chaos, Fractals, and Noise*, volume 97 of Applied mathematical sciences (Springer, Berlin, 2nd edition, 1994).
- [Lee88] K.-Ch. Lee, *Long-time tails in a chaotic system*. Phys. Rev. Lett. **60**, 1991–1994 (1988).
- [Lev89] R.W. Leven, B.-P. Koch and B. Pompe, *Chaos in dissipativen Systemen* (Vieweg, Braunschweig, 1989).
- [Li76] T.-Y. Li, *Finite approximation for the Frobenius-Perron operator. A solution to Ulam's conjecture*. J. of Approx. Th. **17**, 177–186 (1976).
- [Li78] T.-Y. Li and J.A. Yorke, *Ergodic transformations from an interval into itself*. Trans. Am. Math. Soc. **235**, 183192 (1978).
- [Lic92] A.J. Lichtenberg and M.A. Lieberman, *Regular and Chaotic Dynamics*, volume 38 of Applied Mathematical Sciences (Springer, New York, 2nd edition, 1992).
- [Lor63] E.N. Lorenz, *Deterministic nonperiodic flow*. J. Atmos. Sci. **20**, 130–141 (1963).
- [Mac83a] J. Machta, *Power law decay of correlations in a billard problem*. J. Stat. Phys. **32**, 555–564 (1983).
- [Mac83b] J. Machta and R. Zwanzig, *Diffusion in a periodic Lorentz gas*. Phys. Rev. Lett. **50**, 1959–1962 (1983).
- [Mac83c] J. Machta and R. Zwanzig, *Diffusion in a periodic Lorentz gas*. Phys. Rev. Lett. **50**, 1959–1962 (1983).
- [Mac84] R.S. MacKay, J.D. Meiss and I.C. Percival, *Transport in Hamiltonian systems*. Physica D **13**, 55–81 (1984).
- [Mac94] D. MacKernan and G. Nicolis, *Generalized Markov coarse graining and spectral decomposition of chaotic piecewise linear maps*. Phys. Rev. E **50**, 988–999 (1994).
- [Man82] B.B. Mandelbrot, *The Fractal Geometry of Nature* (W.H. Freeman and Company, San Francisco, 1982).
- [Mar71] B.R. Martin, *Statistics for Physicists* (Academic Press, London, 1971).
- [Mei92] J.D. Meiss, *Symplectic maps, variational principles, and transport*. Rev. Mod. Phys. **64**, 795–848 (1992).

- [Mis89] M. Misiurewicz, *Persistent rotation intervals for old maps*. in: Dynamical Systems and Ergodic Theory, volume 23 of Banach Center Publications, pages 119–124. (Polish Scientific Publishers, Warszawa, 1989).
- [Moo75] J.B. Moore and S.S. Sengupta, *Existence and control of Markov chains in systems of deterministic motion*. SIAM J. Control **13**, 1103–1114 (1975).
- [Mor87] B. Moran and W.G. Hoover, *Diffusion in a periodic Lorentz gas*. J. Stat. Phys. **48**, 709–726 (1987).
- [Nob95] B. Nobbe, *Classical motion in two-dimensional crystals*. J. Stat. Phys. **78**, 1591–1605 (1995).
- [Nus88] H.E. Nusse and J.A. Yorke, *Is every approximate trajectory of some process near an exact trajectory of a nearby process?* Commun. Math. Phys. **114**, 363–379 (1988).
- [Ott93] E. Ott, *Chaos in Dynamical Systems* (Cambridge University Press, Cambridge, 1993).
- [Pei92] H.-O. Peitgen, H. Jürgens and D. Saupe, *Chaos and Fractals* (Springer-Verlag, Berlin, 1992).
- [Pos88] H.A. Posch and W.G. Hoover, *Lyapunov instability of dense Lennard-Jones fluids*. Phys. Rev. A **38**, 473–482 (1988).
- [Pos89] H.A. Posch and W.G. Hoover, *Equilibrium and nonequilibrium Lyapunov spectra for dense fluids and solids*. Phys. Rev. A **39**, 2175 (1989).
- [Rec80] A.B. Rechester and R.B. White, *Calculation of turbulent diffusion for the Chirikov-Taylor model*. Phys. Rev. Lett. **44**, 1586 (1980).
- [Rec81] A.B. Rechester, M.N. Rosenbluth and R.B. White, *Fourier-space paths applied to the calculation of diffusion for the Chirikov-Taylor model*. Phys. Rev. A **23**, 2664 (1981).
- [Rei87] F. Reif, *Statistische Physik und Theorie der Wärme* (de Gruyter, Berlin, 3rd edition, 1987).
- [Rei92] L. Reichel and L.N. Trefethen, *Eigenvalues and pseudo-eigenvalues of Toeplitz matrices*. Lin. Alg. Appl. **162-164**, 153–185 (1992).

- [Rei94] P. Reimann, *Suppression of deterministic diffusion by noise*. Phys. Rev. E **50**, 727–735 (1994).
- [Rue78] D. Ruelle, *Thermodynamic Formalism*, volume 5 of Encyclopedia of mathematics and its applications (Addison-Wesley, Reading, Mass., 1978).
- [Rue89] D. Ruelle, *The thermodynamic formalism for expanding maps*. Commun. Math. Phys. **125**, 239–262 (1989).
- [Sac84] L. Sachs, *Angewandte Statistik* (Springer, Berlin, 6th edition, 1984).
- [Sch82] M. Schell, S. Fraser and R. Kapral, *Diffusive dynamics in systems with translational symmetry: A one-dimensional-map model*. Phys. Rev. A **26**, 504 (1982).
- [Sch89] H.G. Schuster, *Deterministic Chaos* (VCH Verlagsgesellschaft mbH, Weinheim, 2nd edition, 1989).
- [Sin68] Ya.G. Sinai, *Construction of Markov partitions*. Funktsional’nyi analiz i Ego Prilozheniya **2**, 70–80 (1968).
- [Sin89] Ya.G. Sinai, *Dynamical Systems*, volume 2 of Encyclopedia of mathematical sciences. (Springer, Berlin, 1989).
- [Sin68] Ya.G. Sinai, *Markov partitions and C-diffeomorphisms*. Funktsional’nyi analiz i Ego Prilozheniya **2**, 64–89 (68).
- [Sta89] J. (Ed.) Stachel, *The collected papers of Albert Einstein*, volume 2. (Princeton University Press, Princeton, 1989).
- [Sto94] R. Stoop, *Bivariate thermodynamic formalism and anomalous diffusion*. Phys. Rev. E **49**, 4913–4918 (1994).
- [Suh94] H. Suhl, *Chaos and the Kubo formula*. Physica B **199**, 1–7 (1994).
- [Tas93a] S. Tasaki, I. Antoniou and Z. Suchanecki, *Deterministic diffusion, de Rham equation and fractal eigenvectors*. Phys. Lett. A **179**, 97–102 (1993).
- [Tas93b] S. Tasaki, Z. Suchanecki and I. Antoniou, *Ergodic properties of piecewise linear maps on fractal repellers*. Phys. Lett. A **179**, 103–110 (1993).
- [Tas94] S. Tasaki and P. Gaspard, *Fractal distribution and Fick’s law in a reversible chaotic system*. in: M. Yamaguti, Hrsg., *Towards the Harnessing of Chaos*, pages 273–288. (Elsevier, Amsterdam, 1994).

- [Tas95] S. Tasaki and P. Gaspard, *Fick's law and fractality of nonequilibrium stationary states in a reversible multibaker map*. J. Stat. Phys. **81**, 935–987 (1995).
- [Tel95] T. Tél, J. Vollmer and W. Breymann, *Nondiffusive transport as transient chaos*. preprint (1995).
- [Tho83] S. Thomae, *Chaos-induced diffusion*. in: C. Benedek et al., Hrsg., *Statics and Dynamics of nonlinear systems*, pages 204–210, Springer, Berlin, 1983.
- [Tod92] M. Toda, R. Kubo and N. Saitô, *Statistical Physics*, volume 1 of Solid State Sciences (Springer, Berlin, 2nd edition, 1992).
- [Tre85] W.F. Trench, *On the eigenvalue problem for Toeplitz band matrices*. Lin. Alg. Appl. **64**, 199–214 (1985).
- [Tro89] G. Troll and U. Smilansky, *A simple model for chaotic scattering*. Physica D **35**, 34–64 (1989).
- [Tro91] G. Troll, *A devil's staircase into chaotic scattering*. Physica D **50**, 276–296 (1991).
- [Tse94] H.-Ch. Tseng et al., *Some exact results for the diffusion coefficients of maps with pruning cycles*. Phys. Lett. A **195**, 74–80 (1994).
- [Umb84] C.P. Umbach et al., *Magnetoresistance of small, quasi one-dimensional, normal-metal rings and lines*. Phys. Rev. B **30**, 4048–4051 (1984).
- [Viv83] F. Vivaldi, G. Casati and I. Guarneri, *Origin of long-time tails in strongly chaotic systems*. Phys. Rev. Lett. **51**, 727–730 (1983).
- [vK92] N. van Kampen, *Stochastic processes in physics and chemistry* (North Holland, Amsterdam, 1992).
- [Vol94] J. Vollmer and W. Breymann, *Scaling behaviour in Lorenz-like maps at the onset of pruning*. Europhys. Lett. **27**, 23–28 (1994).
- [vW95] C.F. von Weizsäcker, *Zeit und Wissen* (DTV, München, 1995), p. 271.
- [Wag92] J. Wagenhuber et al., *Chaos and anomalous diffusion of ballistic electrons in lateral surface superlattices*. Phys. Rev. B **45**, 4372–4383 (1992).
- [Wan66] G.H. Wannier, *Statistical Physics* (Dover, New York, 1966).

- [Wan93] X.-J. Wang and Ch.-K. Hu, *Anomalous diffusion in dynamical systems: Transport coefficients of all order*. Phys. Rev. E **48**, 728–733 (1993).
- [Wax54] N. Wax, *Selected Papers on Noise and Stochastic Processes*. (Dover, New York, 1954), see especially the review articles by S. Chandrasehar, G.E. Uhlenbeck, L.E. Ornstein, and M.C. Wang.
- [Wei91] D. Weiss et al., *Electron pinball and commensurate orbits in a periodic array of scatterers*. Phys. Rev. Lett. **66**, 2790–2793 (1991).
- [Wei95] D. Weiss and K. Richter, *Antidot-Übergitter: Flippern mit Elektronen*. Physikalische Blätter **51**, 171–176 (1995).
- [Wig92] S. Wiggins, *Chaotic Transport in Dynamical Systems*, volume 2 of Interdisciplinary Applied Mathematics (Springer, New York, 1992).
- [Woo71] W.W. Wood and F. Lado, *Monte Carlo calculation of normal and abnormal diffusion in Ehrenfest's Wind-Tree model*. J. Comput. Phys. **7**, 528–546 (1971).
- [Zur84] R. Zurmühl and S. Falk, *Matrizen und ihre Anwendungen*, volume 1 (Springer, Berlin, 5th edition, 1984).